Escuela Politécnica Superior
Departmento de Electrónica

Universidad de Alcalá

Programa de Doctorado en
Electrónica: Sistemas Electrónicos Avanzados. Sistemas Inteligentes

Ultralong continuous wave and ultrafast fibre lasers at telecommunication wavelengths

Tesis doctoral presentada por
FRANCESCA GALLAZZI

Director
Juan Diego Ania-Castañón

Tutor
Miguel González Herráez

Alcalá de Henares, 2019

Abstract

The birth of lasers in 1960 had a strong impact on the development of fibre optics, and consequently on nonlinear optics. Despite the enormous amount of literature concerning fibre lasers, the topic is still actual and thriving and always looking for new solutions addressing the necessities of scientific research and industry for what regards either continuous wave or ultrafast radiation sources.

This thesis develops around two research lines, Raman distributed amplifiers, in the form of ultralong Raman fibre lasers, and passive ultrafast fibre lasers, which we will try to combine for the first time.

The second order Raman distributed amplifier called ultralong Raman fibre laser has proven its suitability and efficiency in both unrepeatered and long-haul optical communication links. Nevertheless relative intensity noise transfer from pump to signal, especially in the case of high power co-propagating pump necessary to achieve the lowest signal power variation in the amplifier cell, may severely hinder the transmission performances. In the first part of the thesis, a characterization of the relative intensity noise transfer in the cavity and an optimization of the architecture of the amplifier (changing the front-end reflectivity and the pump power split) is performed in order to improve the performance in a transmission system, which finds its optimal balance with a 20% forward pump power ratio and 10% front-end reflectivity with a transmission reach of 6479 km.

Ultrafast radiation sources have a widespread use and are highly demanded. Mode-locked fibre lasers attract much attention due to their many advantageous features, such as compactness, low-cost, stability and easy handling. In the second part of the thesis, we focus on ultrafast passively mode-locked fibre lasers trying to overcome one of their usual limits, that is the achievement of high peak power and pulse energies in the femtosecond range. Solutions for a simple, inexpensive, polarisation independent, high peak-power passively mode-locked femtosecond ring fibre laser are developed, relying on standard and commercial components and a novel InN-based semiconductor saturable absorber mirror, that ensures self-starting mode-locking. Using a cavity 2.4 km long it is possible to obtain Gaussian pulses below 250 fs with a peak power over 1 MW and pulse energy over 250 nJ, properties that open up to new power demanding application fields.

The developed laser system is then applied to the generation of supercontinuum and pulse compression, achieved through the addition of an external reel of single mode fibre to the resonator. Fibres with different lengths and dispersion are employed to test the applicability and tunability of this low-cost, simple system. In particular with standard

single mode fibre supercontinuum is generated over 200 nm with pulse compression down to 50 fs. Such radiation source is tested to prove its feasibility for gas sensing.

In the last part, the developed ultrafast laser is used to implement for the first time an ultralong Raman fibre laser into a pulsed laser, with the objective of generating high power ultrashort pulses taking advantage of the virtually lossless and transparent span produced by the Raman cell. Mode-locking with sub-picosecond pulses is maintained in cavity up to 25 km in length, demonstrating this new application area for distributed Raman amplifiers.

Resumen

El nacimiento de los láseres en 1960 tuvo un fuerte impacto en el desarrollo de la fibra óptica y, en consecuencia, de la óptica no lineal. A pesar de la enorme cantidad de literatura sobre láseres de fibra, el tema sigue siendo enormemente vigente y en constante evolución, siempre en busca de nuevas soluciones que respondan a las necesidades de la investigación científica y de la industria en lo que respecta a fuentes de radiación de onda continua o ultrarrápida.

Esta tesis se desarrolla en torno a dos líneas de investigación, los amplificadores Raman distribuidos, en su modalidad de láseres de fibra Raman ultralargos, y los láseres pasivos de fibra ultrarrápidos, combinando adems ambas líneas por primera vez.

El amplificador Raman distribuido de segundo orden basado en cavidades ultralargas, llamado láser de fibra Raman ultralargo, ha demostrado su idoneidad y eficacia tanto en enlaces únicos de comunicación óptica sin amplificación puntual intermedia como en sistemas de largo alcance para comunicaciones transoceánicas. Sin embargo, la transferencia de ruido de intensidad relativa de la fuente de bombeo a la señal, especialmente en el caso de una fuente de bombeo co-propagante de alta potencia (necesaria para lograr la menor variación de potencia de la señal en la cavidad del amplificador), puede limitar seriamente el rendimiento del sistema. En la primera parte de la tesis describiremos la caracterización de la transferencia del ruido de intensidad relativa en la cavidad y la optimización de la arquitectura del amplificador (cambiando la reflectividad del extremo de entrada de la célula y la proporción de la potencia de la fuente de bombeo) para mejorar el rendimiento de un sistema de transmisión coherente de última generación, el cual encuentra su equilibrio óptimo con una proporción de potencia de la fuente de bombeo co-propagante de un 20% y una reflectividad del extremo de entrada de la célula de un 10% y un alcance de transmisión de 6479 km.

Las fuentes de radiación ultrarrápidas tienen una enorme cantidad de aplicaciones tanto industriales como científicas, siendo por tanto muy demandadas y dando lugar a un campo de trabajo en vertiginosa evolución. De entre las diferentes opciones para este tipo de fuentes, los láseres de fibra con anclado de modos llaman especialmente la atención gracias a sus numerosas características ventajosas, como la compacidad, el bajo coste, la estabilidad y la facilidad de manejo. En la segunda parte de la tesis nos centramos en los láseres de fibra con anclado de modos pasivo ultrarrápidos, demostrando la posibilidad de superar uno de sus límites habituales, que es el logro de altas potencias de pico y energías por pulso en el rango de los femtosegundos. Se desarrollan soluciones para un láser de anillo

de fibra de femtosegundo con anclado de modos pasivo de alta potencia, simple, económico e independiente de la polarización, que se basa en componentes estándar y comerciales y en un nuevo absorbente saturable de semiconductor en configuración de espejo basado en InN, que garantiza el autoarranque del anclado de modos. Utilizando una cavidad de 2.4 km de longitud es posible obtener pulsos Gaussianos por debajo de 250 fs con una potencia pico superior a 1 MW y una energía por pulso superior a 250 nJ, propiedades que abren la posibilidad de aplicar este tipo de fuentes a nuevos campos de aplicación con exigencia de potencia elevada, sin necesidad de estapas de amplificacin externas.

El sistema láser desarrollado se aplica a continuación a la generación de supercontinuo, obteniéndose además la compresión de los pulsos, mediante la adición al resonador de un carrete externo de fibra monomodo. Fibras con diferentes longitudes y dispersiones son empleadas para probar la aplicabilidad y sintonizabilidad de este sistema simple y de bajo coste. En particular, con fibra monomodo estándar, el supercontinuo se genera sobre más de 200 nm con una compresión de los pulsos de hasta 50 fs. En esta misma sección se demuestra la viabilidad de dicha fuente de radiación para la detección de gases.

En la última parte, el láser ultrarrápido desarrollado se combina por primera vez con la tecnología de amplificador de láser de fibra ultralargo, con el objetivo de generar pulsos ultracortos de alta potencia aprovechando el tramo virtualmente sin pérdidas y transparente producido por la célula Raman. El anclado de modos con pulsos de sub-picosegundo se mantiene en cavidades de hasta 25 km de longitud, lo que demuestra esta nueva área de aplicación para los amplificadores Raman distribuidos.

Acknowledgements

This thesis won't be here if it wasn't for a number of people.

First of all a huge thanks should go to my supervisor, Dr Juan Diego Ania Castañón. Thank you for giving me this incredible opportunity, introducing me to the wonderful world of optics and photonics, investing me with your passion for science and supporting me all this time. I really wish we could fruitfully collaborate together again in the future.

Many other persons from the Instituto de Óptica "Daza de Valdés" of CSIC have been fundamental for this research. First of all Dr Pedro Corredera, whose expertise and humor are fundamental to move around the lab. Then all past and present members of the Non-linear Dynamics and Fiber Optics group, who are the next level of kindness and helpful. A special thanks goes to Dr Giuseppe Rizzelli, who patiently helped me in the early days of this thesis.

My appreciation also has to go to my connections in the Photonic Engineering group of the Universidad de Alcalá, Dr Marco Jimenez-Rodriguez, Prof Fernando Naranjo and Prof Miguel González Herráez, who introduced me to the magical world of InN. A great part of this thesis won't be here without you.

I cannot forget to mention Prof Paul Harper and all the guys from AIPT, especially Dr Asif Iqbal and Dr Mingming Tan, who took good care of me during my stay at Aston University and taught me a lot. It has been a real pleasure to work with you.

My sincere gratitude goes to ICONE ITN network, that allowed me to start this thesis, and all the ICONE members. You have been a great group and I am honoured to have got to know you all and shared science and good moments. I am still waiting for our meeting in Mallorca.

A truly special thanks goes to past and present members of IOSA, who always remind me why we do science and that science is for everyone. It has been a real pleasure being part of the family, either discussing science, showing science or having a beer. Now it is the time to look up for some inter-chapter international activities.

I have to remember here also the first people that welcomed me in Madrid during my Master (it seems such a long time ago, but, yes, it was 2014!), the Surface Spectroscopies & Surface Plasmon Photonics Group of IEM-CSIC. Without you none of this would have happened. Thank you for introducing me for the first time to proper research and remembering me at the right moment. And thank you for introducing me to TeatrIEM. I never thought it would be so enjoyable to overcome my stage fright.

I have to thank as well the Area of Women in Optics and Photonics of SEDOPTICA.

Although temporally it is the last addition to this section, it is really heartfelt. I am proud to be part of the group and I am sure great things lie ahead. Go girls!

A lot of other people should be mentioned here, but a disclosed list would require another entire publication. Either we shared science, a coffee or a night out in weird places, all of you have been part of this work has well.

A final thanks has to go to my family, which in happiness and sadness has changed over these years, but always accepted and supported my "unusual" choices. I hope to see two little new scientists coming up soon enough. You know you are far away only in space but there is no distance in my thoughts.

More than four years ago I took a maybe not totally considered decision: I took a leap in the dark and I have literally discovered light. And I couldn't be happier for that. I can't picture myself doing anything else now, so I guess it was the right choice. Now a new path is opening and thanks to all of you I am sure it will be great.

Francesca Gallazzi

Sometimes I think I'd let myself be locked in a dungeon ten fathoms under the ground where no light penetrates, if I could thereby discover what it is, light.
And the worst is that what I know, I have to tell others.

Life of Galileo (1938), Bertolt Brecht

Contents

List of Tables

List of Figures

Nomenclature

List of Acronyms

ASE Amplified Spontaneous Emission

ASK Amplitude Shift Keying

BER Bit Error Rate

BW Backward

CW Continuous Wave

DBP Digital Back Propagation

DCF Dispersion Compensating Fibre

DFB Distributed FeedBack laser

DOP Degree Of Polarisation

DP-QPSK Dual Polarisation - Quadrature Phase Shift Keying

DSF Dispersion Shifted Fibre

EDFA Erbium Doped Fibre Amplifier

FBG Fibre Bragg Grating

FEC Forward Error Correction

FML Fundamental Mode Locking

FSK Frequency Shift Keying

FW Forward

FWHM Full Width Half Maximum

FWM Four Wave Mixing

GFF Gain Flattening Filter

GVD Group Velocity Dispersion

HML Harmonic Mode Locking

IM/DD Intensity Modulation / Direct Detection

IR InfraRed

ITU International Telecommunication Union

LEAF Large Effective Area Fibre

LED Light Emitting Diode

LO Local Oscillator

MI Modulation Instability

ML Mode Locking

MZ Mach Zehnder

NALM Nonlinear Amplification Loop Mirror

NF Noise Figure

NLSE NonLinear Schrödinger Equation

NPR Nonlinear Polarisation Rotation

NRZ NonReturn to Zero

OOK On Off Keying

OPC Optical Phase Conjugation

OSNR Optical Signal to Noise Ratio

PAMBE Plasma-Assisted Molecular-Beam Epitaxy

PCF Photonic Crystal Fibre

PM Polarisation Maintaining

PMD Polarisation Mode Dispersion

PRBS Pseudo Random Bit Sequence

PSK Phase Shift Keying

QAM Quadrature Amplitude Modulation

QPSK Quadrature Phase Shift Keying

rDFB random Distributed FeedBack laser

RF Radio Frequency

RIN Relative Intensity Noise

RZ Return to Zero

SA Saturable Absorber

SBS Stimulated Brillouin Scattering

SC SuperContinuum

SESAM SEmiconductor Saturable Absorber Mirror

SMF Single Mode Fibre

SNR Signal to Noise Ratio

SPM Self Phase Modulation

SPV Signal Power Variation

SRS Stimulated Raman Scattering

SSMF Standard Single Mode Fibre

URFL Ultralong Raman Fibre Laser

VOA Variable Optical Attenuator

VRM Variable Reflectivity Module

WDM Wavelength Division Multiplexing

XPM Cross Phase Modulation

Chapter 1

Introduction

This thesis is focused on the study, development and optimisation of ultralong fibre lasers and amplifiers in the continuous wave and ultrafast regimes. Fibre lasers have been widely studied but we will show how some areas are still unexplored or need improvement.

In this first chapter we will disclose the motivation, the objectives and, finally, the structure of this thesis.

1.1 Motivation

The first working laser source appeared almost sixty years ago. Fibre lasers became a viable option at the beginning of the 1990s, especially after the introduction of erbium doped amplification. Their applications are countless and in a variety of areas.

On the other side, low loss fibres gave great impulse to nonlinear optics. Propagation of light with high intensity in fibres rarely follows a completely linear regime. Depending on our aim, nonlinear effects in fibres may be detrimental or advantageous. One of this effects, Raman scattering is the base of a system proposed for the first time in 2004, the ultralong Raman fibre laser (URFL) [1]. It is a Raman distributed amplification scheme able to transform a standard optical fibre span into an ultralong laser cavity. Given the right pumping conditions and fibre length this span is virtually lossless or quasilossless with simultaneous spectral and spatial transparency -Fig.1.1- [2, 3]. This feature is extremely interesting for the implementation of nonlinear systems in optical fibres.

The first application of URFL, as it may be imagined, was in telecommunications. An amplifier made of standard single mode fibre (SSMF) with an extended bandwidth, in

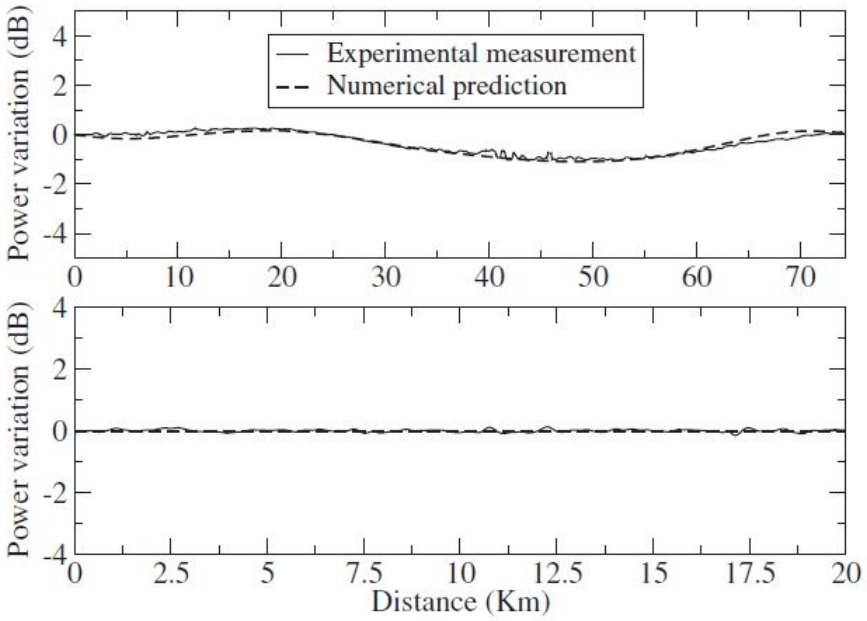

Figure 1.1: Experimental measurements and numerical simulation of the signal power variation for 75 km (upper graph) and 20 km (lower graph). [2]

which the signal power variation over long distances is very low and with a good optical signal to noise ratio (OSNR) is appealing, despite downsides as the necessity of high power pumps or relative intensity noise (RIN) transfer from pump to signal. Though these problems still needs to be considered (especially RIN transfer), the application of URFLs in transmission links has proven to be a good solution, able to help address the increasing bandwidth demand in long-haul telecommunication systems and approaching the nonlinear Shannon limit [4, 5, 6, 7, 8].

But this is not the only possible application of URFLs. The architecture has been successfully used in various fibre sensors [9, 10, 11, 12, 13], where it is useful in extending the range of operation in systems such as Brillouin optical time-domain analysis or phase-sensitive optical time domain reflectometry, again exploiting the virtual transparency given by the URFL over a standard fibre span.

Another application may be suggested but until now it has been impossible to implement: the application of URFLs in pulsed lasers. Mode-locked fibre lasers are extremely common due to their numerous practical advantages, such as simple implementation, low cost, wavelength tunability and feasibility to easily produce ultrafast pulses. This kind of systems does not usually support long cavities, as attenuation and dispersion in the laser cavity become unviable for stable ultrafast pulse propagation. A few attempts able to reach

mode-locking in longer cavities end up well above the femtosecond pulse range [14, 15, 16].

An URFL may be of interest in mode-locked lasers which frequently operate in the solitonic regime, as URFLs can support soliton propagation [17]. Lossless virtual transparency over several kilometers of fibre may be able to support undistorted propagation inside a laser cavity of ultrafast pulses, which would acquire increasing power and energy. But the cavity should be able to meet the soliton requirements and support the resultant high powers and energies maintaining operation stability and without damages to the system.

As we know, high peak power outputs are one of the usual main limitations of ultrafast mode-locked lasers, which frequently need an external amplification stage, precluding their application in energy demanding areas such as material processing. Despite the wide research on mode-locked laser, a simple low cost ultrafast high power fibre laser has not been developed yet, but would be of extreme interest, not only for its operation by itself but also for the possibility of direct and new applications that may become available with the increased power and energy reach. Moreover, such a system would be the perfect test-bed to try and implement an URFL in a mode-locked laser cavity.

This thesis will, thus, follow two lines, which will end up in a third one reconnecting them. We will first try to optimize URFL amplification for telecommunication transmission, considering the impairments caused by RIN transfer. Then we will focus on the development of a high peak power ultrafast passively mode-locked fibre laser and some first direct applications. Finally we will use the experience acquired in the implementation of the mode-locked resonator to apply URFL amplification in a pulsed laser system, with the objective of generate ultrashort high power laser pulses.

1.2 Objectives of the work

This thesis has been devoted to the study, development and optimization of ultralong fibre lasers either in the continuous wave (CW) or pulsed ultrafast regime. With “ultralong” we intend laser cavities longer than usual in their respective areas, meaning several tens of kilometers in the case of CW Raman fibre lasers and from few hundreds of meters to few tens of kilometers in the case of ultrafast mode-locked lasers.

The main objectives of this thesis are:

- The experimental characterization of RIN transfer in 2^{nd} order URFL cavities and

optimization of the transmission performances of such amplifiers, to find the best compromise between cavity architecture and pumping schemes, resulting in the best possible balance between RIN and amplified spontaneous emission (ASE) noise.

- Develop and optimise low cost passively mode-locked ultrafast ring fibre lasers using standard laboratory components and a novel InN-based semiconductor saturable absorber mirrror (SESAM) with the aim of achieving high peak powers retaining the output pulses in the femtosecond range, in order to try to overcome the traditional power limitations of this kind of lasers to open the possibility of using them in power/energy demanding applications, such as material processing.

- The exploration of the possible application of URFLs in a new area, pulsed fibre lasers, to create a virtually lossless span inside a mode-locked laser cavity for the generation of high power ultrafast pulses.

- To start developing some applications for the obtained ultrafast radiation sources:

  - Develop simple low cost supercontinuum laser sources with conventional single mode fibre, exploiting the high power femtosecond pulses generated by the previously developed laser.

  - Potentially apply the developed lasers as sources for spectroscopy, especially in the area of atmospheric gas detection.

1.3 Structure of the thesis

The present thesis has been divided in 7 chapters and an Appendix.

Chapter 1 has been dedicated to outline the motivation, the objectives and the structure of the work.

Chapter 2 presents a general introduction about optical fibres. After some historical notes about optical fibres, lasers and optical communications, the physical characteristics of optical fibres are described. It is then detailed light propagation and linear and nonlinear effects in fibres. Finally an introduction on solitons is presented.

Chapter 3 is dedicated to Raman amplification. Starting from the basics of stimulated Raman scattering in optical fibre, distributed Raman amplification is introduced, with

particular attention to the architecture of ultralong Raman fibre lasers and an introduction about Relative Intensity Noise (RIN) transfer. Afterwards, an introduction about optical transmission systems, amplification systems and modulation formats is delivered. Then we pass to display the experimental results about optimization of URFL systems for transmission: at first the RIN transfer characterization of the cavity and then the optimization of the performances in a 10x30 GBaud DP-QPSK transmission system.

Chapter 4 is dedicated to passively mode-locked ultrafast fibre lasers. After a general introduction, the mechanisms of active and passive mode-locking are introduced and how to practically achieve them. Focus is posed on saturable absorbers (SAs), in particular in the form of SESAMs, as the InN based which have been used in the course of this thesis. An overview on passively mode-locked fibre laser is then reviewed, before starting to describe the experimental set-ups which have been developed. The different configurations of ultrafast passively mode-locked ring fibre lasers with InN SESAM and their performance, aimed to achieve high peak powers and pulse energies, are presented and discussed.

In Chapter 5, a possible first application of the systems reported in Chapter 4 is discussed, supercontinuum generation and pulse compression in single mode fibres using high peak power femtosecond pulses. After introducing theoretically the topics of supercontinuum generation and pulse compression, the experimental set-up is presented, in its variable configurations with fibres with different dispersion and how they are used to tailor and tune the resulting supercontinuum. Finally, a direct application of these supercontinuum laser sources, gas sensing, is presented and preliminary experimental results are reported.

Chapter 6 reunites the URFL architecture from Chapter 3 with the ultrafast passively mode-locked ring fibre lasers from Chapter 4 in a scheme that enables the generation of ultrashort high power pulses in lasers. An experimental implementation of the system is presented and it is introduced how to potentially use the system in any mode-locked fibre laser.

Chapter 7 recollects the conclusions that we can draw from chapter 3 to 6. Finally the hypothesis regarding future lines of study are reported.

In the Appendix the list of publications which have been produced during the PhD are reported.

References

[1] J. D. Ania-Castañón, "Quasi-lossless transmission using second-order raman amplification and fiber bragg gratings," *Optics Express*, vol. 12(19), p. 43724377, 2004.

[2] J. D. Ania-Castañón, T. J. Ellingham, R. Ibbotson, X. Chen, L. Zhang, and S. K. Turitsyn, "Ultralong raman fiber lasers as virtually lossless optical media," *Phys. Rev. Lett.*, vol. 96, p. 023902, 2006.

[3] J. D. Ania-Castañón, V. Karalekas, P. Harper, and S. K. Turitsyn, "Simultaneous spatial and spectral transparency in ultralong fiber lasers," *Phys. Rev. Lett.*, vol. 101, no. 12, pp. 1–4, 2008.

[4] P. Rosa, J. D. Ania-Castañón, and P. Harper, "Unrepeatered DPSK transmission over 360 km SMF-28 fibre using URFL based amplification," *Optics Express*, vol. 22, no. 8, pp. 9687–9692, 2014.

[5] M. Tan, P. Rosa, I. Phillips, and P. Harper, "Extended Reach of 116 Gb/s DP-QPSK Transmission using Random DFB Fiber Laser Based Raman Amplification and Bidirectional Second-order Pumping," *Opt. Fiber Commun. Conf.*, p. W4E.1, 2015.

[6] M. Tan, P. Rosa, S. T. Le, M. A. Iqbal, I. D. Phillips, and P. Harper, "Transmission performance improvement using random DFB laser based Raman amplification and bidirectional second-order pumping," *Opt. Express*, vol. 24, no. 3, p. 2215, 2016.

[7] L. Galdino, M. Tan, D. Lavery, P. Rosa, R. Maher, I. D. Phillips, J. D. Ania-Castañón, P. Harper, R. I. Killey, B. C. Thomsen, S. Makovejs, and P. Bayvel, "Unrepeatered Nyquist PDM-16QAM transmission over 364 km using Raman amplification and multi-channel digital back-propagation," *Optics Letters*, vol. 40, no. 13, pp. 3025–3028, 2015.

[8] I. D. Phillips, M. Tan, M. F. C. Stephens, M. E. McCarthy, E. Giacoumidis, S. Sygletos, P. Rosa, S. Fabbri, S. T. Le, T. Kanesan, S. K. Turitsyn, N. J. Doran, P. Harper, and A. D. Ellis, "Exceeding the nonlinear-Shannon limit using Raman laser based amplification and optical phase conjugation," *Conf. Opt. Fiber Commun. Tech. Dig. Ser.*, pp. 5–7, 2014.

[9] S. Martín-Lopez, M. Alcón-Camas, F. Rodríguez, P. Corredera, J. D. Ania-Castañón, L. Thévenaz, and M. Gonzalez-Herraez, "Brillouin optical time-domain analysis assisted by second-order Raman amplification," *Opt. Express*, vol. 18, no. 18, pp. 18 769–18 778, 2010.

[10] M. González-Herráez, S. Martín-Lopez, M. Alcon-Camas, P. Corredera, L. Thévenaz, and J. D. Ania-Castañón, "Ultra-long range distributed fibre sensing using virtually transparent propagation," in *2011 Conference on Lasers and Electro-Optics Europe and 12th European Quantum Electronics Conference (CLEO EUROPE/EQEC)*, 2011, pp. 1–1.

[11] H. Martins, M. B. Marques, and O. Frazão, "300 km-ultralong Raman fiber lasers using a distributed mirror for sensing applications," *Opt. Express*, vol. 19, no. 19, pp. 18 149–18 154, 2011.

[12] J. D. Ania-Castañón, S. Martín-Lopez, M. Alcón-Camas, F. Rodríguez-Barrios, A. Carrasco-Sanz, P. Corredera, L. Thévenaz, and M. González-Herráez, "Raman-assisted BOTDA sensors," in *IEEE Winter Topicals 2011*, 2011, pp. 167–168.

[13] H. F. Martins, S. Martín-Lopez, P. Corredera, J. D. Ania-Castañón, O. Frazão, and M. González-Herráez, "Distributed Vibration Sensing Over 125 km With Enhanced SNR Using Φ-OTDR Over a URFL Cavity," *Journal of Lightwave Technology*, vol. 33, no. 12, pp. 2628–2632, 2015.

[14] A. Ivanenko, "Mode-Locking in 25-km Fibre Laser," no. 1, pp. 23–25, 2010.

[15] S. M. Kobtsev, S. V. Kukarin, S. V. Smirnov, and Y. S. Fedotov, "High-energy mode-locked all-fiber laser with ultralong resonator," *Laser Phys.*, vol. 20, no. 2, pp. 351–356, 2010.

[16] N. Li, J. Xue, C. Ouyang, K. Wu, J. H. Wong, S. Aditya, and P. P. Shum, "Cavity-length optimization for high energy pulse generation in a long cavity passively mode-locked all-fiber ring laser," *Appl. Opt.*, vol. 51, no. 17, pp. 3726–3730, 2012.

[17] M. Alcon-Camas, A. E. El-Taher, H. Wang, P. Harper, V. Karalekas, J. A. Harrison, and J. D. Ania-Castañón, "Long-Distance Soliton Transmission Through Ultralong Fiber Lasers," *Opt. Soc. Am.*, vol. 34, no. 20, pp. 3104–3106, 2009.

Chapter 2

Introduction to Optical Fibres

2.1 Historical notes

Light has been studied for more than two thousand years since Ancient Greece. Though the theories of the likes of Euclid, Hero and Ptolemy have been overtaken, they show the inner curiosity of mankind surrounding light, vision and optics.

Moving forward towards modern times, the history of fibre optics and lasers are strictly correlated. The advent of the laser revolutionised the way in which we can study and exploit light. Until the 1950s only incoherent light sources were available, while, with the laser, stimulated emission is used to create a monochromatic, coherent and highly directional radiation source. After the maser (Microwave Amplification by Stimulated Emission of Radiation) and several theoretical works [1], the first working pulsed ruby laser was demonstrated by Theodore Maiman in 1960 [2]. Early optical communication systems, such as the optical telegraph, had been soon replaced by electrical systems like the telephone, but the birth of this incredible coherent new light source brought back the idea of optical communications. However, a suitable transmission medium was still missing.

Primitive optical fibres were already available during the 1950s, used mainly for medical devices, but at first they were not considered a viable option for communications due to their extremely high losses. For the first time in 1966 Kao and Hockham theorized the possibility to reduce the losses in optical waveguides [3]. By 1970 losses in fibres were reduced below 20 dB/km [4] and by 1979 to only 0.2 dB/km around 1550 nm [5], which is not far from the losses in modern fibres, due to the physical limit set by Rayleigh scattering.

The path for optical communication was open. The race for continuously increasing

transmission capacity and distance started and in the 1980s deployed commercial system followed closely research and development. Optical amplification schemes became necessary and a big leap was given by the introduction of the Erbium doped fibre amplifiers (EDFAs) in 1987 [6, 7], which are able to efficiently amplify a signal around 1.55 μm, coincident with the region of minimum loss in silica fibres and are still fundamental in long-haul optical communications. Over the years new solutions became available. We will especially focus on Raman amplification in Chapter 3.

The advent of low loss fibres and lasers also brought a revolution in nonlinear optics. A range of nonlinear effects were observed and studied in optical fibres over the 1970s [8, 9, 10, 11, 12, 13, 14] and optical solitons were theorized and observed (see section 2.6). The development of techniques for obtaining ultrashort pulses and the emergence of rare earth doped fibre (mostly Erbium-doped) in the 1990s paved the way for a all new generation of fibre lasers and amplifiers. [15, 16, 17]

2.2 Optical fibre characteristics

The principle that lies behind optical fibres, total internal reflection, was already known in the XIX century, well before fibres and lasers. According to Snell's law, refraction is not possible over a certain incident angle, called critical angle, over which light is fully reflected and confined into the glass in the case of optical fibres. The critical angle in optical fibres can be calculated as

$$\theta_{crit} = arcsin(n_{cladding}/n_{core}). \tag{2.1}$$

An optical fibre is usually constituted by a core, the internal part of the fibre which guides light, made of silica glass surrounded by a cladding (the external part) with lower refraction index (step-index fibre, in contrast with graded-index fibre, where there is a gradual decreasing of the index of refraction towards the boundary, Fig. 2.1). This change in the refractive index is obtained by adding specific dopants to the fused SiO2 molecules of the glass to increase (e.g. GeO2) or decrease (e.g. B and F), in the case of the cladding, the index. Other ions, especially rare-earths, may be used to dope fibres for particular applications, as in fibre amplifiers. The difference between the refractive indexes of core and cladding is engineered to achieve total internal reflection and is usually less than 1% in standard telecommunication fibres, with a critical angle around 82°.

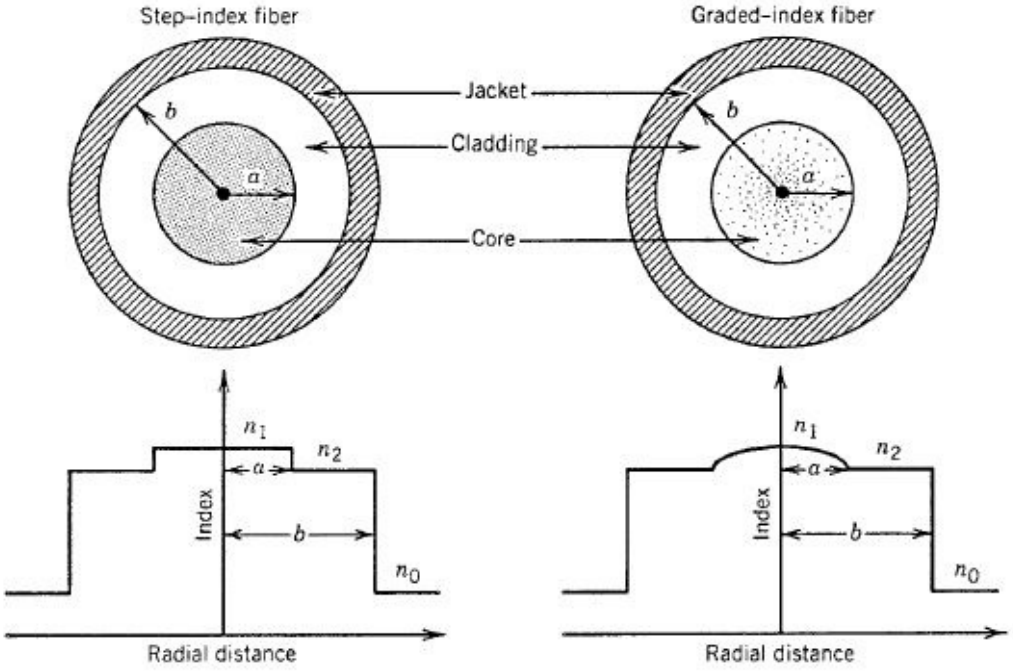

Figure 2.1: Cross section and refractive index profile of a step-index and a graded-index fibre. [15]

We may also consider the acceptance angle, which is the range over which light entering in the fibre will be guided in the core. It is usually expressed through the numerical aperture, NA

$$NA = sin(\alpha_{max}) = n_{core} cos\theta_{crit} = \sqrt{(n^2_{cladding} - n^2_{core})}, \tag{2.2}$$

where α_{max} is the acceptance angle. A large NA corresponds to a higher difference in refractive index.

Another important characteristic is the number of modes which can be supported by the fibre core. The transverse modes inside the fibre core represent a particular distribution or pattern of the electromagnetic field of the radiation observed in the transverse (perpendicular) plane in respect to its propagation direction. It is measured with the V parameter

$$V = \frac{2\pi}{\lambda} NA, \tag{2.3}$$

where λ is the transmitted light. If $V < 2.405$, the fibre can support only one mode at about 1550 nm and it is thus called single-mode fibre. The main difference between a single-mode (SMF) and a multimode fibre, which supports higher modes, is the core

diameter, which is much larger in the second case.

It is worth clarify that mode and channel are not synonyms. A single mode fibre can carry several different optical channels. A channel is a signal transmitted through an optical fibre. Several separated optical channels may be simultaneously transmitted in the same fibre at different wavelengths (wavelength division multiplexing, WDM). [17, 15, 18]

2.3 Light propagation in optical fibres

2.3.1 Maxwell's equations

The propagation of an electromagnetic field in optical fibres fibres follows Maxwell's equations:

$$\nabla \times \mathbf{E} = -\frac{\partial \mathbf{B}}{\partial t}, \tag{2.4}$$

$$\nabla \times \mathbf{H} = \mathbf{J}_f + \frac{\partial \mathbf{D}}{\partial t}, \tag{2.5}$$

$$\nabla \cdot \mathbf{D} = \rho_f, \tag{2.6}$$

$$\nabla \cdot \mathbf{B} = 0, \tag{2.7}$$

being $\mathbf{E}$ the electric field vector and $\mathbf{H}$ the magnetic one, while the corresponding electric and magnetic flux densities are $\mathbf{D}$ and $\mathbf{B}$. $\mathbf{J}_f$ is the current density vector and ρ_f is the charge density, which are the electromagnetic field sources. In optical fibres, given the lack of free charges, these last two values are equal to 0.

Flux densities $\mathbf{D}$ and $\mathbf{B}$ are correlated to field vectors E and H by the constitutive relations:

$$\mathbf{D} = \varepsilon_0 \mathbf{E} + \mathbf{P}, \tag{2.8}$$

$$\mathbf{E} = \mu_0 \mathbf{H} + \mathbf{M}, \tag{2.9}$$

with ε_0 the vacuum permittivity, μ_0 the vacuum permeability, $\mathbf{P}$ the induced electric polarisation and $\mathbf{M}$ the induced magnetic polarisation, which is 0 in the case of optical fibres.

The wave equation describing the propagation of light in an optical fibre can be derived from Maxwell's equations. It is possible to replace $\mathbf{B}$ and $\mathbf{D}$ with $\mathbf{E}$ and $\mathbf{P}$, taking the curl of equation (2.4) and using equations (2.5), (2.8) and (2.9) and the relation $\mu_0 \varepsilon_0 = 1/c^2$,

where c is the light velocity in vacuum. We obtain

$$\nabla \times \nabla \times \mathbf{E} = -\frac{1}{c^2}\frac{\partial^2 \mathbf{E}}{\partial t^2} - \mu_0 \frac{\partial^2 \mathbf{P}}{\partial t^2}. \tag{2.10}$$

The description is completed by introducing the relation between $\mathbf{P}$ and $\mathbf{E}$. If we consider only third order nonlinear effects from $\chi^{(3)}$, the induced polarisation $\mathbf{P}$ is constituted of two parts, a linear one, $\mathbf{P}_L$, and a nonlinear one, $\mathbf{P}_{NL}$, which relations with the electric field are

$$\mathbf{P}_L(\mathbf{r},t) = \varepsilon_0 \int_{-\infty}^{\infty} \chi^{(1)}(t-t') \cdot \mathbf{E}(\mathbf{r},t')dt', \tag{2.11}$$

$$\mathbf{P}_{NL}(\mathbf{r},t) = \varepsilon_0 \int\int_{-\infty}^{\infty} \int \chi^{(3)}(t-t_1, t-t_2, t-t_3) \vdots \mathbf{E}(\mathbf{r},t_1)\mathbf{E}(\mathbf{r},t_2)\mathbf{E}(\mathbf{r},t_3)dt_1 dt_2 dt_3. \tag{2.12}$$

The relations are valid for the electric-dipole approximation, so that there is a local medium response. At this point, several simplifications can be conducted. Equation (2.7) can be solved with $\mathbf{P}_{NL} = 0$, leaving $\mathbf{E}$ as linear. Thus in the frequency domain:

$$\nabla \times \nabla \times \tilde{\mathbf{E}}(\mathbf{r},\omega) + (\omega)\frac{\omega^2}{c^2}\tilde{\mathbf{E}}(\mathbf{r},\omega) = 0, \tag{2.13}$$

where $\tilde{\mathbf{E}}(\mathbf{r},\omega)$ is the Fourier transform of $\mathbf{E}(\mathbf{r},\mathrm{t})$. Equation (2.10) can be further simplified to

$$\nabla \times \nabla \times \mathbf{E} = \nabla(\nabla \cdot \mathbf{E}) - \nabla^2 \mathbf{E} = \nabla^2 \mathbf{E}, \tag{2.14}$$

For all the mathematical passages of the simplification refer to [17].

2.3.2 Nonlinear Schrödinger Equation (NLSE)

Nonlinear and dispersive effects control shape and spectrum of the pulses propagating in a fibre. From equations (2.10), (2.11), (2.12) and (2.14) it can be derived the equation for pulse propagation in nonlinear dispersive fibres:

$$\nabla^2 \mathbf{E} - \frac{1}{c^2}\frac{\partial^2 \mathbf{E}}{\partial t^2} = -\mu_0 \frac{\partial^2 \mathbf{P}_L}{\partial t^2} - \mu_0 \frac{\partial^2 \mathbf{P}_{NL}}{\partial t^2}, \tag{2.15}$$

which describes the relation between the electric field $\mathbf{E}(\mathbf{r},\mathrm{t})$ and $\mathbf{P}_L$, the linear part, and $\mathbf{P}_{NL}$, the nonlinear part of the induced polarisation.

Several assumptions are needed to solve this last equation, as can be more extensively

followed in [17]: $\mathbf{P}_{NL}$ is considered as a weak perturbation of $\mathbf{P}_L$, a scalar approach is conducted by assuming that the optical field maintains its polarisation along the fibre and finally the optical field is considered quasi-monochromatic (assumption which is valid for pulses $\geq$0.1 ps). It is also helpful in the simplification assuming an instantaneous nonlinear response, which finally neglects the contribution of molecular vibrations to $\chi^{(3)}$. It is also useful to separate the slowly varying and rapidly varying part of the electric field in the envelop approximation. To derive the slowly varying amplitude is better to work in the Fourier domain.

Taking into consideration all these assumption it is possible to derive to the so called nonlinear Schrödinger Equation

$$\frac{\partial \mathbf{A}}{\partial z} + \beta_1 \frac{\partial \mathbf{A}}{\partial t} + \frac{i}{2}\beta_2 \frac{\partial^2 \mathbf{A}}{\partial t^2} + \frac{\alpha}{2}\mathbf{A} = i\gamma |\mathbf{A}|^2 A. \tag{2.16}$$

The nonlinearity coefficient γ is

$$\gamma = \frac{n_2 \omega_0}{c\mathbf{A}_{eff}} \tag{2.17}$$

and the pulse amplitude $\mathbf{A}$ is normalized so that $|A|^2$ is the optical power. $\mathbf{A}_{eff}$, the effective core area, which depends on core radius and the difference between core and cladding indexes, can be considered

$$\mathbf{A}_{eff} = \pi w^2, \tag{2.18}$$

if the fundamental mode of the fibre can be approximated to a Gaussian. The width w depends on the fibre parameters (it can vary from 1 to 100 μm^2 at 1.5 μm).

Equation (2.16) is used to describe optical pulse propagation in a single mode fibre and takes into consideration fibre losses (α), fibre nonlinearities (γ) and chromatic dispersion (β_1 and β_2). The group velocity dispersion (GVD) is due to β_2 and is typically negative at 1.55 μm ($\beta_2 \approx$ - 20 ps^2/km).

2.4 Linear effects

Depending on to the propagation regime, linear and nonlinear effects can have more or less repercussions. Let's start with a brief overview of the main linear impairments: fibre

attenuation, chromatic dispersion and polarisation mode dispersion.

2.4.1 Fibre losses

The power loss between input and output in a fibre in the transmission of optical signals is a fundamental parameter. Fibre losses are mainly due to imperfect light coupling at the ends of the fibre, absorption and scattering (along the entire length of the fibre). Without amplification, attenuation is a fundamental limitation for the distance that the optical pulses are able to cover in the fibre, as their power gradually diminish with distance. This is especially important in telecommunication systems because the signal needs to to have a minimum optical power to be correctly detected at the receiver.

For input power $\mathbf{P}_0$, the transmitted power $\mathbf{P}_T$ at a specific point or at the end of the fibre is

$$\mathbf{P}_T = \mathbf{P}_0 exp(-\alpha \mathbf{L}), \tag{2.19}$$

where $\mathbf{L}$ is the fibre length and α is the attenuation coefficient or fibre loss, which is usually expressed in dB/km using the following relation between α and α_{dB}

$$\alpha_{dB} = -\frac{10}{L} log \frac{\mathbf{P}_T}{\mathbf{P}_0} = 4.343\alpha. \tag{2.20}$$

In Fig. 2.2, fibre loss dependence on light wavelength is shown, with a minimum around 1.55 μm of about 0.15-0.20 dB/km. Attenuation in silica fibres is very low in comparison to other waveguides. Among the factor contributing to loss in the fibre, the most important are material absorption and Rayleigh scattering.

Material absorption can vary greatly and depends on the material itself and the wavelength of the light. Silica glass has low absorption in the region between 0.5 and 2 μm, though even minimum impurities can cause significant absorption in that same window. Consider, for example, how notable are the OH^- ion vibrational absorption peaks, especially the overtone in the region of 1.4 μm. This can be reduced using particular precautions in the fabrication process, which remove the impurities and give high transparency at telecommunication wavelengths.

Rayleigh scattering is inevitable in every material, as atoms and molecules always scatter some of the incident light. So it is not related directly to the type of material, but

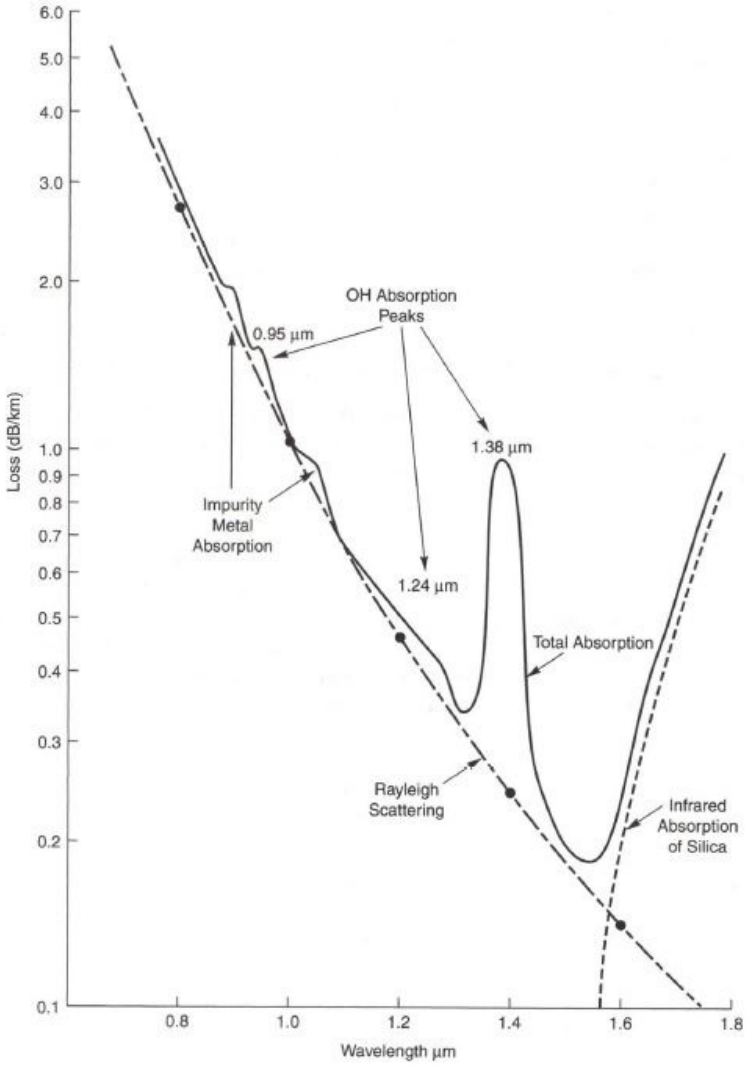

Figure 2.2: Loss spectrum of a single-mode fibre as function of the wavelength [18]

more on the relative dimensions of the particle and the light wavelength. In the fused silica of optical fibres local density fluctuations of the refractive index produce scattering in every direction. Rayleigh scattering loss, like absorption, is cumulative, prevalent at short wavelengths and correlated to λ^{-4}, setting an ultimate intrinsic loss limit. In dB/km, the intrinsic loss level can be estimated as

$$\alpha_R = \frac{\mathbf{C}}{\lambda^4}, \tag{2.21}$$

where $\mathbf{C}$ is a constant dependent on the constituents of the fibre core. As can be seen in

Fig. 2.2, losses at 1.55 μm are mainly due to Rayleigh scattering.

Other factors that can affect the losses are fibre bending or leaking, scattering at the interface between core and cladding and splicing in the case of systems.

2.4.2 Chromatic dispersion

The phase and group velocities of light as it propagates in a transparent medium depend on the optical frequency ω. This phenomenon is called chromatic dispersion and it is mainly due to the interaction of light with the bound electrons of a dielectric optical medium as an optical fibre. The effect results in a frequency dependence of the refractive index $n(\omega)$.

Dispersion is critical for short pulse propagation in fibre, as the different spectral components of the pulse will travel at different speeds following $c/n(\omega)$. In a mostly linear regime, the spectral broadening induced by dispersion can be extremely relevant (and in many cases detrimental, for example in telecom systems), while in a nonlinear regime the interaction of dispersion and nonlinearities can produce different outcomes.

Expanding β, the mode propagation constant, in a Taylor series about the central pulse frequency ω_0, the effects of dispersion can be accounted for:

$$\beta_0 = n(\omega)\frac{\omega}{c} = \beta_0 + \beta_1(\omega - \omega_0) + \frac{1}{2}\beta_2(\omega - \omega_0)^2 + \frac{1}{6}\beta_3(\omega - \omega_0)^3 + ..., \tag{2.22}$$

where

$$\beta_m = \left[\frac{d^m\beta}{d\omega^m}\right]_{\omega=\omega_0} (m = 0, 1, 2, ...). \tag{2.23}$$

β_1 and β_2 are correlated to the refractive index n and its derivatives, so that

$$\beta_1 = \frac{1}{\nu_g} = \frac{n_g}{c} = \frac{1}{c}\left[n + \omega\frac{dn}{d\omega}\right] \tag{2.24}$$

and

$$\beta_2 = \frac{1}{c}\left[2\frac{dn}{d\omega} + \omega\frac{d^2n}{d\omega^2}\right], \tag{2.25}$$

with n_g being the group index, which is dependent on the wavelength in fused silica, and ν_g being the group velocity.

Parameter β_2 covers the dispersion of group velocity responsible of pulse broadening, a phenomenon called group velocity dispersion (GVD), which has β_2 as parameter. In

practice also **D**, the dispersion parameter, is used, which relates to β_2 as:

$$\mathbf{D} = \frac{d\beta_1}{d\beta} = -\frac{2\pi c}{\lambda^2}\beta_2 = -\frac{\lambda}{c}\frac{d^2 n}{d\lambda^2}. \tag{2.26}$$

As visible in Fig. 2.3, for fused silica GVD and dispersion are not constant, but vary with the wavelength. The point where **D** and β_2 cross zero and change sign is called zero-dispersion wavelength (λ_D). For ultrashort pulse propagation close to λ_D, it is necessary to take into consideration β_3, the third order dispersion, and other higher order dispersive effects, since ultrashort pulses can be distorted in both the linear and the nonlinear regime.

For standard single mode fibres the zero-dispersion wavelength is usually close to 1.31 μm, but optimizing fibre design λ_D can be shifted in the proximity of 1.55 μm, the area of minimum loss in fibres. This type of fibres are called dispersion-shifted (DSF). Also, β_2 may have a large positive value if λ_D is shifted over 1.6 μm, as in dispersion-compensating fibres (DCF). We will see later some applications for these particular kinds of fibres.

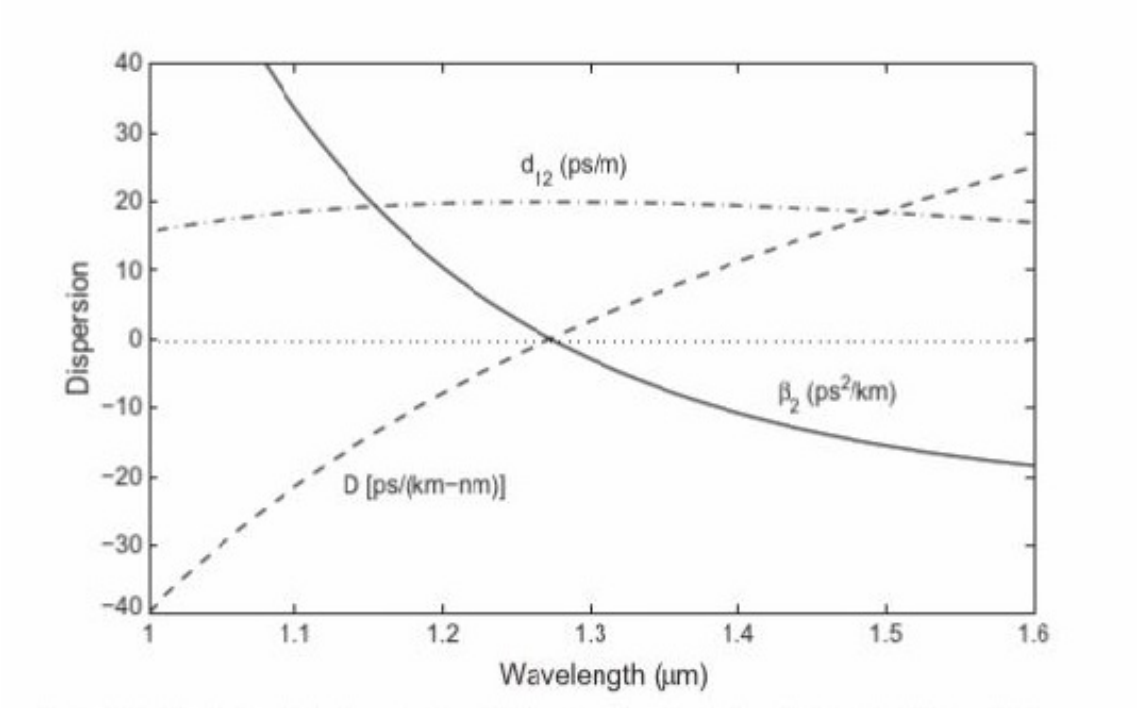

Figure 2.3: Dispersion as function of the wavelength [17]

For $\lambda < \lambda_D$, or $\beta_2 > 0$, a fibre presents normal dispersion, where the low-frequency components of a pulse travel faster than the high-frequency components. The opposite case, $\lambda > \lambda_D$ and $\beta_2 < 0$, is called anomalous dispersion regime. Nonlinear effects can have a different impact depending on the dispersion regime. Especially the anomalous

dispersion one is interesting as the balance of nonlinearities and dispersion allows for soliton propagation in optical fibres.

2.4.3 Polarisation mode dispersion

Even single-mode fibres transmit light in two orthogonally polarised degenerate modes. In an ideal system, a perfectly cylindrical, symmetrical and stress-free fibre, the x and y polarisation modes would not couple. But in an actual fibre there are some variations departing from perfect symmetry and external forces can cause minor differences in the refractive index (birefringence), so that the mode degeneracy will cease. The anisotropy causes mode-propagation constant β to change for the two orthogonally polarised mode (modal birefringence). A dimensionless parameter describes modal birefringence

$$B_m = \frac{|\beta_x - \beta_y|}{k_0} = |n_x - n_y|, \tag{2.27}$$

n_x and n_y being the two modal refractive indexes. For a fixed B_m, the two modes propagate in the fibre with a period called beat length, L_B

$$L_B = \frac{2\pi}{|\beta_x - \beta_y|} = \frac{\lambda}{B}. \tag{2.28}$$

The two axis for which the mode index is either smaller or larger are called fast and slow respectively, because the group velocity for that direction of the light is larger (fast axis) or smaller (slow axis).

Standard optical fibres do not have a constant modal birefringence B_m due to core shape fluctuations and anistotropic stress. This means that polarised light injected in a fibre changes its polarisation state randomly and the two polarisation components travel at different velocities along the fibre. This results in a broader output pulse, a stochastic phenomenon which is called polarisation mode dispersion (PMD) and may be relevant in long-haul optical links. The time delay between the two polarisation components, ΔT, is useful to estimate the pulse broadening along a length of fibre, L with constant B_m

$$\Delta T = \Big|\frac{L}{\nu_{gx}} - \frac{L}{\nu_{gy}}\Big| = L|\beta_{1x} - \beta_{1y}| = L\delta\beta_1, \tag{2.29}$$

where $\delta\beta_1$ is related to group velocity mismatch. This last equation is effective in describing

PMD for standard telecom fibres with random birefringence changes, because they tend to equalize the propagation times of the different polarisation component. This is why PMD is calculated as the root-mean-square of ΔT, obtained averaging over random perturbations:

$$\sigma_T^2 = \langle(\Delta T)^2\rangle = 2(\Delta\beta_1 l_c)^2[exp(-L/l_c) + L/l_c - 1], \tag{2.30}$$

where $\Delta\beta_1 \equiv \Delta\tau/L$ ($\Delta\tau$ is the differential group delay along the principal polarisation states), and l_c is the correlation length (the length, usually in the order of 10 m, over which two polarisation components are correlated). In case of L >100 m, using $l_c << L$, we obtain

$$\sigma_T \approx \Delta\beta_1\sqrt{2l_cL} \equiv D_p\sqrt{L}, \tag{2.31}$$

with D_p as the PMD parameter, that for standard telecommunication fibres is typycally between 0.1-1 ps/$\sqrt{km}$. We can observe that the variance is dependent on $\sqrt{L}$, from which derives that pulse broadening induced from PMD is smaller than the GVD-induced. Still it can be limiting in high-speed optical communications.

A particular type of fibres have been developed for applications where lights need to be transmitted without changing polarisation, the polarisation maintaining (PM) fibres. In these fibres, the design is modified to introduce a large amount of birefringence. As a consequence, only the favored state of polarisation is transmitted, and the impact of the small birefringence fluctuations is greatly reduced.

2.5 Nonlinear effects

A number of nonlinear phenomena are relevant in fibre optics systems. Silica is not a highly nonlinear material, but light interaction, especially of high intensity, over long lengths of fibre acquires great relevance. We will briefly discuss here the more relevant effects for the understanding of the results presented in this thesis.

2.5.1 Kerr effect

The Kerr effect should be described first among the nonlinear phenomena because lies amid the causes behind some of them (especially self phase modulation). It is an optical nonlinear effect taking place in fibres (but also other media) when light with a high optical power

travels along them. Its origin resides in the instantaneous third order nonlinearity and the nonlinear polarisation generated in the material, that modifies the light propagation. The Kerr effect can, thus, be described as an instantaneous modification of the refractive index due to a nonlinear response [10]. The index of refraction n of the high intensity beam is altered as

$$\Delta n = n_2 I, \tag{2.32}$$

where n_2 is the nonlinear Kerr index and I is the optical intensity. In silica n_2 is about 2.5x10^{-20} m^2/W, a low value if compared with other crystalline materials or glasses.

2.5.2 Self Phase Modulation

Self-phase modulation (SPM) is a phenomenon responsible for spectral broadening of the optical pulses and is caused by intensity-dependent refractive index in a nonlinear optical medium, which induces phase modulation in an optical pulse. In a long fibre a temporally dependent phase delay between the different part of a pulse may increase and result in a noticeable phase modulation, to which frequency broadening is associated. Together with GVD it would expand the pulse spreading, fact that may be severely limiting in an optical transmission system. Also, as the time dependent phase shift caused by the Kerr effect is related to the time dependent pulse intensity, a pulse, initially unchirped, may develop a chirp (temporally varying instantaneous frequency) [14].

Numerical solutions of the NLSE are necessary to obtain a general description of SPM. Normalizing the amplitude $U(z,T)$ and considering $\beta_2 = 0$, the propagation equation results in

$$\frac{\partial \mathbf{U}}{\partial z} = -\frac{ie^{-\alpha z}}{L_{NL}}|\mathbf{U}|^2\mathbf{U}, \tag{2.33}$$

where the nonlinear length is $L_{NL} = (\gamma P_0)^{-1}$, the peak power is P_0 and γ is related to the nonlinear Kerr coefficient. The general solution of equation (2.33) can be obtained as

$$\mathbf{U}(L,T) = \mathbf{U}(0,T)exp[i\phi_{NL}(L,T)], \tag{2.34}$$

$\mathbf{U}(0,T)$ being the amplitude of the field at $z = 0$, so that the nonlinear phase shift is

$$\phi_{NL}(L,T) = |\mathbf{U}(0,T)|^2(L_{eff}/L_{NL}), \tag{2.35}$$

considering the effective length

$$L_{eff} = [1 - exp(-\alpha L)]/\alpha. \tag{2.36}$$

From these last equations is clear that, though SPM induces an intensity-dependent phase shift, the temporal pulse shape does not change and that for increasing fibre length L there is an increase in nonlinear phase shift ϕ_{NL}. SPM causes modifications in the optical spectrum as a consequence of the time dependent ϕ_{NL}. If the phase varies temporally, the instantaneous optical frequency over a pulse is different from that at its center, with

$$\delta\omega(T) = -\frac{\partial\phi_{NL}}{\partial T} = -\Big(\frac{L_{eff}}{L_{NL}}\Big)\frac{\partial}{\partial T}|\mathbf{U}(0,T)|^2, \tag{2.37}$$

where $\delta\omega$ is the frequency chirping. SPM-induced chirp magnifies with propagation distance, always broadening the optical spectrum of an initially unchirped pulse, while it can either induce a spectral broadening or narrowing, if the input pulse already has an opposite chirp. The changes of the chirp across an optical pulse are vastly dependent on the pulse shape. High power pulses and long fibres may have a very high nonlinear phase shift and the optical spectrum of a pulse can be widely broadened by SPM. For example, SPM, together with other nonlinear effects (four wave mixing, stimulated Raman scattering...), is one of the processes behind supercontinuum generation, where the spectrum of intense ultrashort pulses can be extended over 100 THz (we will describe more extensively supercontinuum generation in Chapter 5).

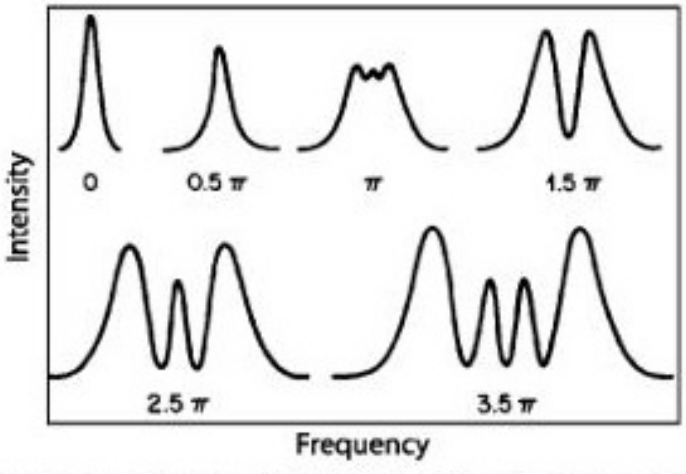

Figure 2.4: SPM-induced broadening of an initially unchirped Gaussian pulse. [17]

An oscillatory structure visible over all the frequency range, which leaves many visible peaks throughout the spectrum, can be associated with SPM spectral broadening. These peaks derive from the time dependency of SPM-induced frequency chirp. A pulse has the same instantaneous frequency in two different points (it has the same chirp for two different T). Like two waves with same frequency but dissimilar phases, according to their relative phases, they can display constructive of destructive interference.

2.5.3 Cross Phase Modulation

As SPM, cross-phase modulation (XPM) is due to the intensity dependence of the refractive index. When two or more pulses or optical channels of different wavelength co-propagate simultaneously in a fibre, each pulse/channel interacts with the other through cross-phase modulation (inducing chirping, for example), as in a nonlinear medium the effective refractive index for an optical beam is not only dependent on its intensity but also on that of any other co-propagating optical field. In conjunction with other nonlinear processes as four wave mixing, stimulated Raman scattering and stimulated Brillouin scattering, it may lead to the generation of new waves. XPM and SPM are strictly related when we have the simultaneous presence of more than one optical field in a fibre.

If we consider a multiplexed system, the nonlinear phase shift of a particular channel is conditioned by the power of the other channels:

$$\phi_j^{NL} = \gamma L_{eff}\Big(P_j + 2\sum_{m\neq j} P_m\Big), \tag{2.38}$$

with the sum extending over all the channels. The factor 2 (which comes from the nonlinear susceptibility) states that the effect of XPM is double of that of SPM for the same power.

The effect of XPM over multiplexed signals is not trivial to estimate. Different channels do not propagate at the same speed and XPM induces phase shift only in pulses overlapping in time, so it is usually an issue mainly in neighbouring channels. This means that the walk-off between the two signals is fundamental for the resulting spectral broadening and shape induced from XPM [19].

2.5.4 Four Wave Mixing

Four-wave mixing (FWM) emerges from the third-order nonlinear susceptibility $\chi^{(3)}$. Over long lengths of fibre the interactions between optical fields travelling simultaneously may become relevant. In FWM three carrier frequencies, ω_1, ω_2 and ω_3, co-propagating in an optical fibre interact to generate a fourth frequency ω_4, following the relation $\omega_4 = \omega_1 \pm \omega_2 \pm \omega_3$. Tough theoretically all the combinations are possible, many of them do not fulfil the phase-matching requirements deriving from momentum conservation, while others are problematic for multiplexed systems, impacting their performances. The phase mismatch of four waves propagating in the same direction is

$$\Delta = \beta_{\omega 3} + \beta_{\omega 4} - \beta_{\omega 1} - \beta_{\omega 2}, \tag{2.39}$$

with β_ω being the propagation constant of the optical field of frequency ω.

Though FWM is a weak effect, it becomes relevant if the signals are phase matched over long fibre distances, as when $\beta_2 = 0$ or is very close to it. The pulses propagating near zero-dispersion at different wavelengths over different channels keep the same relative position along the fibre. FWM is increased and noise signal is built up, fact that may induce interchannel crosstalk. That is why in multiplexed systems the zero-dispersion wavelength is located outside the transmission band. Dispersion, even if low, greatly reduces FWM.

2.5.5 Modulation instability

Modulation instability (MI) is a nonlinear process where nonlinearities and dispersion interactions produce the growth of phase modulations and amplitude in a wave. This phenomenon appears in many different nonlinear systems and it was initially studied not only in nonlinear optics but in diverse fields, as plasma physics or fluid dynamics. In optical fibres, MI appears in the anomalous dispersion regime as a breakup of CW radiation in ultrashort pulses.

MI can be considered analogous to stimulated FWM, though the phase matching requirements are different in this case. Phase matching in MI is usually self-generated by anomalous dispersion and index nonlinear change, conditions which may occurr in single-mode fibres [20, 21].

2.5.6 Stimulated Light Scattering

While Rayleigh scattering is elastic, so the scattered light doesn't change in frequency, in an inelastic scattering, such as Raman and Brillouin scattering, the light frequency is shifted, resulting in a photon of (more commonly) lower energy, while the energy difference takes the form of a phonon (optical in the case of Raman scattering and acoustic for Brillouin scattering). Inelastic scattering, in both mentioned forms, is quite weak at low powers because of the reduced scattering cross section. But for incident power levels over a certain threshold stimulated inelastic scattering grows exponentially and becomes critical.

Stimulated Raman Scattering (SRS) and Stimulated Brillouin Scattering (SBS) have been observed in optical fibres since the 1970s. We will extensively discuss SRS in Chapter 3, where we will explain how this nonlinear effect can be harnessed to turn an optical fibre span into a distributed amplifier.

Stimulated Brillouin scattering (SBS), has some similarities with SRS but also differences which arise from the fact that acoustic phonons are at the base of SBS. A Stokes wave downshifted in frequency in respect to that of the incident light is generated, but, unlike in SRS (which can propagate in either direction), it propagates only backwards in an optical fibre. The Stokes shift for SBS is only ∼10 GHz, while it is abount 13 THz for SRS. SBS manifests at much lower powers than SRS and the spectral width of the pump wave influences the threshold power. It can be very low for CW pumps or wide pulses (1 mW), but with pump pulses shorter than 1 ns SBS is not triggered.

SBS produces an acoustic wave at a frequency Ω for an oscillating field at the pump frequency Ω_p. SBS can be understood as the scattering of the pump wave from this acoustic wave, which generates a wave at the frequency of the pump Ω_s. The process has to conserve the energy, so the Stokes shift is $\Omega = \omega_p - \omega_p$, and the momentum, which means that the wave vectors respect $k_A = k_p - k_s$. If the dispersion relation is $|k_A| = \Omega/\nu_A$, the acoustic frequency is

$$\Omega = |k_A|\nu_A = 2\nu_A|k_p|sin(\theta/2), \tag{2.40}$$

where ν_A is the acoustic velocity, $|k_p| \approx |k_s|$ and θ is the angle between pump and scattered waves. We can extrapolate that for $\theta = 0$ (forward direction) Ω is null, while for $\theta = \pi$ (backward direction) Ω is maximum. Since in single-mode fibres light only propagates in those two directions, SBS only occurs in the backwards direction with $\Omega = 2\nu_A|k_p|$.

2.6 Introduction to solitons

Though the first account of solitary waves in water dates back to the observations of Scott Russell in 1834 [22], the term soliton was first used in 1965 [23] and describes a particular type of wave, resulting from the interplay of dispersive or diffractive and nonlinear effects, that is able to propagate over long distances without changing temporal and spectral shape, even after collisions. Solitons are present in various areas of physics. Their presence in optical fibres was discovered in 1973 [24] and potential applications in optical communications were immediately suggested.

It is useful to normalize the NLSE equation to have a better comprehension of soliton waves. The dimensionless variables

$$U = \frac{A}{\sqrt{P_0}}, \quad \xi = \frac{z}{L_D} \quad \text{and} \quad \tau = \frac{T}{T_0}, \tag{2.41}$$

can be introduced, with P_0 as the peak power, L_D as the dispersion length and T_0 as the width of the incident pulse. So the NLSE can be written as

$$i\frac{\partial U}{\partial \xi} = sgn(\beta_2)\frac{1}{2}\frac{\partial^2 U}{\partial \tau^2} - N^2|U|^2U \tag{2.42}$$

with the soliton order N

$$N^2 = \frac{L_D}{L_N L} = \frac{\gamma P_0 T_0^2}{|\beta_2|}. \tag{2.43}$$

The parameter N can be written out the equation (2.42) using

$$u = NU = \sqrt{\gamma L_D}A. \tag{2.44}$$

So equation (2.42) takes the usual form of the NLSE

$$i\frac{\partial u}{\partial \xi} + \frac{1}{2}\frac{\partial^2 u}{\partial \tau^2} + |u|^2u = 0, \tag{2.45}$$

where $sgn(\beta_2) = -1$ reflects the case of anomalous dispersion.

In a fundamental or first-order soliton ($N = 1$) its shape does not undergo changes during propagation, as there is a specific balance between dispersion, pulse duration and peak power. T_0 and P_0 of an hyperbolic secant pulse can be chosen to have $N = 1$ in

equation 2.43. If such a pulse were to be injected in an ideal (lossless) fibre the pulse would in fact propagate without distortions over long lengths of fibre, characteristic that may be extremely interesting in telecommunication systems. If we fix $N = 1$, the peak power necessary for the propagation of the fundamental soliton would be

$$P_0 = \frac{|\beta_2|}{\gamma T_0^2} \cong \frac{3.11|\beta_2|}{\gamma T_{FWHM}^2}, \tag{2.46}$$

with $T_{FWHM} \cong 1.76 T_0$.

It is not the same case for higher order solitons ($N > 1$), where the necessary peak power can be calculated with equation 2.43. They can take various forms, experience breathing or periodical evolution while propagating, with period

$$z_0 = \frac{\pi}{2} L_D = \frac{\pi}{2} \frac{T_0^2}{|\beta_2|} \approx \frac{T_{FWHM}^2}{2|\beta_2|}. \tag{2.47}$$

The NLS equation can give various other solitary waves solution and several types of solitons have been observed in fibres, especially when the nonlinear and dispersive properties of the system are modified. For example, several communication or ultrafast laser system exploit some kind of dispersion management to improve their performances. This is usually obtained by introducing fibres with different GVD parameters. Though locally the dispersion may be high, due to β_2 of opposite sign, the average dispersion of the system results very reduced.

In this situation, pulse-like periodic solutions may be found for the NLSE, which are called dispersion managed solitons, that present some characteristics different from those of the usual solitons. In fact in these pulses, width and amplitude may oscillate periodically, the frequency may vary across the pulse, which means that they are chirped and their shape is usually Gaussian instead of $sech^2$ [17, 25].

Another interesting solution is related to the dissipative solitons, which are an extension of the conventional soliton idea that can exist in dissipative systems. In a real system with loss, the balance between nonlinear and dispersive effects is not possible for long distances, and other factors need to be taken into consideration, especially a correct balance between gain and losses, which allow to produce stationary localized solutions. As we will see in later chapters, the features of the dissipative solitons are of great interest in mode-locked

laser systems [26].

References

[1] A. L. Schawlow and C. H. Townes, "Infrared and optical masers," *Physical Review*, vol. 112, no. 6, pp. 1940–1949, 1958.

[2] T. H. Maiman, "Stimulated optical radiation in Ruby," *Nature*, vol. 187, no. 4736, pp. 493–494, 1960.

[3] K. C. Kao and G. A. Hockham, "Dielectric-fibre surface waveguides for optical frequencies," *Proceedings of the Institution of Electrical Engineers*, vol. 113, no. 7, pp. 1151–1158, 1966.

[4] F. P. Kapron, D. B. Keck, and R. D. Maurer, "Radiation losses in glass optical waveguides," *Applied Physics Letters*, vol. 17, no. 10, pp. 423–425, 1970.

[5] T. Miya, Y. Terunuma, T. Hosaka, and T. Miyashita, "Ultimate low-loss single-mode fibre at 1.55 μm," *Electronics Letters*, vol. 15, no. 4, pp. 106–108, 1979.

[6] R. J. Mears, L. Reekie, I. M. Jauncey, and D. N. Payne, "Low-noise erbium-doped fibre amplifier operating at 1.54 μm," *Electronics Letters*, vol. 23, no. 19, pp. 1026–1028, 1987.

[7] E. Desurvire, J. R. Simpson, and P. C. Becker, "High-gain erbium-doped traveling-wave fiber amplifier," *Opt. Lett.*, vol. 12, no. 11, pp. 888–890, 1987.

[8] R. H. Stolen, E. P. Ippen, and A. R. Tynes, "Raman oscillation in glass optical waveguide," *Applied Physics Letters*, vol. 20, no. 2, pp. 62–64, 1972.

[9] E. P. Ippen and R. H. Stolen, "Stimulated scattering in optical fibers," *IEEE Journal of Quantum Electronics*, vol. 8, no. 6, p. 549, 1972.

[10] R. Stolen and A. Ashkin, "Optical Kerr effect in glass waveguide," *Applied Physics Letters*, vol. 22, no. 6, pp. 294–296, 1973.

[11] R. G. Smith, "Optical Power Handling Capacity of Low Loss Optical Fibers as Determined by Stimulated Raman and Brillouin Scattering," *Appl. Opt.*, vol. 11, no. 11, pp. 2489–2494, 1972.

[12] K. O. Hill, D. C. Johnson, B. S. Kawasaki, and R. I. MacDonald, "CW threewave mixing in singlemode optical fibers," *Journal of Applied Physics*, vol. 49, no. 10, pp. 5098–5106, 1978.

[13] R. Stolen, "Phase-matched-stimulated four-photon mixing in silica-fiber waveguides," *IEEE Journal of Quantum Electronics*, vol. 11, no. 3, pp. 100–103, 1975.

[14] R. H. Stolen and C. Lin, "Self-phase-modulation in silica optical fibers," *Physical Review A*, vol. 17, no. 4, pp. 1448–1453, 1978.

[15] G. P. Agrawal, *Fiber-optic communication systems*. Wiley, 2010.

[16] M. D. Al-Amri, M. El-Gomati, and M. S. Zubairy, *Optics in our time*. Springer, 2016.

[17] G. P. Agrawal, *Nonlinear fiber optics*. Academic Press, 2012.

[18] J. Hecht, *Understanding fiber optics*. Laser Light Press, 2015.

[19] M. N. Islam, L. F. Mollenauer, R. H. Stolen, J. R. Simpson, and H. T. Shang, "Cross-phase modulation in optical fibers," *Opt. Lett.*, vol. 12, no. 8, pp. 625–627, 1987.

[20] K. Tai, A. Hasegawa, and A. Tomita, "Observation of modulational instability in optical fibers," *Physical Review Letters*, vol. 56, no. 2, pp. 135–138, 1986.

[21] V. E. Zakharov and L. A. Ostrovsky, "Modulation instability: The beginning," *Physica D: Nonlinear Phenomena*, vol. 238, no. 5, pp. 540–548, 2009.

[22] S. Russell, "Report on waves," *Report of 14th Meeting of the British Association for Advancement of Science*, pp. 311–390, 1844.

[23] N. J. Zabusky and M. D. Kruskal, "Interaction of "solitons" in a collisionless plasma and the recurrence of initial states," *Physical Review Letters*, vol. 15, no. 6, pp. 240–243, 1965.

[24] A. Hasegawa and F. Tappert, "Transmission of stationary nonlinear optical pulses in dispersive dielectric fibers. I. Anomalous dispersion," *Applied Physics Letters*, vol. 23, no. 3, pp. 142–144, 1973.

[25] S. K. Turitsyn, B. G. Bale, and M. P. Fedoruk, "Dispersion-managed solitons in fibre systems and lasers," *Physics Reports*, vol. 521, no. 4, pp. 135 – 203, 2012.

[26] P. Grelu and N. Akhmediev, "Dissipative solitons for mode-locked lasers," *Nature Photonics*, vol. 6, no. 2, pp. 84–92, 2012.

Chapter 3

RIN characterization and performance optimization of URFL transmission systems

Raman amplification for optical transmission systems was proposed quite early. Raman amplification in optical fibres was already studied in the 1970s and proposed for transmission in the 1980s, but the difficulties in its implementation and, then, the widespread appearance of EDFA amplification in the early '90s prevented its adoption for a while. Nonetheless the appearance of the proper pumping sources has brought Raman amplification to the fore in recent years. As opposed to traditional EDFA amplification, Raman amplification is an interesting solution for distributed amplification, with a number of well-known potential benefits arising from its improved balance between noise and nonlinear impairments [1, 2].

After a general introduction on Raman amplification and telecommunication transmission systems, in this chapter we will focus on a particular type of amplifier, the Ultralong Raman Fibre Laser (URFL) [3] and the work which has been carried out about RIN transfer characterization and optimization of URFLs cavities to improve transmission performances.

3.1 Stimulated Raman Scattering

Stimulated Raman scattering is the enabling effect of Raman amplification. Although this nonlinear effect can be detrimental for transmission along fibre optics, it is also able to turn the fibre itself into a broadband amplifier.

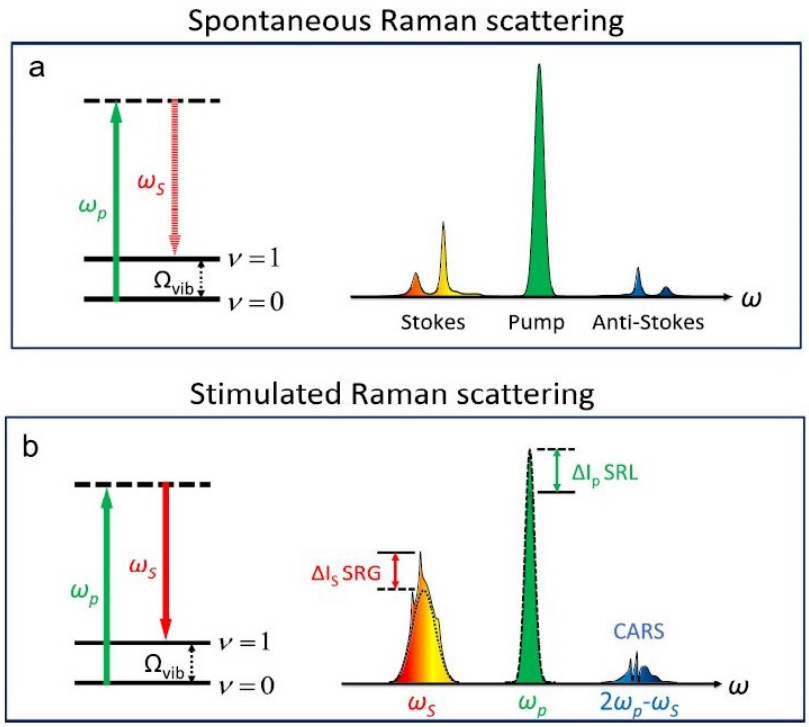

Figure 3.1: Spontaneous (a) and stimulated (b) Raman scattering [4].

The Raman effect was predicted theoretically by the physicist Adolf Smekal in 1923 [5] and then discovered experimentally by Raman and Krishnan in 1928 [6, 7]. Shortly later the Smekal-Raman effect was reported in crystals by Landsberg and Mandelstam [8]. Today the observation and exploitation of Raman scattering is much more easily implementable thanks to the use of lasers as energy source, a clear example being Raman spectroscopy.

The Raman effect is the inelastic scattering of photons. Spontaneous Raman scattering is a weak nonlinear phenomenon. When light interacts with a material, a small part is not scattered elastically, but at frequencies different from those of the incident light. If the shift is towards lower frequencies (alas the scattered photon has lower energy than the incident one), we speak about Stokes components, while we refer to anti-Stokes Raman scattering in the case of photons shifted to higher frequencies (with more energy than the incident ones) -Fig. 3.1. This second effect is orders of magnitude less intense than Stokes scattering. The analysis of this shift, which is characteristic for the vibrational energy levels in the molecules of each material, is at the basis of Raman spectroscopy. In fact, a molecule is excited by the incident photon to a higher energy level, called virtual level, but decays just afterwards to a lower energy level while emitting another photon. Molecular

vibrations of the material account for the energy difference between the incident and the emitted photon.The Stokes and anti-Stokes shift and the Raman gain shape depend on these vibrational levels. In standard fibres the Raman gain is described by a broad curve, given by the amorphous structure of the material, and the peak of the Stokes shift is around 13.2 THz [9, 10].

Here we are interested in stimulated Raman scattering (SRS), a stronger effect which usually occurs when the excitation source is an intense laser beam, as it is the gain mechanism underlying Raman amplification. In this case 10% or more of the incident photons energy is converted in Stokes frequency and emitted in forward and backward directions. SRS happens when Stokes components are already present in the medium, the fibre in our case. If the frequency difference between the incident beam (the pump) and the Stokes wave already present is equal to the Stokes shift, new photons are generated at the Stokes frequency, which results amplified.

It is important to take into consideration a few points which display the possible advantages of Raman amplification over EDFA amplification. SRS does not need special fibres as the EDFA and, in fact, it can occur in any fibre. Moreover, since the pump photon is excited to a virtual level, it is possible to choose the signal wavelength at which the Raman gain is going to happen by appropriately selecting the wavelength of the pump, while the resonant levels of the erbium limit the wavelengths of EDFA operation. Finally, Raman gain is a very fast process in comparison with the energy transfer in erbium [9, 10, 11].

3.2 Raman Amplification

As we said, SRS is the nonlinear phenomenon that can turn a standard optical fibre into a broadband Raman amplifier.

As all telecommunication systems, a system exploiting Raman amplification carries a signal from a transmitter (Tx) to a receiver (Rx). Fig. 3.2 depicts a general example of a Raman amplifier, where, besides the transmitter and receiver, one or more pumps are located at one or both extremes of the standard single mode fibre span. If this span is the actual transmission fibre in which the signal travels, usually tens of kilometers long, the system is called a distributed Raman amplifier, because the gain is distributed along the

entire fibre. On the contrary, in conventional point or lumped amplifiers (as the EDFAs), gain is punctual, the signal power decreases gradually in the transmission span and is recovered at the end of each section. If the pump propagates in the same direction as the signal, it is called a forward or co-propagating pump, whereas if the pump travels in the opposite direction it is called a backward or counter-propagating pump. On the other hand, if the amplifier contains a gain fibre of only a few kilometers length, used exclusively for lumped amplification, it is called a discrete Raman amplifier. In this work we will focus mainly on distributed Raman amplifiers (we will later introduce a particular type called Ultralong Raman Fibre Laser).

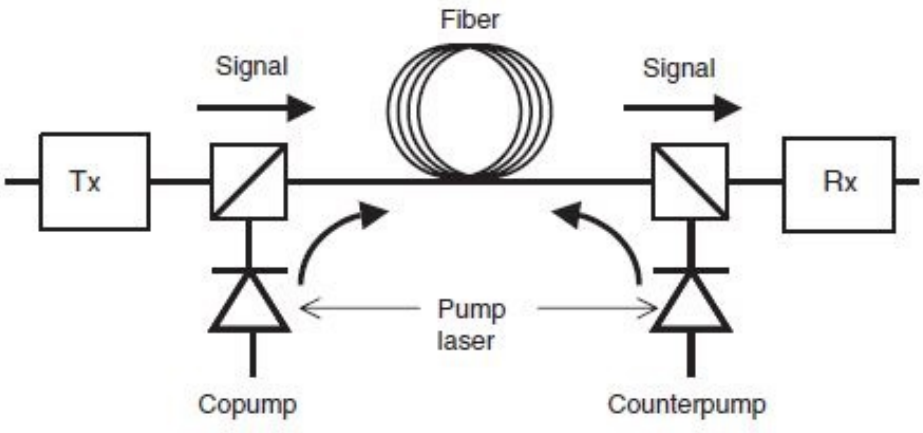

Figure 3.2: Scheme of a transmission system with Raman amplification [10].

So, in a Raman amplifier the pump and the signal, usually both CW, are injected in the same fibre. The following equations, generically describe the average power evolution in a Raman amplifier of the signal P_s, and the forward (+) or backward (-) pump, P_p, along the fibre z:

$$\frac{dP_s}{dz} = -\alpha_s P_s \frac{g}{A_{eff}} P_p^{\pm} P_s \tag{3.1}$$

and

$$\frac{dP_p^{\pm}}{dz} = \mp\alpha_p P_p^{\pm} \mp \frac{\nu_p}{\nu_s}\frac{g}{A_{eff}} P_s P_p^{\pm}, \tag{3.2}$$

where α_s and α_p are the fibre attenuation at signal and pump frequencies ν_s and ν_p, g is the Raman gain coefficient and A_{eff} is the fibre effective area. If we don't

consider pump depletion in Eq. (3.2), which is the second term on the right-end side, it is possible to solve Eq. (3.2) as $P_p(z) = P_p(0)exp^{-\alpha_p z}$ for a co-propagating pump and as $P_p(z) = P_p(L)exp^{-\alpha_p(L-z)}$ for a counter-propagating pump. It is subsequently possible to solve Eq. (3.1) analytically, describing the evolution of the signal in the fibre, as

$$P_s(L) = P_s(0)exp\Big(\frac{g}{A_{eff}}P_0 L_{eff} - \alpha_s L\Big), \tag{3.3}$$

where the effective length, L_{eff}, is defined as

$$L_{eff} = \frac{[1 - exp(-\alpha_p L)]}{\alpha_p}. \tag{3.4}$$

Moreover, from the integration of Eq. (3.1) the signal gain is

$$G(z) = \frac{P_s(z)}{P_s(0)} = exp\Big(\frac{g}{A_{eff}}\int_0^z P_p(z)dz - \alpha_s z\Big). \tag{3.5}$$

The signal power varies along the length of a distributed amplifier and different pumping schemes may be applied to exert control over this evolution. However finding an "optimal" configuration is not easy, because it depends on several parameters, as we will see later. Usually the total pump power is selected so that the Raman gain is capable of fully compensating the fibre losses ($G_L = 1$, the net signal gain). It is practical to introduce the concept of on-off Raman gain

$$G_A = \frac{P_s(L)\text{with pump on}}{P_s(L)\text{with pump off}} = exp\Big(\frac{g}{A_{eff}}P_0 L_{eff}\Big), \tag{3.6}$$

that describes the total amplifier gain distributed over the length L_{eff}.

Raman amplification presents some advantages in transmission systems, such as an improved noise figure (NF) of the amplifier, which is the ratio of the input to the output signal-to-noise-ratio (SNR), and the possibility to achieve a flat gain profile. However, also some disadvantages appear in Raman amplification: spontaneous Raman scattering, PMD (these two effects are an issue also in Er-doped amplification), double Rayleigh backscattering in the fibre, noise figure tilt and especially noise transfer from the pump to the signal, where fluctuations in the pump may cause fluctuations in the Raman gain and thus the signal power (we will return to this topic in section 3.3).

3.2.1 Raman gain spectrum

The Raman gain coefficient is related to the cross section of spontaneous Raman scattering and shows the Stokes power transfer as a function of the frequency shift from the pump to the signal.

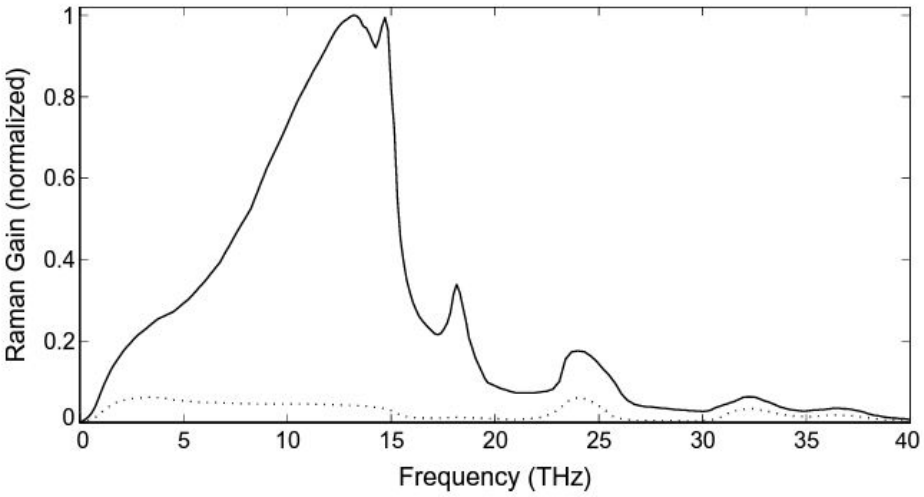

Figure 3.3: Normalized Raman gain spectrum for co-pololarised (solid line) and orthogonally polarised (dashed line) pump and Stokes [12].

The Raman gain spectrum (Fig.3.3) is well known for silica fibres, expanding over a wide range of frequencies, with a broad peak at 13.2 THz. This is due to the amorphous structure of the material, where the molecular vibrational frequencies create a continuum, in contrast with materials with a crystalline structure that present Raman gain at specific frequencies. This is the underlying feature of broadband amplification. Raman gain is also strongly dependent on the polarisation. It differs for co-polarised (it is maximum) or orthogonally polarised (it almost disappears) pump and signal. To avoid polarisation dependent gain, the pumps used for Raman amplified systems are preferably unpolarised.

3.2.2 Ultralong Raman Fibre lasers

A distributed Raman amplified system can adopt several different configurations. The architecture and length of the cavity and the distribution, number and wavelength of the pumps (pumping scheme) are customized trying to achieve the best signal power evolution along the transmission fibre and improve system performance.

A backward-pumping configuration exploits the fact that the fluctuations in the pump

power are averaged out as signal and pump travel in opposite directions. In forward-pumping the fluctuations are, instead, directly transferred to the signal gain, due to the fast response time (<100 fs) of Raman scattering. The application of bi-directional pumping (combining forward and backward pumping) is used to reduce the signal power variation over the transmission span -Fig. 3.4.

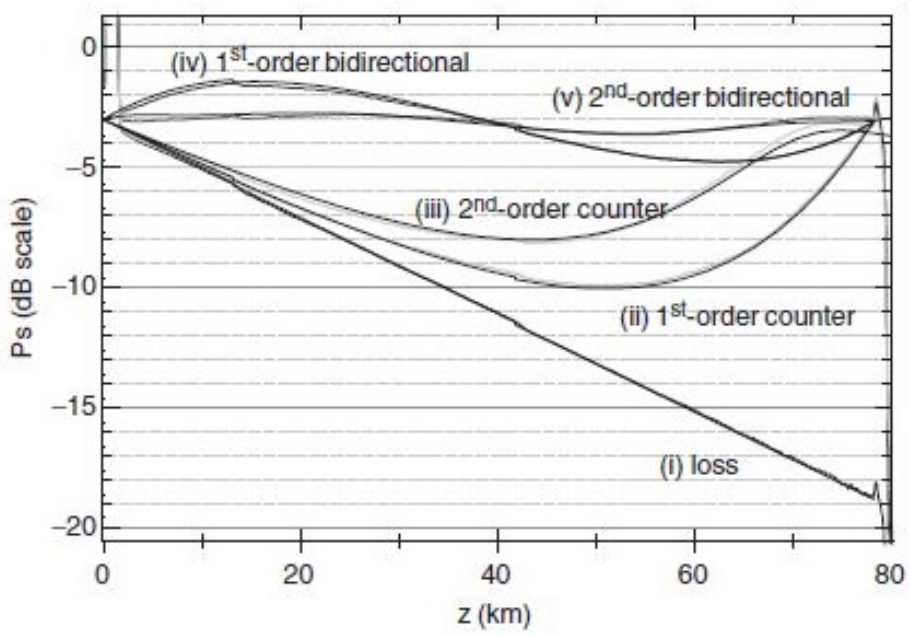

Figure 3.4: Signal evolution in a transmission fibre for different pumping schemes [10].

It is also interesting to control the wavelength of the pumps. The Raman gain is able to directly amplify a signal that is upshifted around 13.2 THz (the first Stokes shift) from the pump wavelength. In a Raman amplifier using a 1^{st}-order pumping scheme we have uni- or bi-directional pumps located around 13.2 THz (around 100nm) apart from the signal (if we consider the standard telecommunication C-band between 1530 nm and 1565 nm for transmission, the pumps will have a wavelength around 145x nm). But we may employ also a higher order (or cascaded pumping), which indirectly amplifies the signal, where one or more sets of pumps are located two (2^{nd}-order pumps) or more Stokes shift away from the signal wavelength. We talk about dual-order Raman amplification, when the 2^{nd}-order pumps (for example at 1365 nm) amplify the 1^{st}-order pumps (at 1455 nm), that in turn amplify the signal (at 1550 nm).

The architecture -Fig. 3.5- that we are going to take especially in consideration is a type of 2^{nd}-order bi-directional pumping scheme called ultralong Raman fibre laser [3]. In

this amplifier the 1^{st}-order pumps are replaced by two high reflectivity fibre Bragg gratings (FBG) that delimit the cavity. The gratings' central wavelength is selected around 1455 nm to be located in proximity of the Stokes peak of the pumps at 1365 nm at the ends of the cell. When the total pump power compensates the first Stokes attenuation, a new pump at 1455 nm is generated in the fibre constituting the cavity from the ASE noise. This generated bidirectional pumping at 1455 nm is now able to amplify a signal at the traditional transmission wavelength around 1550 nm.

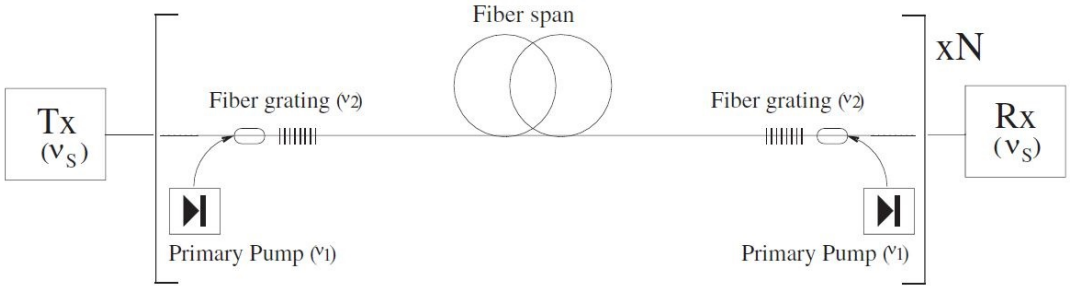

Figure 3.5: URFL architecture [13]

A variation of this scheme is the so called random distributed feedback Raman laser (rDFB) [14], in which one or both FBG reflectors are removed and the cavity relies on random distributed Rayleigh backscattering to provide feedback. This type of cavity may prove advantageous over the URFL in some situations, as we will explain later in section 3.5, at the cost of a lower efficiency.

The URFL scheme presents advantages in terms of the average power evolution along the length of the cavity, as to achieve quasi-lossless transmission over the fibre. This evolution can be represented by the following equations, which include pump depletion, ASE and double Rayleigh backscattering:

$$\frac{dP_{p1}^{\pm}}{dz} = \mp\alpha_1 P_{p1}^{\pm} \mp g_1 \frac{\nu_1}{\nu_2} P_{p1}^{\pm}(P_{p2}^{+} + P_{p2}^{-} + 4h\nu_2\Delta\nu_2(1 + \frac{1}{e^{h(\nu_1-\nu_2)/K_BT} - 1})) \pm \varepsilon_1 P_{p1}^{\mp}, \quad (3.7)$$

$$\begin{aligned}\frac{dP_{p2}^{\pm}}{dz} = {} & \mp\alpha_2 P_{p2}^{\pm} \pm g_1(P_{p2}^{\pm} + 2h\nu_2\Delta\nu_2(1 + \frac{1}{e^{h(\nu_1-\nu_2)/K_BT} - 1}))(P_{p1}^{+}P_{p1}^{-}) \\ & \mp g_2 \frac{\nu_2}{\nu_s} P_{p2}^{\pm}(P_s + N_s^{+} + N_s^{-} + 4h\nu_s\Delta\nu_s(1 + \frac{1}{e^{h(\nu_2-\nu_s)/K_BT} - 1})) \pm \varepsilon_2 P_{p2}^{\mp}, \quad (3.8)\end{aligned}$$

$$\frac{dP_s}{dz} = -\alpha_s P_s + g_2 P_s(P_{p2}^{+} + P_{p2}^{-}), \quad (3.9)$$

$$\frac{dN_s^+}{dz} = -\alpha_s N_s^+ + g_2(N_s^+ + 2h\nu_s\Delta\nu_s(1 + \frac{1}{e^{h(\nu_2-\nu_s)/K_BT} - 1}))(P_{p2}^+ P_{p2}^-)\varepsilon_s N_s^-, \quad (3.10)$$

$$\frac{dN_s^-}{dz} = \alpha_s N_s^- - g_2(N_s^- + 2h\nu_s\Delta\nu_s(1 + \frac{1}{e^{h(\nu_2-\nu_s)/K_BT} - 1}))(P_{p2}^+ P_{p2}^-)\varepsilon_s(P_s N_s^+). \quad (3.11)$$

Eq. (3.7) describes the 2^{nd}-order forward (+) and backward (-) pump powers, P_{p1}, and Eq. (3.8) the 1^{st}-order pump powers, P_{p2}, generated with the FBGs at 1455 nm. P_s is the signal power and N_s are the forward (+) and backward (-) signal noise powers. α is the attenuation at the corresponding pump or signal wavelength, g are the Raman gain coefficients normalized for the effective area, ν are the frequencies, $\Delta\nu$ are the effective bandwidths and ε are double Rayleigh backscattering of the fibre at each frequency. Moreover, h is the Planck's constant, K_B is the Boltzmann's constant and T is the absolute temperature of the fibre. The equations (3.7)-(3.11) are solved with the following boundary conditions

$$P_{p1}^+(0) = P_{p1}^-(L) = P_0; \quad P_{p2}^+(0) = R_1 P_{p2}^-(0); \quad P_{p2}^-(L) = R_2 P_{p2}^+(L); \quad (3.12)$$

$$N_s^+(0) = N_0; \quad N_s^-(L) = 0; \quad P_s(0) = P_{IN}; \quad (3.13)$$

where R_1 and R_2 are the FBGs reflectivities at the extremes of the cell and L is the length of the transmission span [3].

3.3 RIN transfer

The relative intensity noise (RIN) is a standard way to measure the amplitude noise of a laser, as it is a frequency dependent value that quantifies the power fluctuations of a laser. A variable degree of intensity fluctuations is present in all lasers. The spectrum of power or intensity fluctuations represented by RIN is defined as

$$\frac{\sigma_p^2}{\langle P_0\rangle^2} = \int_0^\infty \mathbf{RIN}_p(f)df, \quad (3.14)$$

where σ_p^2 is the variance of the pump-power fluctuations and $\langle P_0\rangle$ is the average pump power. If we include pump noise, fluctuations are present also in the amplified signal and

so the RIN of the amplified signal is

$$\frac{\sigma_s^2}{\langle P_s(L)\rangle^2} = \int_0^\infty \mathbf{RIN}_s(f)df. \tag{3.15}$$

The enhancement of the signal noise at a specific frequency f is represented by the pump-noise transfer function:

$$H(f) = \mathbf{RIN}_s(f)/\mathbf{RIN}_p(f). \tag{3.16}$$

Since pump and signal don't have the same wavelength, they do not propagate along the fibre with the same speed, which is dependent on the fibre dispersion. The pump-noise transfer is, thus, affected by the length of the amplifier, the pumping scheme and the dispersion of the fibre.

The pump configuration and the noise frequency affect the noise transfer from pump to signal, as fluctuations in the pump cause fluctuations in the Raman gain and thus in the signal power. Noise at low frequencies is amplified and transferred to the signal, while transfer at higher frequencies is reduced thanks to the averaging effect of pump and signal walkoff.

Since in a Raman amplifier the gain is exponentially dependent on the pump power, fluctuations in the latter will be reflected in the signal power. The amplifier length, the pumping scheme and the dispersion of the fibre are all factors on which the noise transfer depends.

Counter-propagating pumping is also preferred to reduce RIN transfer, since it averages out the impact of pump fluctuations on signal gain, as explained in section 3.2. [10]

3.4 Basics of optical transmission systems

An optical communication system in its simplest implementation -Fig. 3.6- may be described as an optical transmitter, an optical receiver and a communication channel between them, that in our case is an optical fibre.

The objective of the communication channel is transporting the signal from transmitter to receiver without distortions. We have described optical fibres and their characteristic in Chapter 2. The properties that make them very suitable for a lightwave system are the low

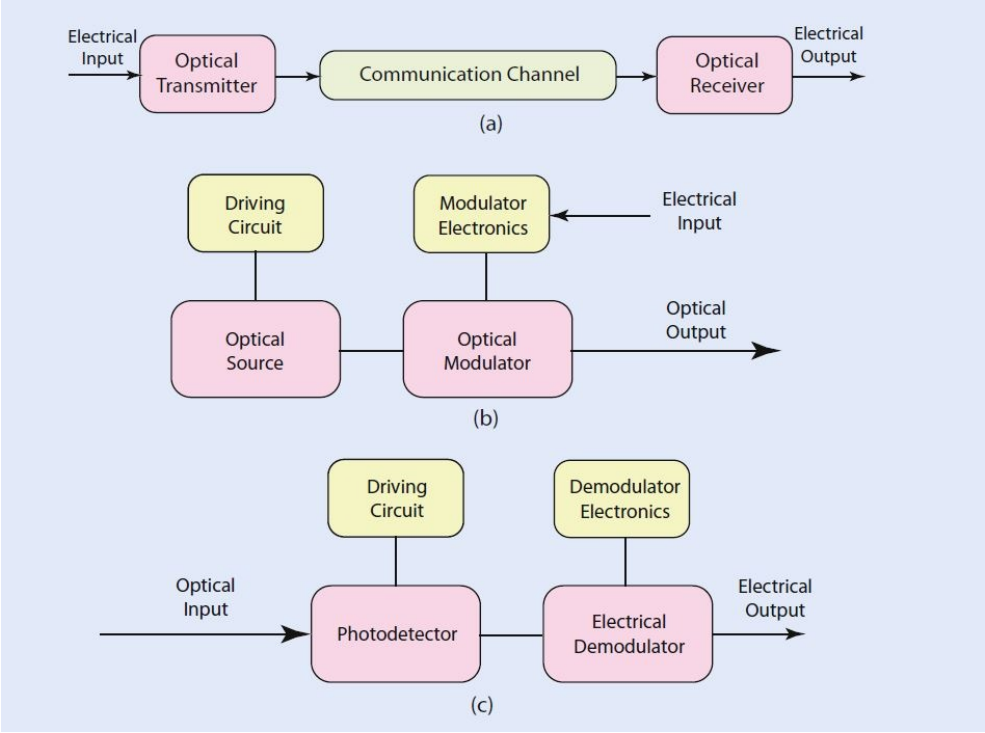

Figure 3.6: General scheme of an optical telecommunication system (a), a transmitter (b) and a receiver (c) [15].

losses and dispersion low enough to be acceptable in most applications. Anyway both these features becomes an issue especially in long-haul and high speed systems, which eventually need amplifiers or repeaters to compensate the losses and to control the spectral width of the optical source and compensate for dispersion. Despite that, dispersion-induced pulse broadening finally poses a limit on the bit rate, as the pulses tend to broaden outside their bit slot degrading the signal.

Optical fibre communications operate in a reduced region in the near infrared. This range is usually subdivided in "telecom windows":

- The first window (800-900 nm) was the originally employed, but it is suitable only for short distance transmission, because at these wavelengths fibre losses are quite high and there are not efficient amplifiers.
- The second window (1260-1460 nm) has lower losses in fibre and very low dispersion, which is why was used in the first long-haul transmission systems. However amplifiers in this window are not as convenient as the ones used in the third window.
- The third window (1460-1675) is the most used in modern systems. It is the region where losses in silica are the lowest and in which Erbium-doped amplifiers (see section

3.4.1) operate. This window is usually divide in bands as follows:

- S band (short wavelengths), between 1460 and 1530 nm;
- C band (conventional), between 1530 and 1565 nm;
- L band (long wavelengths), between 1565 and 1625 nm;
- U band (ultralong wavelengths), between 1625 and 1675 nm;

The most commonly used band is the C band, because it corresponds with the region of operation of the EDFAs.

The optical transmitter translates an electrical signal into an optical one which is launched into the optical fibre. Its basic blocks are the optical source, the modulator and the channel coupler. Usually the source is a semiconductor laser or a light emitting diode, which are easily coupled with an optical fibre. The optical signal is generated modulating the carrier wave of the source. Modulation can be either direct or external and is used to generate the bit stream. We will describe modulation formats in section 3.4.2. Direct modulation consist in modulate the signal by increasing the drive current, and so the output power, of the light source. While diode lasers have a very quick response to increased current, LEDs are slower. So direct modulation can be good for a cheap transmitter, but it is not suitable for high speeds due to excessive chromatic dispersion and limited maximum frequency modulation.

As said, external modulators are necessary for higher speeds, as fibre optics systems demand modulation at gigabit rates. There are two types of modulators: electro-optic modulators and electro-absorption modulators. Electro-optic modulation depends on a change in the refractive index in response to a voltage applied across the material of the waveguide (usually $LiNbO_3$). The phase of the light passing through is modulated. To add intensity modulation to the device, a Mach-Zehnder (MZ) interferometer, where the two arms are $LiNbO_3$ waveguides, is included. An electro-absorption modulator is a waveguide device made of a material similar to the semiconductor laser which favours their integration on the same substrate. It makes use of the Franz-Keldysh effect, which means that the semiconductor bandgap is reduced when an electric field is applied through it. So the modulator starts to absorb light when an external voltage reduces electronically the bandgap of its material.

The optical receiver at the end of the communication channel converts the optical signal back to an electric signal. It is composed of a channel coupler, a photodetector and a demodulator. The channel coupler delivers the signal to the photodetector, which is a device based on optical absorption and, for compatibility with the system, is usually a semiconductor photodiode (commonly a $p-n$, $p-i-n$ or avalanche photodiode). It is in this stage that light is converted to electricity through the photoelectric effect. Then the signal passes to the demodulator which varies according to the modulation format used in the system. For some modulation formats direct or incoherent detection is feasible while others require coherent detection, either homodine or heterodine.

A common low-cost scheme deployed is called intensity modulation with direct detection (IM/DD), in which the intensity of the incoming radiation is converted into an electric signal and demodulated with a decision circuit that distinguishes the transmitted bits as 0 and 1. Demodulation depends on the amplitude of the signal and no phase or frequency information are used. The signal-to-noise ratio of the electrical signal at the photodetector stage determines the accuracy of the decision circuit, diminishing the probability of error (sampling time is a decisive parameter).

Coherent detection merges coherently the incident optical signal with an optical field before it reaches the detector. Contrary to direct detection, in this case it is possible to recover information from the phase of the signal, as its variations are converted into amplitude variations. A narrow linewidth laser, the local oscillator (LO), generates a coherent field at the receiver which is combined with the incoming optical field through a beam splitter. If the incoming optical signal is

$$E_s = A_s exp[-1(\omega_0 t + \phi_s)], \tag{3.17}$$

where A_s is the amplitude, ω_0 is the carrier frequency and ϕ_s is the phase, the local oscillator field is

$$E_{LO} = A_{LO} exp[-1(\omega_{LO} t + \phi_{LO})], \tag{3.18}$$

and we assume that E_s and E_{LO} have the same polarisation. The optical power incident on the photodetector results

$$P = |E_s + E_{LO}|^2, \tag{3.19}$$

or, using the previous equations

$$P(t) = P_s + P_{LO} + 2\sqrt{P_s P_{LO}} cos(\omega_{IF} t + \phi_s - \phi_{LO}), \tag{3.20}$$

with

$$P_s = A_s^2, \quad P_{LO} = A_{LO}^2 \quad \text{and} \quad \omega_{IF} = \omega_0 - \omega_{LO}, \tag{3.21}$$

where $\nu_{IF} = \omega_{IF}/2\pi$ is the intermediate frequency, which is not always necessary. Depending on whether ω_{IF} equals zero or not, we can distinguish two different coherent techniques, homodyne and heterodyne. In homodyne detection $\omega_{IF} = 0$, as ω_{LO} is selected to coincide with ω_0, while in heterodyne detection ω_{LO} differs from the signal carrier frequency ($\omega_{IF} \neq 0$). In both coherent detection techniques the information can be coded in the amplitude, phase and frequency modulation of the optical carrier, which is an advantage over direct detection. Also they have an improved SNR, derived from the fact that the local oscillator amplifies by a large factor the received signal (homodyne detection has a larger value than heterodyne). But they also present the disadvantage of being phase sensitive. ϕ_s and ϕ_{LO} fluctuate randomly with time, while ideally they should stay constant. In homodyne detection the difference $\phi_s - \phi_{LO}$ is forced to remain constant through an optical phase-locked loop, which design is quite complex. Moreover, matching ω_s and ω_{LO} needs specific optical sources fulfilling stringent linewidth requirements. Heterodyne detection has a 3-dB penalty in the SNR in respect to homodyne detection, but, because of this, the optical phase-locked loop is not needed anymore, so it has the advantage of a simpler receiver. Still, the linewidth of the optical sources needs to be controlled [16, 17].

It is worth define a few useful terms:

- a bit is the basic unit of information and correspond to a binary digit;
- a bit stream is a sequence of bits;
- the bit rate is the number of bits that are transmitted or processed per unit of time;
- the bit error rate (BER) is the average probability to incorrectly identify a bit (a standard operation value is a BER of 10^{-9}). It is used to evaluate the performance of a transmission system.

3.4.1 Amplification systems

Another block is usually needed in an optical transmission system: amplification. Passing through any transmission medium a signal undergoes distortion and attenuation and each of these factors increase with the travelled distance compromising the signal strength. If the signal decays too much it is difficult for the receiver to demodulate it with a good quality and the bit error rate increases. That is why amplification or regeneration of the signal is necessary.

In early fibre optics communication systems optical amplifiers were not available, so a regeneration process was required at intervals of 80-100 km. The signal had to pass through a repeater, which was essentially a back-to-back receiver and transmitter, where the optical signal was at first converted into an electrical signal, amplified and then regenerated back into an optical signal.

Optical amplifiers appeared in the late 1980s. In optical amplification conversion to the electrical domain is not necessary and the optical signal is directly amplified (which means that also the accumulated noise in the same spectral band is amplified). Optical amplifiers present several advantages, for example they can directly amplify several separate wavelengths travelling along the fibre, as it happens in multi-channel systems.

Also, optical amplifiers are based on stimulated emission (as the laser): a weak input signal enters the material of which is constituted the optical amplifier, it stimulates the excited molecules and they produce energy as photons, which have the same features of the incident signal in regards to wavelength and phase. This way the input signal is strengthened. As the probability of stimulated emission varies with the wavelength depending on the material and its structure, optical amplifiers function over a limited range of wavelengths in which we are able to stimulate the emission.

In fibre optics systems three types of amplifiers are generally used. We have already spoken of Raman amplifiers, which can spread over many kilometers of fibre and do not require doped fibres. Semiconductor optical amplifiers are similar to semiconductor lasers, though they do not have a mirror enclosed cavity. As in semiconductor lasers, a current flowing through a semiconductor produces the energy. Their gain is comparable with that of the third kind of amplifiers, doped fibre amplifiers.

Doped fibre amplifiers are the most commonly used and rely on special fibres in which

the core is doped with an element (usually a rare earth). An external laser pumps light through the fibre core where light is amplified thanks to stimulated emission. The most widespread doped amplifiers are erbium-doped fibre amplifiers (EDFAs), which have become standard for long haul transmission systems. EDFAs are particularly convenient because they work in a frequency range from 1530 nm to 1625 nm, which is the region of minimum attenuation in optical fibres and corresponds to the usual transmission window. Their use was fundamental for the increase of transmission capacity in the 1990s, as they can amplify WDM signals. [17]

3.4.2 Modulation formats

The process of conversion from electrical binary signal to optical bit stream is fundamental in the design of an optical communication system. The task is usually performed by an electro-optical modulator. If the system is capable of coherent detection then it is possible to encode information in the amplitude, frequency or phase of the optical signal. Three types of modulation approaches are thus possible: amplitude-shift keying (ASK), frequency-shift keying (FSK) and phase-shift keying (PSK). The electric field of the optical signal is

$$E_s(t) = A_s(t)cos[\omega_0 t + \phi_s(t)], \tag{3.22}$$

where A_s is the amplitude, ω_0 is the frequency and ϕ_s is the phase.

In the case of ASK only the amplitude is modulated. In the most straightforward case, on-off keying (OOK), A_s has just two fixed values. The time slot allocated to one bit either contains (1) or not (0) an optical pulse, thus transmitting the correspondent bit. No coherent detection is required to extract the information from a signal with ASK-only modulation.

ASK modulation can present two variants: return-to-zero (RZ), where the bit slot (the time slot allocated for one bit) is longer than the optical pulse correspondent to bit 1, so that amplitude comes back to zero within the slot , and nonreturn-to-zero (NRZ), where the amplitude of the optical pulse does not return to zero before the end of the bit slot and so between successive bits 1 (the bit pattern determines the pulse width) -Fig. 3.7-. Though more control on the pulse width is necessary with the NRZ format, it has the advantage of requiring about half of the signal bandwidth of RZ format. RZ format is

especially useful for high-capacity systems: the pulses spread over the bit slots, lowering power and thus detrimental nonlinear effects, but are compressed to the original width with dispersion-management techniques (chirped RZ).

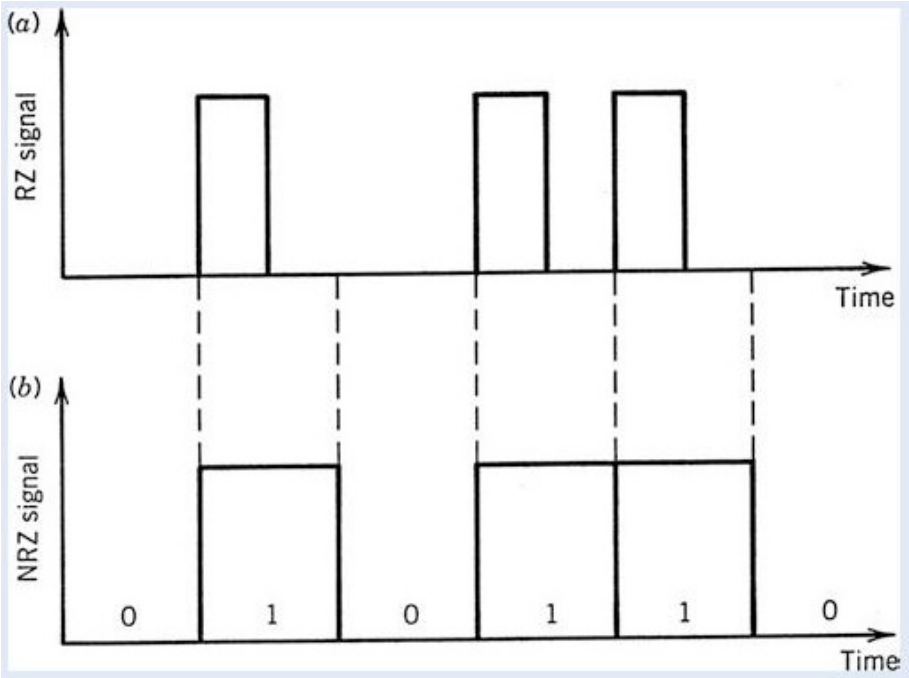

Figure 3.7: Bit stream encoded with return-to-zero and non-return-to-zero formats [15].

In FSK modulation, information is located in the optical carrier frequency ω_0, which can have two values, $\omega_0 + \Delta\omega$ or $\omega_0 - \Delta\omega$, for a 1 or 0 bit. The quantity $\Delta f = \Delta\omega/2\pi$ is referred as frequency deviation and depends on the available bandwidth. The usual bandwidth of an FSK signal is $2\Delta f + 2B$, where B is the bit rate.

Finally in PSK, the phase ϕ_s is modulated. The phase takes different values, which usually are 0 and π. The optical intensity does not need to change over different bits in PSK.

Other formats exist, which combine two of these basic modulation schemes. For example Quadrature Amplitude Modulation (QAM) allows the simultaneous modulation of amplitude and phase. Moreover, a binary scheme may be surpassed in the coding by using a multi-level format which is less demanding for high speed bandwidth needs of the electronic circuits and opto-electronic components. In multi-level modulation two or more (2^{bits}) bits can be encoded in one symbol, reducing the optical bandwidth utilisation. All the standard modulation formats may have a multi-level version. For example we can have Quadrature Phase Shift Keying (QPSK), where we are in the condition 2^2, that means

that 2 bits per symbol can be transmitted, compressing the necessary bandwidth. It is also possible to use polarisation multiplexing as additional way to increase the channel capacity: two different signals may be sent with orthogonal polarisation over the same wavelength. The transmission experimental results presented later in this chapter are obtained using Dual Polarisation - Quadrature Phase Shift Keying (DP-QPSK) as modulation format. All these higher level formats need coherent detection, so the downside of a more complex receiver is balanced by with the advantages over bandwidth capacity. [16, 15, 18, 19]

3.4.3 The nonlinear Shannon limit

Since their introduction in the 1970s, the capacity (bit rate) of optical communication channels has increased exponentially, to the point that continuous bandwidth demand is pushing close to the theoretical maximum capacity in single-mode optical fibres. The Shannon limit [20] states the maximum capacity C of a linear noisy communication channel as

$$C_s = \Delta\nu_{ch} log_2\Big(1 + \frac{P_s}{N}\Big), \tag{3.23}$$

where ν_{ch} is the channel bandwidth, P_s is the average signal power and N is the average noise power. From the equation we can deduce that if there is a low noise level able to maintain a high SNR, the system capacity can exceed the bandwidth of the channel. Equation (3.23) can be used as theoretical upper limit for the capacity of a linear system, but does not always apply to a system with nonlinear effects. In such system this limit can be overcame and capacity increased, setting a new limit, the nonlinear Shannon limit. This limit is theoretical and it has been proven that it can be exceeded with proper amplification and nonlinear compensation techniques (it was achieved in [21] using URFL amplification and optical phase conjugation). The continuous request to increase bandwidth availability is pushing for more studies in this area [16, 22].

3.5 RIN transfer characterization and transmission performance optimization in ultra-long Raman fibre lasers

High-order Raman amplification using URFLs [3, 13] has proven to be a promising solution for long-haul and unrepeatered communication links, combining a simple design with low

signal power variation and superior optical signal to noise ratios (OSNRs) [23, 24]. Its combination with different nonlinear mitigation techniques, such as digital backpropagation (DBP) [25] or optical phase conjugation (OPC) [21] has given excellent results, leading to record transmission capacities at long distances.

As previously mentioned, the performance of URFL amplifiers is inevitably limited by RIN transfer (see section 3.3) from pump to signal, due to the fact that, through the fast process of Raman amplification, oscillations on the pump intensity are passed onto the signal. This effect is maximised for co-propagating pumps, due to the superposition of the pump and signal during transmission [26, 27]. URFLs rely on cascaded pumping to efficiently distribute the gain along the transmission link. As we mentioned before, in a low-depletion regime symmetric pumping leads to the lowest signal power variation (SPV) along the span, and hence to the best possible balance between ASE noise and nonlinear impairments. But high forward pump powers, necessary to maintain symmetry in long spans or when amplifying a high number of channels, may be detrimental for transmission performance, as it is directly related to an increased RIN transfer from the pump to the propagating signal [28, 29, 30]. In order to overcome the problem of RIN transfer, the use of Raman amplification based on certain configurations of ultralong random distributed feedback (DFB) fibre lasers has been recently proposed and successfully demonstrated in coherent transmission schemes. In such lasers, the FBG at the beginning of the cavity is removed, leaving a half open cavity which reduces front-end backreflections to zero, with the downside of reduced forward (FW) pump efficiency [31].

In the following sections we are first going to present a characterization of RIN in a 2^{nd}-order Raman amplifier, in particular how RIN transfer increases with increasing reflectivity at the front end of the cavity, as well as with forward pump powers [30]. After that, we are going to evaluate the direct impact of RIN on transmission performance, using a 30 GBaud DP-QPSK system transmitting 10 WDM signal channels in the C-band, using a cavity in which it is possible to vary both front-end FBG reflectivity and pump power split in order to control RIN transfer in the URFL amplification scheme.

3.5.1 Experimental set-up

Figure 3.8 represents the set-up of the 2^{nd}-order URFL amplifier tested for the experimental characterization of RIN transfer and its impact on transmission performance.

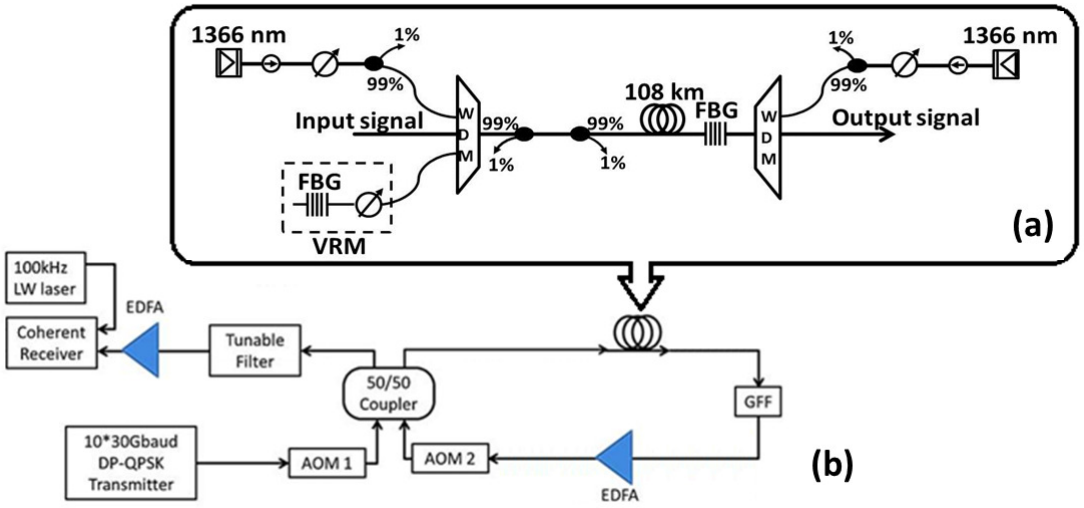

Figure 3.8: Set-up of the 2^{nd}-order URFL amplifier (a) and the 10x30 GBaud DPQPSK transmission system (b).

It is built with 100 km (for the RIN characterization) and 108 km (for the transmission optimization) of standard telecommunication single mode fibre (SSMF) pumped bidirectionally by two equal highly depolarised Raman fibre laser operating at 1366 nm, acting as second order pumps. The basic cavity is enclosed by two FBGs, centered around 1454 nm corresponding to the pumps first Stokes wavelength. Two wavelength division multiplexers (WDM) are employed to couple and split pumps, signals and first Stokes components at the two sides of the cavity. The FBG at the end of the cavity presents a high (>95%) fixed reflectivity at its central wavelength (1454 nm), whereas the front-end reflector is actually a variable reflectivity module (VRM), combining a high-reflectivity FBG (>95%) and a variable optical attenuator (VOA), which allows testing of the cavity performance over a continuum of FBG reflectivities, controlling the amount of backreflections into the cavity. Back-to-back 99%-1% splitters inside the cavity allow for the real-time monitoring of the VRM reflectivity. The effective reflectivity is measured and calculated as the ratio of the power reflected at the 1% tap on the right in Fig. 3.8(a) of the back-to-back 99%-1% splitters divided by the power incident at the tap on the left (that is the ratio of the power back-reflected by the VRM to the power incident on the VRM). Due to the insertion losses caused by the taps, VOA and WDM, the maximum effective reflectivity achievable with the VRM was 40% in the case of RIN characterization and 20% in the transmission experiment. Other two VOAs are located at the pumps output to adjust the pump powers, in order to keep the pump RIN fixed and independent from pump power, as it is known that fibre

pump lasers present a RIN level which depends on their drive current. The pumps are, thus, set to the maximum power needed, which is then attenuated to obtain the necessary pump split for each measurement. The forward (FW) pump ratio is calculated as the percentage of the total pump power supplied by the forward pump. We tested different configurations of front-FBG reflectivity and pump power ratio adjusting the amplifier through the VOAs located at the pump outputs and in the VRM at the front end of the cavity.

In order to monitor the transmission performance, different URFL configurations are employed to fully compensate for the Raman span and passive component losses in a 10 x 30 GBaud coherent detection DP-QPSK transmission system, as shown in Fig. 3.8(b). In this set-up, the 108 km transmission span is included in a recirculating loop. The transmitter comprises ten 100 GHz spaced distributed feedback lasers located between 1542.94 nm and 1550.12 nm. In order to test each available channel, the grid is combined with a 100 kHz linewidth tunable laser that replaces the corresponding DFB laser during the measurement cycle. In each channel, the multiplexed signals were QPSK modulated with normal and inverse 231 -1 PRBS patterns at 30 Gb/s with a relative delay between I (in-phase) and Q (quadrature) of 18 bits. The PolMux was implemented with a delay of 300 bits between the two polarisation states. The total transmission rate was 10 x 120 Gb/s. No temporal decorrelation is applied to the data transmitted at each wavelength, but fibre dispersion effectively decorrelates the 10 WDM channels temporally. The modulated DP-QPSK signals are launched into the previously described transmission span in the recirculating loop. The output spectrum is equalized by a gain flattening filter (GFF) and an EDFA compensates for the losses of the loop before the coherent receiver. A detailed description of a similar transmission system is available in [21]. The resultant traces are post-processed off-line with digital signal processing (DSP). Finally, the Q-factors are calculated from measured bit error rates (BERs), averaged over two million bits.

3.5.2 Experimental characterization of RIN transfer

In the described cavity RIN was measured using a low noise photodetector with a bandwidth of 125MHz and it was integrated over the first 1 MHz [30].

As we mentioned, pump RIN varies with its direct output power. We can see in Fig. 3.9 that the output signal RIN, accordingly, varies when the pumps do not operate with a fixed pump RIN, that is when the pump power is directly changed as opposed to the

case in which pump power is fixed and then externally attenuated. The figure presents the two extreme cases of reflectivity obtainable with the VRM, 40% and 1.5%, which is obtained by substituting the VRM with a flat FC/PC connector. While the RIN level is comparable in all cases when FW pump power is absent, as the FW pump is introduced and increased we start to observe a different behaviour. The case in which RIN transfer is lower is the cavity with low front-end reflectivity and variable pump RIN, where up to 30% FW pump ratio the penalty on the output signal RIN is negligible. For the cavity with the same reflectivity but fixed pump RIN, at 30% FW pump ratio a much higher (10 dB) RIN penalty is detected. The same trend is visible in the case of 40% front-end reflectivity, though integrated RIN penalty is higher and starts to grow at a lower forward pump power ratio.

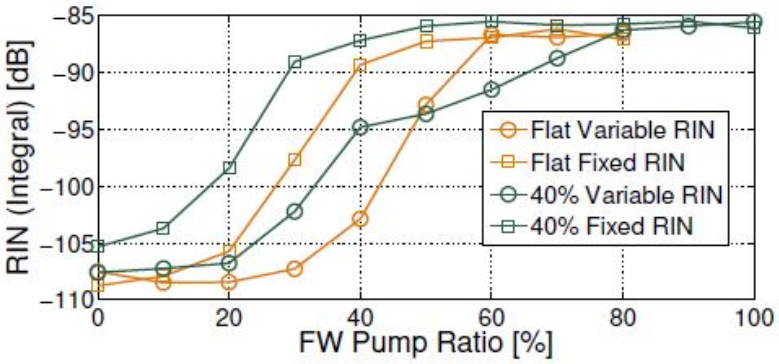

Figure 3.9: Integrated signal RIN over 1 MHz for variable (solid lines) and fixed (dashed lines) pump RIN for 1.5% (flat, yellow lines) and 40% (green lines) front-end reflectivity [30].

To analyse the combined effect of FW pump power and front-end reflectivity on the RIN transfer, in the following results pump RIN levels were kept fixed, unless is specified otherwise.

In figure 3.10 we can see the complete experimental RIN characterization for all the tested cavities, from rDBF (half-open cavity) to 40% reflectivity, as the integrated signal RIN is depicted as a function of the FW pump power. It is clear that all the cavities are subjected to a higher RIN transfer as the FW pump power increases. Moreover, for increasing front-end reflectivity, the signal RIN starts to grow at a lower FW pump power ratio and with a steeper slope. Also, RIN transfer reaches saturation above 50% of FW pump power ratio, remaining in a plateau for higher FW pump powers.

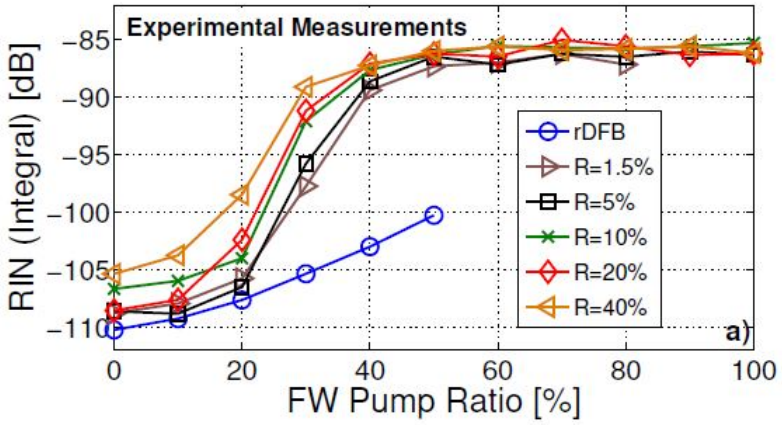

Figure 3.10: Experimental signal RIN integrated over 1MHz as a function of the FW pump ration and front-end reflectivity for a 100 km 2nd-order URFL amplifier [30].

In [28, 29], models of RIN transfer in 2^{nd} order URFLs and rDFB lasers are presented. In [30] numerical simulations of the cavities presented in Fig.3.10, which follow those models, are shown. The simulated signal RIN displays a very good agreement with the experimental results which we have just presented, with only minor differences ascribable to deviations of the fibre characteristics in the experiment and in the simulations.

It is clear that we have to take into consideration this characterization of RIN transfer and the impact of front-end reflectivity and pump power ratio when considering the optimization of the transmission performances in a URFL amplifier.

3.5.3 Performance optimization in ultra-long Raman laser amplified 10x30 GBaud DP-QPSK transmission

Different configurations of the URFL cavity are tested to investigate their transmission performances, considering the impact that RIN transfer may have on them. Q-factors are obtained for front-end FBG reflectivities of 1.5% (obtained with a flat-end PC connector substituting the VRM), 10% and 20% and forward pump power ratios of 10%, 20% and 40%. Q-factors for 0% (backward pumping only) FW pump power ratio are measured only for the case of 20% front-end reflectivity without loss of generality, since, as previously shown in [31], the performance is not altered in this case by variations in front-end FBG reflectivity. Please note that, unlike the FBG reflector, which acts as a sharp filter around the Stokes wavelength, the flat-end connector (giving a 1.5% reflectivity) reflects all wavelengths

equally, including the pump ones.

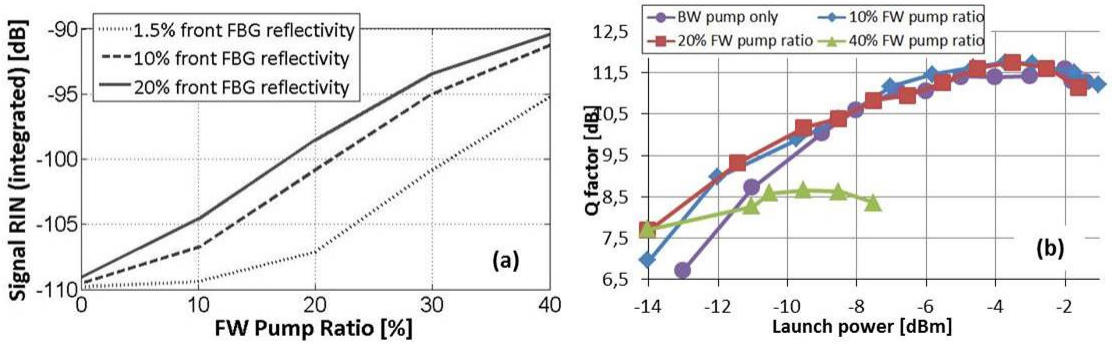

Figure 3.11: Simulated signal RIN integrated over 1 MHz as a function of FW pump power ratio and front-FBG reflectivity (a). Launch power versus Q-factors at 2159 km, measured at 1545.32 nm for 20% front-FBG reflectivity (b).

Figure 3.11(a) shows the simulated signal RIN, integrated over 1 MHz, obtained from the calculated RIN transfer function for each of the investigated cases, taking as input the measured pump RIN. From the figure it is clear how RIN increases both with FW pump ratio and front-FBG reflectivity. 3.11(b) shows the variation of the Q-factors of the measured channel at 1545.32 nm versus signal launch power at different forward pump power ratios maintaining a 20% front-FBG reflectivity and a fix transmission distance of 2159 km in the recirculating loop. Optimal signal launch powers are between -2 dBm and -4 dBm for FW pump ratios up to 20% of total pump power, while they shift down to between -8 dBm and -9 dBm for a FW pump ratio of 40%. This reduction in the optimal signal power is typical of quasi-lossless URFL amplification, and thus to be expected as gain becomes more evenly distributed as we approach to equal bidirectional pumping [32]. Please note that 40% FW pump ratio is the highest for which it has been possible to achieve a BER below the forward error correction (FEC) threshold (corresponding to Q-factors above 8.5 dB). This is in line with the build-up of the RIN in the cavity, which can be expected to hinder the transmission performance.

Figures 3.12(a), (b) and (c) show the achievable Q-factors of the channel at 1545.32 nm as a function of transmission distance for the different cavity configurations. A maximum reach of 5399 km is achievable for the 1.5% flat-end connector -Fig. 3.12(a)- with 10% and 20% FW pump ratios (the second one giving the best results), but RIN transfer at 40% FW ratio quickly degrades performance despite the improved OSNR offered by the URFL configuration. The flat connector configuration offers, in any case, worse performance

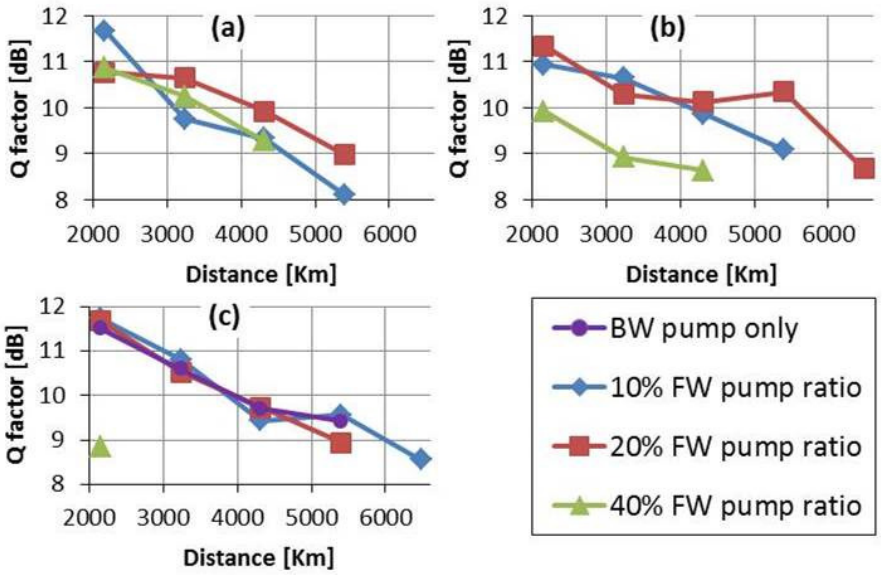

Figure 3.12: Transmission distance versus Q-factors measured at 1545.32 nm for 1.5% (a), 10% (b) and 20% (c) front-end reflectivity.

than any of the FBG-based configurations tested, possibly due to its extended reflection bandwidth. For a 10% reflectivity front-FBG -Fig. 3.12(b)-, reach is extended to 6479 km for a 20% FW pump ratio, which offers the best trade-off between OSNR and RIN performance. The 20% reflectivity front-FBG -Fig. 3.12(c)- case can offer a similar reach of 6479 km (with better pump conversion efficiency) for a 10% FW pump ratio, but the performance is degraded for higher FW pump ratios due to RIN transfer, as well as for the backward-only pump case, in which ASE dominates. Regarding the results obtained with 40% FW pump ratio, it is clear that, besides allowing for shorter reaches (down to only 2159 km for 20% front-end reflectivity), the starting performance itself is worse than in the cases with lower FW pump ratios (which allow for Q-factors close to or over 11 dB at a 2159 km distance) and decreasing for higher front-FBG reflectivities.

Figure 3.13 displays the measured optical spectra and the Q-factors of the 10 WDM channels at maximum worst-channel attainable reach after FEC. As seen above, 10% and 20% FW pump ratios allow for sweet spot configurations in which OSNR and RIN impairments are balanced, which lead to reaches of at least 5399 km for the 10 channels, with good gain flatness resulting in a variation of less than 0.7 dB between the Q-factors of the different channels, except, as it may be expected, in the case of the flat connector (1.5%), in which performance is limited to 4319 km. The best performance is obtained

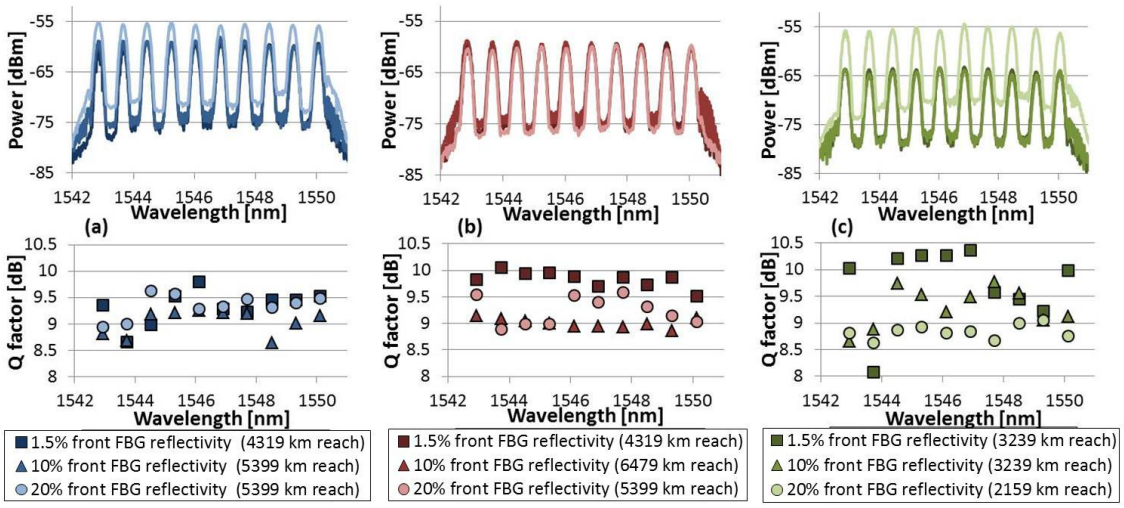

Figure 3.13: Measured spectra and Q-factors at maximum reach of the 10 channels for 10% (a), 20% (b) and 40% (c) FW pump ratio.

for the case of 10% reflectivity and 20% FW pump power, with a 6479 km reach for all channels, with a Q-factors maximum variation between channels of 0.28 dB. Performance for the 40% FW pump ratio is poor for all cases, and down to 2159 km for the 20% front-FBG reflectivity, with higher variability between channels Q-factors.

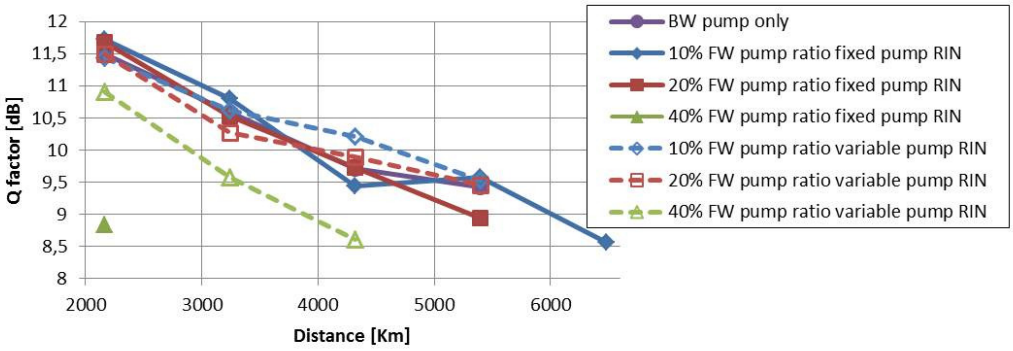

Figure 3.14: Comparison fixed (solid) and variable (dashed) pump RIN: transmission distance versus Q-factors measured at 1545.32 nm for 20% front-end reflectivity.

As mentioned in the description of the experimental set-up, the measurements are performed with fixed high output pump powers, which each time are attenuated by means of the variable optical attenuators located at the lasers outputs to obtain the necessary pump power ratio. Since pump RIN is dependent on pump power, controlling the output pump power as mentioned above, the pump RIN is kept fixed and it is possible to eliminate its dependence from the power variation of the pumps. It is, thus, possible to isolate the effect of RIN transfer, taking into account that the pump always delivers the same

RIN. Since we want to check the impact of RIN transfer on transmission performance, we perform the measurements with the described method. It is worth to mention though, as it has been shown in [27], that the signal RIN increases differently compared to what is presented in Fig. 3.11(a) when changing directly the pumps power in respect with the fixed pump RIN approach. In particular, for high front-end reflectivity of the cavity and high FW pump power ratio, the signal RIN is higher in the case of fixed pump RIN. We verify here this behavior on the transmission performance, presented in Fig. 3.14, where the Q-factors as function of transmission distance in a cavity with 20% front-end reflectivity are compared for the cases of fixed and variable pump RIN. While for low FW pump ratios they show comparable performances, it is clear that, increasing the FW pump to 40%, the set-up with variable RIN offers better performances incrementing the maximum reach from 2159 km of the fixed pump RIN case up to 4319 km.

3.6 Conclusions

We have evaluated the impact of front-FBG reflectivity and pump split on long-haul URFL-amplified systems performance. First we have experimentally characterised RIN transfer in an ultralong 2^{nd}-order Raman fibre amplifier with variable front-end reflectivity and pump split, observing how RIN transferred from pump to signal increases with increasing VRM reflectivity and FW pump power.

Then we have tested the transmission performances. For the considered span length we can conclude that forward pump ratios above 20% with noisy fibre laser pumps should be avoided in general in combination with any kind of front-FBG reflector for the Stokes component, but the use of lower pump ratios can offer ASE noise reduction without compromising system performance because of RIN. For a 108 km ultra-long Raman laser amplifier, a 20% forward pump power ratio and 10% front-FBG reflectivity offered the best performance, allowing us to reach transmission distances of 6479 km for all the 10 channels between 1542.94 nm and 1550.12 nm.

References

[1] I. Nasieva, J. D. Ania-Castañón, S. K. Turitsyn, C. Borsier, E. Pincemin, and M. P. Fedoruk, "Span design for reduced noise and nonlinear impairments in a dispersion-managed Raman amplified system," *Opt. Quantum Electron.*, vol. 36, no. 8, pp. 725–732, 2004.

[2] W. Pelouch, "Raman amplification: An enabling technology for high- capacity, Long-Haul transmission," *Opt. Fiber Commun. Conf. OFC 2015*, vol. 34, no. 1, pp. 6–19, 2015.

[3] J. D. Ania-Castañón, "Quasi-lossless transmission using second-order raman amplification and fiber bragg gratings," *Optics Express*, vol. 12(19), p. 43724377, 2004.

[4] H. J. Lee and J. X. Cheng, "Imaging chemistry inside living cells by stimulated Raman scattering microscopy," *Methods*, vol. 128, pp. 119 – 128, 2017.

[5] A. Smekal, "Zur quantentheorie der dispersion," *Naturwissenschaften*, vol. 11(43), p. 873875, 1923.

[6] C. Raman, "A new radiation," *Indian Journal of Physics*, vol. 2, p. 387, 1927.

[7] C. V. Raman and K. Krishnan, "A new type of secondary radiation," *Nature*, vol. 121, pp. 501–502, 1928.

[8] G. Landsberg and L. Mandelstam, "Uber die lichtzerstreuung in kristallen," *Zeitschrift für Physike*, vol. 50(11), pp. 769–780, 1928.

[9] R. W. Boyd, *Nonlinear optics*. Academic Press, 2008.

[10] C. Headley and G. P. Agrawal, *Raman amplification in fiber optical communication systems*. Elsevier Academic Press, 2005.

[11] N. Bloembergen, "The stimulated raman effect," *American Journal of Physics*, vol. 35, no. 11, pp. 989–1023, 1967.

[12] G. P. Agrawal, *Nonlinear fiber optics*. Academic Press, 2012.

[13] J. D. Ania-Castañón, T. J. Ellingham, R. Ibbotson, X. Chen, L. Zhang, and S. K. Turitsyn, "Ultralong raman fiber lasers as virtually lossless optical media," *Phys. Rev. Lett.*, vol. 96, p. 023902, 2006.

[14] S. Turitsyn, S. A. Babin, A. E. El-Taher, P. Harper, D. V. Churkin, S. I. Kablukov, J. D. Ania-Castañón, V. Karalekas, and E. V. Podivilov, "Random distributed feedback fibre laser," *Nature Photonics*, vol. 4(4), p. 231235, 2010.

[15] M. D. Al-Amri, M. El-Gomati, and M. S. Zubairy, *Optics in our time.* Springer, 2016.

[16] G. P. Agrawal, *Fiber-optic communication systems.* Wiley, 2010.

[17] J. Hecht, *Understanding fiber optics.* Laser Light Press, 2015.

[18] E. Lach and W. Idler, "Modulation formats for 100g and beyond," *Optical Fiber Technology*, vol. 17, p. 377386, 2011.

[19] K. Roberts, M. O'Sullivan, K. T. Wu, H. Sun, A. Awadalla, D. J. Krause, and C. Laperle, "Performance of Dual-Polarization QPSK for Optical Transport Systems," *Journal of Lightwave Technology*, vol. 27(416), pp. 3546–3559, 2009.

[20] C. E. Shannon, "A mathematical theory of communication," *Bell System Technical Journal*, vol. 27, no. 3, pp. 379–423, 1948.

[21] I. D. Phillips, M. Tan, M. F. C. Stephens, M. E. McCarthy, E. Giacoumidis, S. Sygletos, P. Rosa, S. Fabbri, S. T. Le, T. Kanesan, S. K. Turitsyn, N. J. Doran, P. Harper, and A. D. Ellis, "Exceeding the nonlinear-Shannon limit using Raman laser based amplification and optical phase conjugation," *Conf. Opt. Fiber Commun. Tech. Dig. Ser.*, pp. 5–7, 2014.

[22] A. D. Ellis, J. Zhao, and D. Cotter, "Approaching the non-linear shannon limit," *J. Lightwave Technol.*, vol. 28, no. 4, pp. 423–433, 2010.

[23] P. Rosa, J. D. Ania-Castañón, and P. Harper, "Unrepeatered DPSK transmission over 360 km SMF-28 fibre using URFL based amplification," *Optics Express*, vol. 22, no. 8, pp. 9687–9692, 2014.

[24] M. Tan, P. Rosa, I. Phillips, and P. Harper, "Extended Reach of 116 Gb/s DP-QPSK Transmission using Random DFB Fiber Laser Based Raman Amplification and Bidirectional Second-order Pumping," *Opt. Fiber Commun. Conf.*, p. W4E.1, 2015.

[25] L. Galdino, M. Tan, D. Lavery, P. Rosa, R. Maher, I. D. Phillips, J. D. Ania-Castañón, P. Harper, R. I. Killey, B. C. Thomsen, S. Makovejs, and P. Bayvel, "Unrepeatered Nyquist PDM-16QAM transmission over 364 km using Raman amplification and multi-channel digital back-propagation," *Optics Letters*, vol. 40, no. 13, pp. 3025–3028, 2015.

[26] C. R. S. Fludger, V. Handerek, and R. J. Mears, "Pump to signal RIN transfer in Raman fiber amplifiers," *J. Light. Technol.*, vol. 19, no. 8, pp. 1140–1148, 2001.

[27] B. Bristiel, S. Jiang, P. Gallion, and E. Pincemin, "New model of noise figure and RIN transfer in fiber raman amplifiers," *IEEE Photonics Technol. Lett.*, vol. 18, no. 8, pp. 980–982, 2006.

[28] M. Alcón-Camas and J. D. Ania-Castañón, "RIN transfer in 2nd-order distributed amplification with ultralong fiber lasers," *Opt. Express*, vol. 18, no. 23, p. 23569, 2010.

[29] J. Nuño, M. Alcon-Camas, and J. D. Ania-Castañón, "RIN transfer in random distributed feedback fiber lasers," *Adv. Photonics Congr.*, vol. 20, no. 24, p. JM5A.7, 2012.

[30] G. Rizzelli, M. A. Iqbal, F. Gallazzi, P. Rosa, M. Tan, J. D. Ania-Castañón, L. Krzczanowicz, P. Corredera, I. Phillips, W. Forysiak, and P. Harper, "Impact of input fbg reflectivity and forward pump power on rin transfer in ultralong raman laser amplifiers," *Optics Express*, vol. 24, no. 25, pp. 29 170–29 175, 2016.

[31] M. Tan, P. Rosa, S. T. Le, M. A. Iqbal, I. D. Phillips, and P. Harper, "Transmission performance improvement using random DFB laser based Raman amplification and bidirectional second-order pumping," *Opt. Express*, vol. 24, no. 3, p. 2215, 2016.

[32] L. Barker, A. E. El-Taher, M. Alcon-Camas, J. D. Ania-Castañón, and P. Harper, "Extended bandwidth for long haul DWDM transmission using ultra-long Raman fiber lasers," *Eur. Conf. Opt. Commun. ECOC*, vol. 1-2, pp. 23–25, 2010.

Chapter 4

Ultrafast ring fibre lasers with InN SESAM

The origin of ultrafast optics can be traced back to the seminal research on mode-locking in solid-state lasers carried out by De Maria et al. [1] in 1966, followed by the generation of sub-picosecond pulses in passively mode-locked organic dye lasers by Shank and Ippen [2] in 1974. In parallel to those remarkable achievements, the theoretical foundations for this new field were laid down in pioneering contributions by researchers such as Haus and New [3, 4] throughout the 70's and 80's. From the beginning, the tremendous potential of femtosecond lasers was recognized and applied to areas as varied as medicine, telecommunications, metrology, spectroscopy, material processing or energy research [5, 6]. Ultrashort pulse generation has been explored over a large variety of active media over time, with each choice available presenting a different set of virtues and drawbacks that limit their potential fields of application.

Several of the topics (light propagation in fibres, linear and nonlinear effects, solitons) discussed in Chapter 1 will be useful for the understanding of this chapter, as they play an important role in the implementation of fibre lasers. We will focus especially on passively mode-locked fibre lasers which make use of saturable absorbers to achieve self-starting mode-locking. After an introduction about ultrafast fibre lasers and how to achieve mode-locking lasers, we will take a closer look to the semiconductor saturable absorber mirror (SESAM) used in the set-ups presented in this thesis and to the fibre lasers themselves and their performances.

4.1 Introduction to ultrafast fibre lasers

The idea of fibre lasers is almost as old as that of the laser itself [7], but it is especially in the past three decades that research in this area has been boosted, after the introduction of fibre amplifiers (as the EDFAs). Ultrashort pulsed fibre lasers have proven themselves capable of offering simple implementation solutions at a reduced cost, over a range of energies, wavelengths and temporal pulse widths [8]. They combine stability, efficiency, compactness and easy integrability, are nearly maintenance-free and allow for convenient output beam handling, which makes them highly attractive in a broad variety of applications.

As any laser, a fibre laser needs a gain medium, an energy source and a mean to achieve optical feedback. We can see a fibre laser as a fibre amplifier located inside a cavity so as to have optical feedback. Various rare earth ions (erbium, ytterbium, neodymium...) in the fibre can induce stimulated emission, allowing fibre lasers to operate at very different wavelengths, in a range that may extend from 0.4 μm to 4 μm.

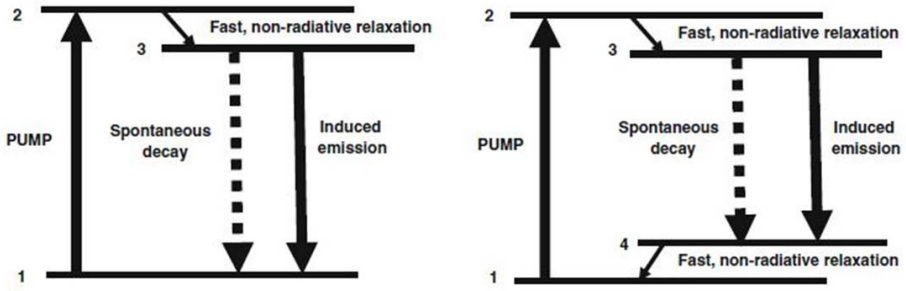

Figure 4.1: Three-energy-level and four-energy-level diagrams of laser operation [9].

Fibre lasers usually work with a three or four -level pumping scheme of stimulated emission (as described in Fig. 4.1). Since the appearance of Er-doped fibre amplifiers and their great impact on optical communications, Er-doped fibre lasers have drawn a lot of attention. Er-doped fibre lasers exploit a three-level pumping scheme, where pumping is usually provided by a semiconductor laser at 980 nm or 1480 nm (an EDFA could be used, combining pump and gain medium in one device). Though they can operate at various wavelengths, the 1.55 μm region is the most used one, as it coincides with the region of lowest loss in optical fibre and the C-band in telecommunication window.

The physics of fibre lasers is obviously very similar to that of traditional laser cavities. One of the main differences is the geometry of the gain medium, which, being an optical

fibre, is usually much longer and have a very reduced cross-section. This parameter foster the relevance of optical nonlinearities, which have to be taken into consideration when designing a fibre laser.

Given their flexibility, fibre laser cavities can be implemented in a variety of ways. For example, Fabry-Perot cavities are very common, where the gain medium is enclosed by two high reflectivity reflectors, which can be applied directly at the fibre end, as fibre Bragg gratings for example. Ring cavities may also be advantageous, can avoid the use of mirrors, be all-fibre and operate in an unidirectional way, but usually need to have some kind of polarisation control. Mode-locked lasers may also present a double ring cavity, called figure-of-eight, where one of the rings acts as a nonlinear amplifying loop mirror, which allows passive mode-locking without a saturable absorber. Others configurations are possible and are used in a variety of situations. [9, 10, 11]

Fibre lasers can operate in different regimes. The main ones are:

- Continuous wave (CW), where the laser emission is quasi-constant in intensity. CW lasers are generally used when high average power is needed.

- Q-switching, which relies on the fact that the laser Q factor (quality factor) quickly changes when the losses inside the cavity change and are modulated from high to low. The Q factor of an resonator or oscillator is a parameter measuring the strength of the damping of its oscillations. In the case of Q-switched lasers, when the Q factor is suddenly increased, an intense laser pulse is produced. So, it is used to generate pulses of high energy and peak power in the range of the nanoseconds.

- Mode-locking, where through different devices, many modes oscillating in the cavity can be locked in. In this case, we are talking about longitudinal modes, which are stationary waves forming a pattern with nodes located axially along the length when they are confined in a laser cavity. They are the result of constructive interference in the cavity, while the other wavelengths are suppressed. It is used to generate ultrashort pulses in the range of picoseconds and femtoseconds. This group of methods will be explained more extensively in the next subsection.

Others regimes are possible, as well as intermediate or hybrid regimes. Q-switching and mode-locking, for example, can be present in the same laser.

4.2 Introduction to passively mode-locked fibre lasers

As said, in this chapter we will focus on passively mode-locked fibre lasers and their development. We will firstly describe the mode-locking mechanism, how it is achieved and the possible shapes that a passively mode-locked laser can take.

4.2.1 Mode-locking

In a fibre laser we can have the presence of many simultaneous longitudinal modes in the same gain wavelength region. When the phase of different axial modes is synchronised so that the phase difference between two neighbouring modes is locked to a value $\phi = \phi_m - \phi_{m-1}$, which is constant, the laser is in mode-locking condition. An intracavity modulation produces a rapid modulation of the laser output, which generates ultrashort optical pulses. The pulses recirculate inside the cavity and a regular pulse train is emitted at the laser output with a repetition rate equal to the round trip time of the pulse inside the cavity (condition of fundamental mode-locking, FML, one pulse at time is recirculating in the cavity). If more than one pulse is recirculating at the same time inside the cavity (harmonic mode-locking, HML), the repetition rate is a multiple of the fundamental one, according to the number of pulses simultaneously present in the cavity with equal spacing. At the same time at each round trip the energy lost by the pulse at the laser output is regained at its passage through the gain medium. Mode-locking can occur in two ways: actively or passively.

Active mode-locking is achieved with an amplitude or phase modulator (usually an acousto-optic or electro-optic modulator) inside the cavity, that actively modulates the losses of the resonator simultaneously with its round trips. It is produced by the modulation of amplitude or phase of the internal optical field at a frequency which is equal (or multiple) of the mode spacing frequency. In this way modulation sidebands appear and overlap with those of neighbouring modes, leading to phase synchronization. The pulses reach the modulator when there are less losses, so that the slightly higher losses at the pulse wings shorten the pulses. The steady state, where this shortening is counterbalanced by pulse broadening, is reached after thousands of round trips. The pulses generated with this mechanism usually do not go below the few tens of picosenconds in duration.

On the contrary, passive mode-locking is able to generate ultrashort pulses, using,

instead of an active modulator, a passive nonlinear device, such as a saturable absorber (SA), whose behaviour depends on the intensity of the incident optical pulse and modulates losses in the cavity faster than an active modulator. Several effects result in a shorter pulse duration, which is finally given by the balance between the SA pulse shaping action, the pulse broadening due to limited gain bandwidth, the chromatic dispersion and the nonlinear effects. The saturable absorber and the laser architectures can take many forms, which we will discuss in the next sections [10, 12, 13].

4.2.2 Saturable absorption and passively mode-locked fibre lasers

Among the different existing options for the implementation of ultrafast sources, those relying on passive mode-locking in optical fibre have been the subject of much attention and constant development since the early 90's. Today most of the ultrafast fibre laser rely on passively mode-locked oscillators, to which amplification may be added at a later stage. Erbium (1.55 μm) and ytterbium (1.05 μm) lasers are especially common, with numerous commercial solutions, but solution with thulium and holmium, in the mid-infrared region are getting more and more attention. Moreover, the vast availability of commercial fibre optics components allows simple implementation of "in-house" solutions. [5]

We have already described in section 4.2.1 that in mode-locking multiple axial modes in the cavity are locked through phase coherence. A synchronous modulation with the laser radiation round trip can build up a pulse, which can be shortened at every passage through the resonator. This shortening finds its limit in the limited gain bandwidth of the laser. One of the objectives in the study of this kind of lasers has always been the generation of shorter pulses. Passive mode-locking is especially suited for this. [12]

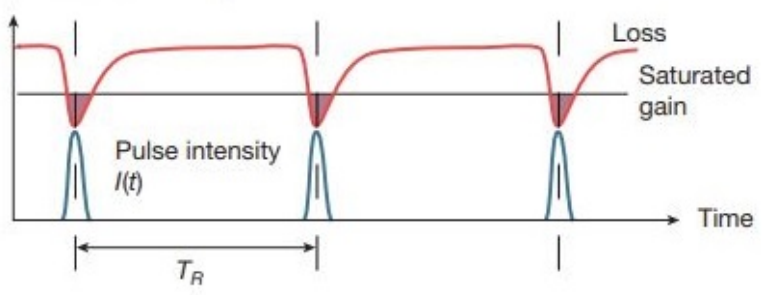

Figure 4.2: Active and passive mode-locking scheme [14]

As we said passive mode-locking needs some mechanism of passive modulation inside

the cavity to modulate the intensity inside the resonator. It builds up the pulses around the area of minimum loss modulation, in accordance with the round trip time, and so with the length of the cavity (which determines the repetition frequency of the laser) -Fig. 4.2. The theory of mode-locking in laser has been studied extensively and can be found, among others, in [3, 12, 15, 16]. The model described by Haus' master equation is well established:

$$T_R \frac{\partial}{\partial T} A(T,t) = \Big(-iD\frac{\partial^2}{\partial t^2} + i\delta|A|^2 \Big) A + \Big(g - l + D_{g,f}\frac{\partial^2}{\partial t^2} - q(T,t) \Big) A, \tag{4.1}$$

where T_R is the round trip time, $A(T,t)$ is the slowly varying field envelope, D is the group delay dispersion, δ is the SPM coefficient, g is the saturated gain, l is the round trip loss, $D_{g,f}$ is the gain and frequency dependent dispersion and $q(T,t)$ is the response of the saturable absorber. The gain saturates after many pulses. It can be assumed that it saturates with average power

$$P(T) = E_P(T)/T_R. \tag{4.2}$$

In consequence the saturated gain is

$$g(T) = \frac{g_0}{1 + \frac{E_P(T)}{P_L T_R}}, \tag{4.3}$$

where E_P is the pulse energy, g_0 is the small signal gain and P_L is the saturation power of the gain medium.

As we see from equation 4.1 gain and saturable absorption play an important role in cavity dynamics. In the following paragraphs we will describe the properties and mechanism of saturable absorbers (of which SESAMs are particularly important in this study), which is the most common way to achieve passive mode-locking. But the modulation of the losses can be achieved also in other ways. We will thus also present a short summary of the possible implementation methods of passively mode-locked fibre lasers, with special regard to erbium fibre lasers, which are the ones that have been implemented in this thesis.

Saturable absorbers

Saturable absorbers were the first method employed to achieve passive mode-locking in the 1970s, but they can also be used in Q-switching. The optical absorptions of these materials are constant at low intensity levels, but as the laser intensity rises they saturate or are

reduced to lower values.

Semiconductors are frequently used as SA. In them incident photons with an energy similar to that of the band gap are mostly absorbed before the spontaneous decay time, so for high optical intensities the conduction band may be saturated by the electrons. If more photons incide on the material, it is less probable that they are absorbed, which means that the absorption coefficient is reduced and the transmission of the semiconductor raises. For low optical intensities saturable absorption does not occur because less electrons are excited from the valence band to the conduction band and the latter does not saturate.

After being reduced due to saturation from an optical pulse, the absorption returns to its initial level, thanks to intraband thermal relaxation (a process that takes around 50 to 100 fs) and then recombination (a slower process in the range of tens or hundreds of picoseconds). SAs can be divided into fast and slow saturable absorbers depending on their recovery time. If it is shorter than the pulse duration, it is referred to as fast SA. If it is longer or similar to the duration of the pulse, it is considered a slow SA. This definition implies that the same saturable absorber may be considered fast or slow, depending on the pulses generated by the laser, where duration may vary noticeably according to the cavity configuration.

SAs can be used either in transmission or reflection (some materials may work in both configurations with due structure adjustment). A common and advantageous type of SA which functions in reflection is the semiconductor saturable absorber mirror (SESAM), firstly introduced by Keller in solid state lasers [17]. In this case the SA is still based on a semiconductor but a reflective element (as a mirror or a Bragg mirror) is added to it and its reflectivity increases for high optical intensities. Besides the complete control over design parameters, the reflection configuration translates in a doubling of the interaction effective length of the absorber. Thanks to these features, SESAMs have proven to enhance the performances in lasers, in terms of pulse width, average power and repetition rate. A particular type of SESAM has been used in the work presented in this thesis and it will be presented in section 4.3.

There are several properties that have to be characterised in a saturable absorber [18, 13]. The most important are:

- Modulation depth, which is the maximum nonlinear change in reflectivity, which

is dependent on the thickness of the absorber, the type of material, the optical wavelength and the optical field penetration in the absorber.

- Non-saturable losses, which are generally unwanted. They are usually higher if there is a high modulation depth and fast recovery.
- Linear losses, which are losses due to linear absorption in the material.
- Saturation fluence, which is the energy per unit area (fluence) of an incident pulsed necessary to cause significant absorption saturation. It is dependent on the material, the wavelength and the field penetration in the absorber.
- Saturation energy, which is the saturation fluence times the mode area.
- Damage threshold, which can be expressed as an intensity or fluence and is the upper limit of operation of the SA, above which the material can be damaged.

Other mechanisms of saturable absoption

In some cases an all-fibre laser may be necessary, condition that may not be met with a semiconductor SA. A solution, which was proposed in the early 1990s [19, 20], is the use of nonlinear fibre-loop mirrors implemented in figure-of-eight lasers, whose name denotes their particular configuration as visible in Fig. 4.3(a). The system is composed of two loops, the main oscillator and the NALM (nonlinear amplifying loop mirror) which are connected at the center by a 50-50 coupler-splitter, which function is to equally divide the radiation in two counterpropagating directions. The location of the doped fibre in the NALM is selected so that one wave is amplified just after the entrance of the loop, while the other is amplified just before the exit. In this way they will accumulate different nonlinear phase shift during the round trip of the NALM. The outcome of this process is the narrowing of the pulse exiting the loop, in a similar way of what happen with a SA [10].

320 fs soliton pulses were generated with this method in a passively mode-locked erbium fibre laser as soon as 1991. [21]. Though pulses shorter than 100 fs may be difficult to achieve with a NALM, by amplifying and then compressing the laser output with a dispersion shifted fibre, pulses as short as 30 fs have been observed [22]. Placing a short length of dispersion shifted fibre inside the NALM itself may also be an option (98 fs pulses were achieved in [23]). Finally, a way of increasing the usual limited energy of the pulse is

to introduce normal dispersion fibre. Pulse widths of 125 fs and pulse energies of 0.5 nJ were reached in [24].

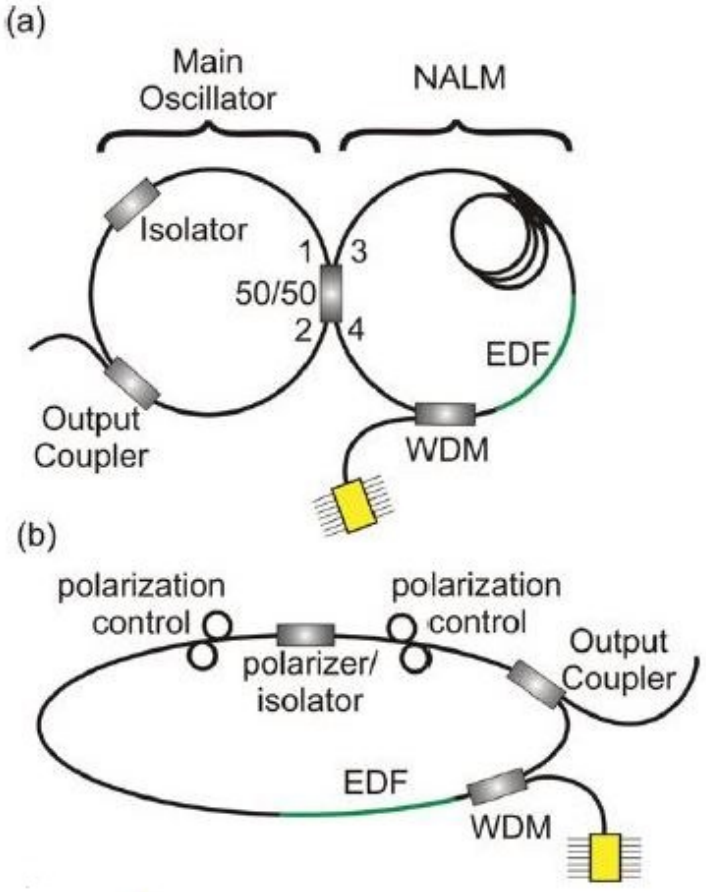

Figure 4.3: Different oscillator designs. Figure-of-eight laser (a) and ring resonator [25].

Another passive mode-locking method is nonlinear polarisation rotation (NPR), which uses the intensity dependent changes in the state of polarisation of orthogonally polarised pulse components propagating in a fibre, due to nonlinear effects as SPM or XPM. Firstly developed in the same period at the beginning of the 1990s [26], NPR is a mode-locking mechanism similar to that of NALM, based on additive pulse mode-locking, only in this case the two components are the orthogonally polarised states. The cavity design, though, is simpler, as only one loop is necessary -Fig. 4.3-. The passive mode-locking device is basically a linear polariser placed between two polarisation controllers. The first polarisation controller sets linear polarisation in the center of the pulse. The polariser (which is also an isolator) lets pass the central part of the pulse but not the wings with less intensity. The second polarisation controller has the function of changing the polarisation state of the linearly polarised light exiting the polariser into elliptical. Due to nonlinear effects during

the propagation of the pulse, as phase shift is induced and the polarisation state becomes not uniform across the pulse. Thanks to this mechanism the pulse is shortened [10].

Already in 1992, NPR lasers with additive pulse mode-locking were able to produce 452 fs pulses from a self-starting single ring with erbium doped fibre [27]. Pulses could be shortened and energy increased by adding a section of positive dispersion Er-doped fibre, resulting in 77 fs pulses with pulse energy of 90 pJ and peak power >1 kW for a 45 MHz repetition frequency [28]. Performances could be further improved with cavities with positive net dispersion [29]. This may be achieved simply by adjusting the relative length of the fibres with opposite dispersion, creating a dispersion managed resonator. In the section with normal GVD the pulses experience pulse stretching, which aids in the generation of higher energies. In this type of lasers the position of the output coupler plays an important role on the pulse width, as it varies throughout the cavity [30]. A drawback is that the length of the cavity, which is important to create the nonlinear phase shift, may be an important source of environmental instability.

It is worth notice how all these cavities rely on an unidirectional ring configuration, which has been proven to facilitate self-starting mode-locking [31, 32], because mode pulling decreases mode coherence time and reflections, which will cause it, are reduced in a ring cavity [11].

4.3 InN as Semiconductor Saturable Absorber Mirror

Typical semiconductors used as saturable absorbers are InGaAs and GaAsSb, for example [33]. Besides such traditional semiconductors, several materials and structures have been proposed and implemented over time as saturable absorbers, such as graphene, carbon nanotubes, few layers transition metal dichalcogenides, golden nanoparticles, black phosphorus and topological insulators, among others [34, 35, 36, 37, 38, 39, 40]. Although all these materials have interesting properties, they present a drawback which is their damage threshold, which is quite low limiting their power range of operation.

Also, III-nitrides semiconductors, as AlN, GaN, InN and their alloys, can behave as saturable absorbers for the C-band, because they have a direct optical band gap. Moreover, they have high thermal and chemical stability and high nonlinearities due to their asymmetrical crystalline structure.

In the work related with this thesis we have used a novel non-commercial SESAM based on InN. InN was proposed, characterised and tested for the first time as saturable absorber both in transmission and reflection configuration by our collaborators of the Photonics Engineering Group from Universidad de Alcalá (Alcalá de Henares, Spain) [41, 42, 43]. The SESAM sample used in this study was provided by Dr Eva Monroy of Université Grenoble-Alpes, CEA-RIG-PHELICS (Grenoble, France).

Wurtzite (0001)-oriented InN displays some outstanding properties as a saturable absorber, including high thermal and chemical stability, extremely high fluence tolerance (> 1 TW/cm^2), high nonlinear absorption (thus, high modulation depth) and insensitiveness to polarisation, which is extremely practical for operation in an ultralong cavity. The InN-based SESAM proposed consists of a 1-μm-thick InN thin film grown by plasma-assisted molecular-beam epitaxy (PAMBE) on a commercial 4-μm-thick GaN-on-sapphire template (details on the process can be found in [41]). The characterization of the InN-based SA in trasmission operation can be found in [42], but in the current project the material has been used as a SESAM [43]. For that, a mirror of 300-nm-thick layer of highly reflective aluminum has been deposited on the InN layer by RF sputtering at room temperature. From the experimental data, a saturation fluence of 226 $\pm$ 23 μJ/cm^2 (which translates into a saturation intensity of 2.0 GW/cm^2), a linear reflectance of 25 $\pm$ 3%, a nonlinear reflectance of 50 $\pm$ 5% and a modulation depth of 25% are estimated (considering that the effective length of the active layer increases in respect to that of the same saturable absorber in transmission). The nonlinear reflectance curve of the SESAM can be seen in Fig. 4.4

4.4 Basic laser and optical pulse parameters

It is worth define and remember how are calculated some laser and optical pulse parameters -Fig. 4.5- before exploring the experimental results obtained.

- $\Delta\tau$, temporal pulse width or pulse duration, is the time evolution at full width half maximum (FWHM) of the temporal intensity of a pulse. It is expressed in a unit of time, generally fs or ps for ultrashort pulses.

- $\Delta\lambda$, spatial pulse width, is the length of the optical spectrum of the pulse at FWHM in the spatial domain. It is usually measured in nm.

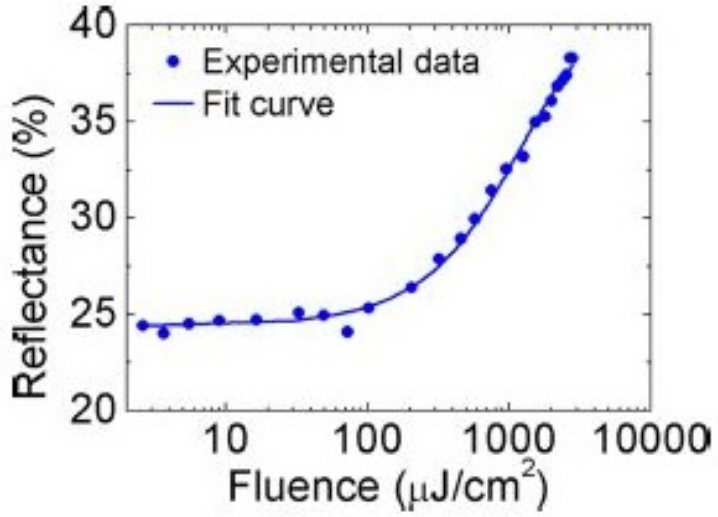

Figure 4.4: Nonlinear reflectance (%) curve of InN SESAM as a function of the incident fluence (J/cm2) [43].

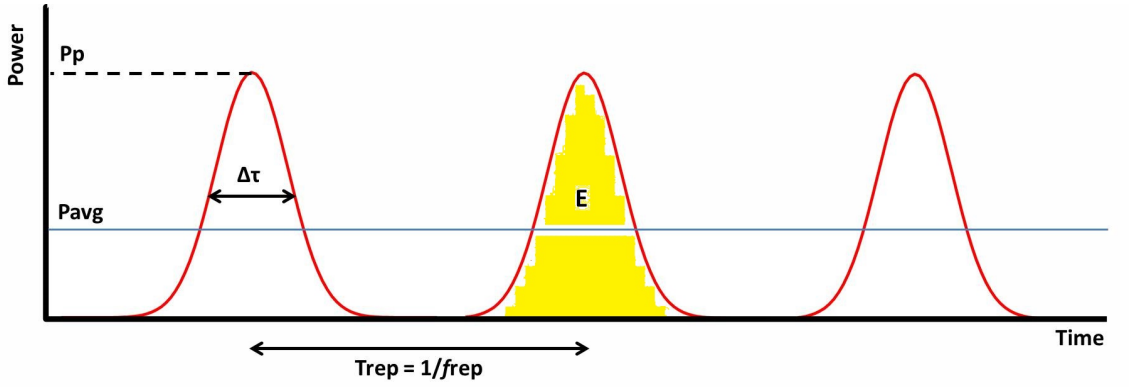

Figure 4.5: Scheme of the paramaters of a pulse.

- f_{rep}, repetition frequency or rate, is the frequency of a regularly emitted pulse train defined as the number of emitted pulses per second, which is the same as the inverse temporal pulse spacing: $f_{rep} = 1/T_{rep}$, where T_{rep} is the pulse period, the temporal separation between consecutive pulses. Fibre lasers may present a wide range of repetition frequencies.

- P_{avg}, average power, is the power averaged over a period which can be directly measured at the output of the laser and give information about the total power recirculating in the cavity. It is usually in the order of mW.

- E_p, pulse energy, is the total energy contained in a single pulse. It is usually measured in nJ or pJ in ultrafast lasers.

- P_p, peak power, is the maximum power reached by the pulse, which is usually no more than a few tens of kW in an ultrafast laser. In the case of a square pulse the peak power equals the rate of energy flow: $P_p = E_p/\Delta\tau$, with $\Delta\tau$ the pulse FWHM. For different types of pulses it can be calculated as as this rate times a constant factor that depends on the pulse shape. The peak power and the average power are thus related by:

$$P_p = CP_{avg}\frac{T_{rep}}{\Delta\tau} = C\frac{P_{avg}}{f_{rep}\Delta\tau}. \tag{4.4}$$

  Where C usually takes a value close to 1 (0.88 for solitonic pulses and of 0.94 for Gaussian pulses, for example). So through the direct measure of P_{avg} and T_{rep}, we can calculate E_p and thus estimate P_p from the pulse duration $\Delta\tau$ and its shape.

4.5 Ultrafast passively mode-locked ring fibre laser with InN SESAM: overcoming the megawatt peak power

As we have previously explained in this chapter, passive self starting mode-locking is a convenient feature in fibre lasers, which may be easily achieved using a ring configuration for the resonator and introducing some form of saturable absorber in the cavity, leading to the production of very short pulses [1, 3, 11]. Among the possible configurations for the implementation of the saturable absorption in the laser device, the use of a SESAM has been shown to be both highly efficient in achieving mode-locking and simple to implement.

In spite of their undeniable advantages, ultrafast passively mode-locked fibre lasers' application is still restricted in certain areas, mostly due to their achievable pulse energy and peak power (in particular if a "simple" system needs to be maintained), with the latter limited in practice up to date to the few hundreds of kW for ultrashort pulses in the femtosecond range. This constrain hinders their use in the power-demanding materials processing or industrial solutions, where other options, such as solid-state lasers, dominate.

The most straightforward way to increase pulse energy would be to increase the resonator length, but the usual outcome of this procedure in fibre ring lasers is the extension of the temporal width of the pulses to the nanoseconds range [44, 45, 46, 47, 48, 49] due to dispersive effects. Although recent times have seen the development of passively mode-locked fibre lasers capable of reaching the MW pulse peak power through the use of

specifically engineered photonic crystal fibre [50, 51], such goal seemed unattainable using low-cost conventional communications fibre.

In this work we have exploited InN as the basis for a novel polarisation insensitive semiconductor saturable absorber mirror [41, 42], operating in the telecommunication C-band, in combination with the use of ultralong fibre laser cavities [52, 53] and standard telecommunication-grade Erbium-doped fibre amplifiers, with the objective of overcoming of the previous power limitations of conventional fibre-based passively mode-locked ring fibre lasers to develop a high-power ultrafast ring fibre laser, paving the way for a new generation of compact, low-cost and reliable sources to be applied in highly power-demanding materials processing and operating at standard telecommunications wavelengths.

4.5.1 Experimental set-up

Figure 4.6 represents the basic configuration of the proposed high-power ultrafast ring fibre laser, operating counter-clockwise according to the depicted scheme. The resonator uses an off-the-shelf EDFA with on-off operation (non-adjustable gain level) and a maximum output saturated power of 24 dBm as the gain medium, and relies on a SESAM. A polarisation-independent Faraday fibre isolator is located at the output of the EDFA to ensure unidirectionality of the cavity. The ring cavity is made of a 16 m piece of Erbium-doped fibre in the EDFA and a selectable reel of standard single-mode fibre of multiple possible lengths and characteristics, ranging from a few hundred meters to a few kilometers, located between the EDFA and the SESAM. The SESAM section is a free space set-up in which losses have been adjusted to be of the order of 24 dB. Although losses could be reduced through efficient alignment and beam focusing in the coupling to the small-core area fibre, as we will see below, having the SESAM operate in a fairly lossy regime eliminates the need for the insertion of an additional attenuator.

Standard, off-the-shelf fibre optical components are used to complete the experimental scheme: an optical circulator to connect the cavity with the SESAM, a variable optical attenuator (VOA) located before the EDFA to control the ingoing power into the amplifier and a fibre coupler at the laser output (a 70%/30% coupler was chosen, since it resulted in the highest output powers under mode-locking conditions). A part from the EDFA, all the other components rely on standard single-mode telecommunications optical fibre, so the resonator can be considered to operate in the anomalous dispersion regime.

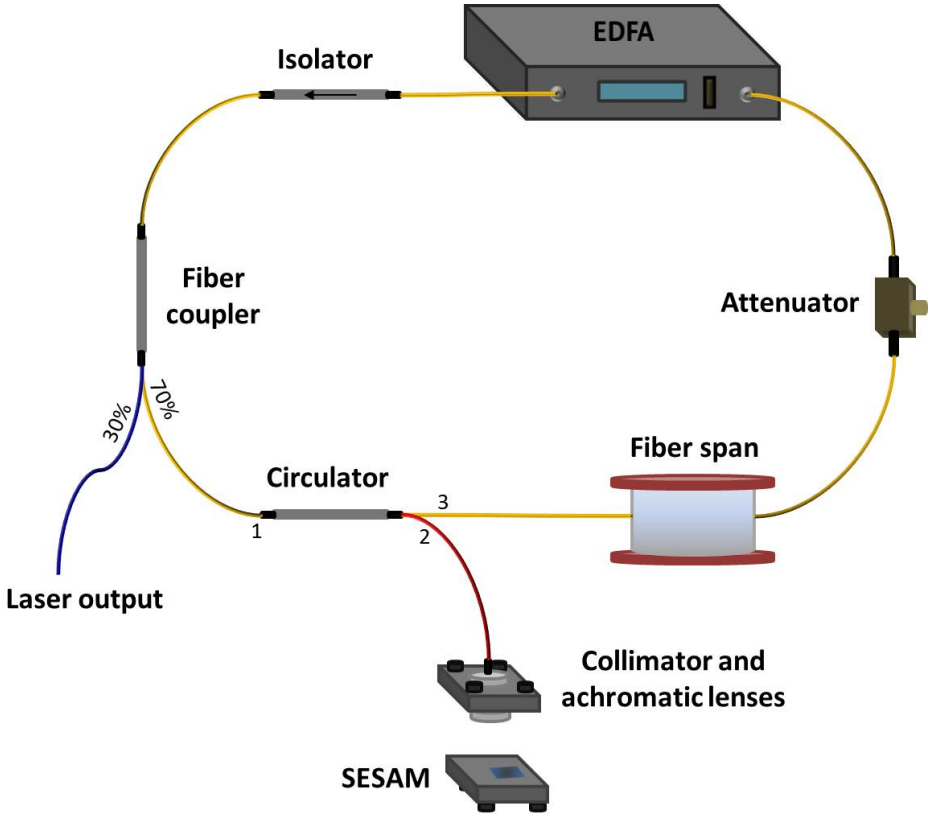

Figure 4.6: Fibre laser set-up. The operation of the laser is counter-clockwise.

The InN based SESAM was described in section 4.3. As a reference, the performance of the system is compared to that of the same setup relying instead on a commercially available GaAs-based SESAM (SAM-1550-55-2ps-x from BATOP Optoelectronics) operating at the same wavelength and consisting of a GaAs-based thin film on a distribute Bragg reflector mirror. According to the manufacturer, the maximum of absorption for this material is found around 1550nm, where a linear reflectance between 40 - 45% is obtained. Due to the strong dependence on polarisation of the active layer, it was not possible to directly measure its full characteristics in the same way as with the InN-based SESAM, but a saturation fluence of 40 $\mu J/cm^2$ and a linear and non-saturable reflectances of 45% and 79% respectively have been calculated, thus a modulation depth of 34% is estimated.

4.6 Experimental measurements

In order to study the stable pulse train obtained at 1.56 μm, autocorrelation traces for the measurement of the duration of the pulses, optical spectra, radio frequency (RF) spectra for the measurement of the repetition frequency and round trip period, and average power

are recorded at the laser output. These direct measurements will allow us to get the information about peak power and pulse energy, as we saw in section 4.5. Four different ring configurations (based on their length) and their operation (when pulsed regimes are achievable) with both SESAMs have been studied: the basic ring (no added SSMF span is introduced), which is around 40 m long, a 1.05 km long cavity (where a 1 km SSMF span is inserted in the ring), a 1.67 km long cavity and a 2.37 km long cavity. Further measurements were undertaken with the InN-based setup for longer ring configurations to study higher harmonics mode-locking.

4.6.1 Basic ring configuration

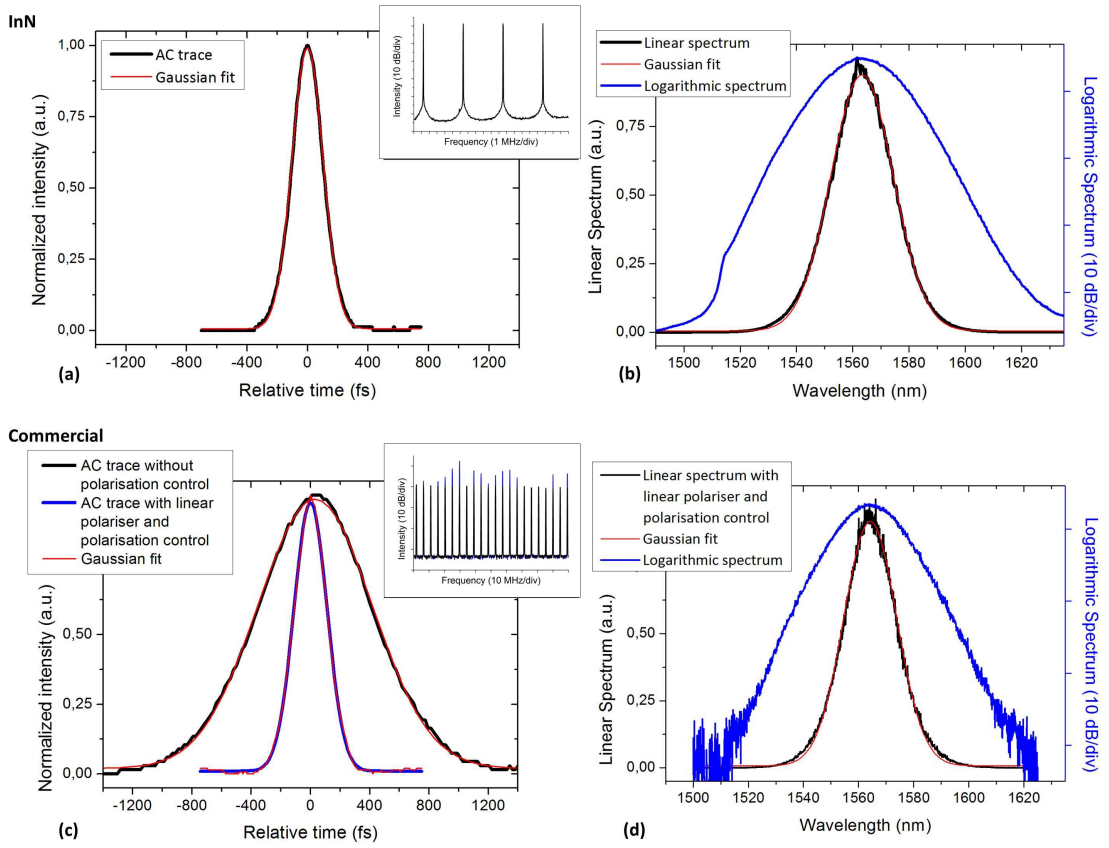

Figure 4.7: Autocorrelation traces (a, c) and optical spectra (b, d) in linear (black line, Gaussian fit in red) and log scale (blue line) of the basic ring configuration with InN (a, b) and commercial SESAM with linear polariser and polarisation control (c, d). Inset: corresponding RF spectrum.

Given the polarisation-insensitive response of the InN, no polarisation control is needed in the system to achieve stable mode-locking. The basic ring locks to its fundamental mode generating a 239 ± 6 fs Gaussian pulse train with a repetition rate around 5 MHz and a

spectral bandwidth of 24.6 ± 0.5 nm (hence not transform-limited). Average output power is around 33 mW, which translates into a peak power of the pulse of around 26 kW and an energy around 6 nJ -Fig. 4.7 (a) and (b). The insertion of a polarisation controller anywhere in the ring does not have an impact on pulse characteristics. With or without polarisation control, the output degree of polarisation is low, between 1% and 15%.

Polarisation control has, on the other hand, an important impact on pulse generation when using the commercial GaAs-based SESAM. Without polarisation control, mode-locking to 0.9 ± 0.1 ps Gaussian-like pulses is obtained, with maximum output peak powers of 5.3 kW and energies of about 5.8 nJ. The insertion of a polarisation controller before the EDFA allows for tunable pulse widths up to 1.1 ± 0.1 ps. Still, at such powers, Kelly side-bands appear, and fundamental mode-locking is highly unstable. Variations of the polarisation state allow for the switching between fundamental and either 2^{nd} or 3^{rd} order mode-locking.

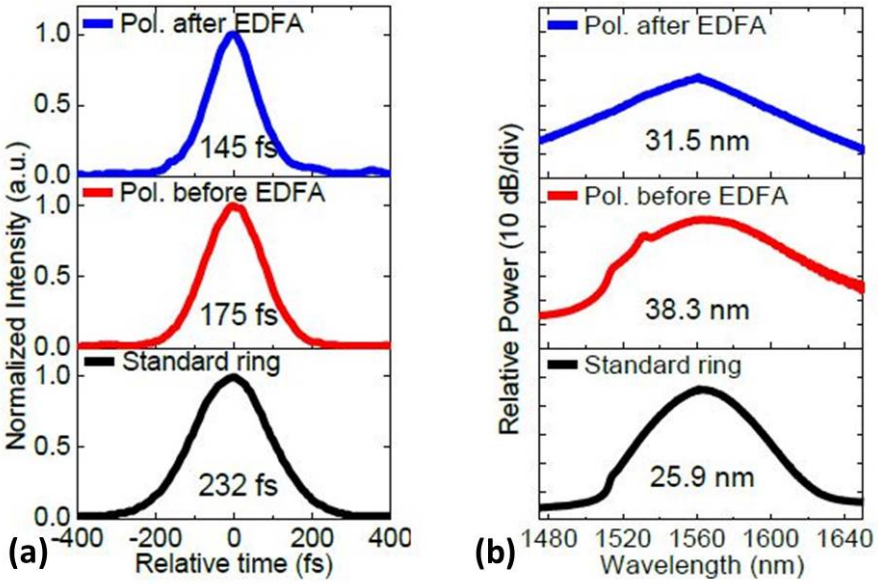

Figure 4.8: Autocorrelation traces (a) and optical spectra (b) with and without polarisation control. Temporal and spectral widths at FWHM shown in figure [54].

Although polarisation control alone does not have any effect on the performance of the InN SESAM based ring laser, the introduction of an additional nonlinear polarisation rotation evolution absorber module in the ring can offer some control over pulse characteristics. This can be easily achieved by placing a linear polariser and a polarisation controller before amplification stage. The combined effects of the new saturable absorbtion module and the InN SESAM make it possible to tune pulse duration between 170 and 320

fs through selection of the state of polarisation of the input signal into the EDFA, always without losing stable mode locking to the fundamental (single soliton) mode - Figs. 4.8(a) and (b)-. The polarisation control system may also be introduced after the EDFA. In this case the spectral shape of the output pulses changed, with a temporal pulse-width of 150 fs, also becoming soliton-like, in contrast with the other two configurations (without any polarisation control and with polarisation control before the EDFA), where more clearly Gaussian-like pulses were obtained. In the polarisation-controlled configurations, the laser output is of course highly polarised.

Introducing the same kind of polarisation control (linear polariser and polarisation control before the EDFA) in the ring with the commercial SESAM, it is possible to switch from the regime with unstable 0.9 ps pulses and visible Kelly side-bands to 260 fs pulses with Gaussian spectra locked to the fundamental mode in the optimal configuration -Fig. 4.7 (c) and (d). Mode-locking in this case is actually caused exclusively by nonlinear polarisation rotation, which was verified by removing the SESAM itself, obtaining identical pulse characteristics.

4.6.2 Optimal cavity length: 1.05 km long resonator

As mentioned above, increasing pulse energy by the simple method of extending cavity length (i.e. reducing the repetition rate) while maintaining average output power, eventually leads to pulse degradation in passively mode-locked fibre ring lasers through fibre dispersive effects, pulse destabilization due to polarisation, power loss through Raman conversion, distortion due to increased nonlinear effects and, if energies are high enough, potential damage to the saturable absorber. As we will see, all these deleterious effects have been avoided by using a polarisation-insensitive SESAM and moderate average powers leading to first-order mode-locking in solitonic regimes.

We tested this hypothesis by initially extending our ring cavity with a 1 km standard telecommunication single-mode fibre (ITU G.652) span, relying on the two different SESAMs. Mode-locking is in this case not achievable by using only the polarisation rotation setup (linear polariser + polarisation control). On the other hand, mode-locking to higher harmonics is easily achievable with both SESAMs. In the case of the commercial SESAM polarisation needs to be controlled, while this is not necessary for the InN SESAM. Finally, in order to obtain fundamental mode-locking, cavity losses need to be increased by

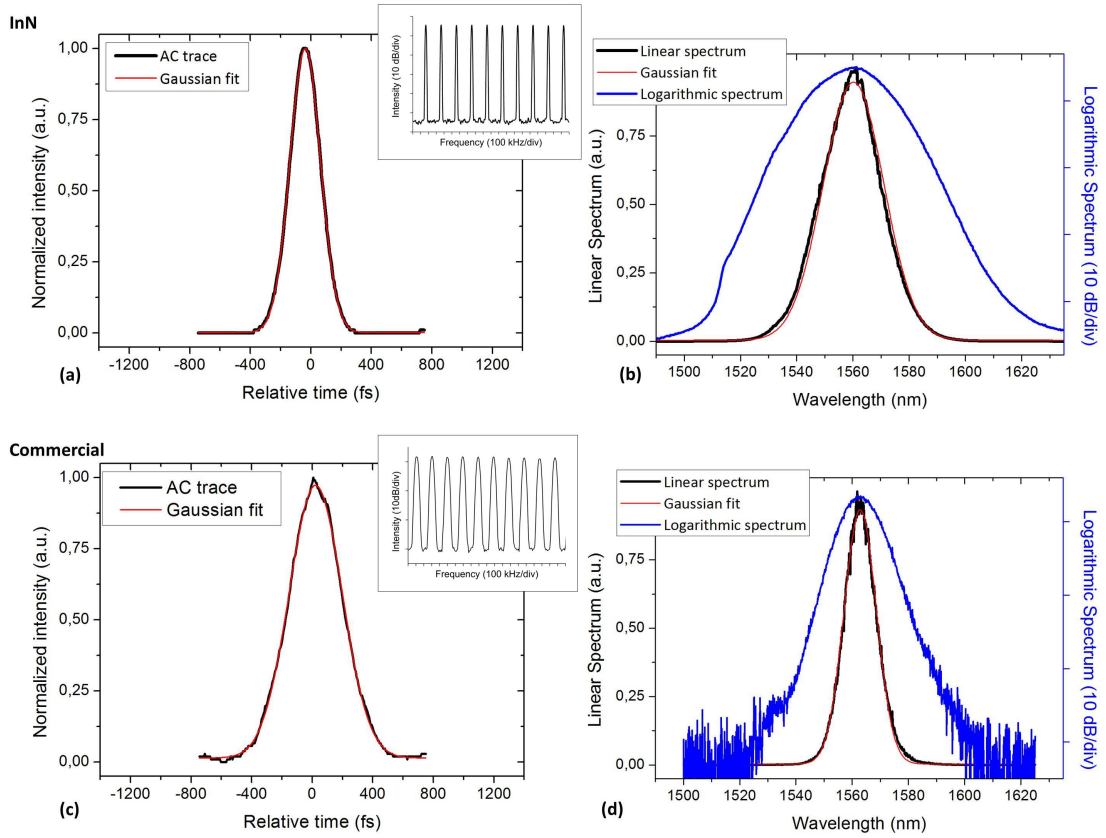

Figure 4.9: Autocorrelation traces (a, c) and optical spectra (b, d) in linear (black line, Gaussian fit in red) and log scale (blue line) of the 1.05-km-long ring configuration with InN (a, b) and commercial SESAM with linear polariser and polarisation control (c, d). Inset: corresponding RF spectrum.

means of the VOA. At this point, the difference between the response of the two materials becomes clear. Fundamental mode-locking is easily obtained with the InN-based SESAM, where the average output power is lowered only by a few mW, whereas the commercial SESAM requires lowering the average power below 20 mW. Relying on the commercial SESAM, linear polariser and polarisation controller, pulses temporally broaden to up to ∼410 ± 10 fs in the much longer cavity as can be appreciated from Fig. 4.9 (c) and (d), with a spectral width at FWHM of 13.5 ± 0.5 nm. In contrast, the pulses obtained with the InN SESAM are still very similar to those obtained from the basic resonator, with a temporal width at FWHM of 239 ± 6 fs and a spectral width of 25.4 ± 0.5 nm. Symmetric and clean Gaussian spectra are obtained, without significant contribution of EDFA-generated ASE contributing to the inter-pulse continuous white noise component, so almost all the energy is contained in the pulses. Indeed, the integrated energy in the signal spectrum deviates less than 0.1% from that of a perfect Gaussian pulse train at the

output of an ideal laser with identical repetition rates and output average powers. For the InN-based set-up, pulses with a peak power of 650 kW and pulse energy of 155 nJ are produced, with a measured repetition rate of 196 kHz (in perfect agreement with the cavity round-trip for a 1.05 km length) and an average output power of 30.5 mW. The solution based on the commercial GaAs SESAM offers a maximum peak power of 236 kW and a pulse energy of 97 nJ, with much broader pulses and average powers below 20 mW. Please note that the insertion losses between the output of the EDFA and the entrance to the standard single-mode fibre span have been measured to be of the order of 27 dB. This leads to peak powers for the generated pulse train of approximately 1.3 kW at the entrance to the SMF, slightly above the fundamental soliton peak power for the pulse duration, but well below the maximum peak power for solitons of order $N = 2$.

4.6.3 Performance improvement: megawatt femtosecond ultralong ring fibre laser

The 1.05 km resonator with the InN-based configuration achieves stable mode locking with extremely clean Gaussian pulses in both the autocorrelation trace and the optical spectra, but it is possible to further increase peak power and energy by increasing cavity length while still achieving mode-locking to the fundamental mode. On the other hand, mode-locking in longer resonators is not feasible with the commercial SESAM. As it can be seen in Fig.4.10 (c) and (d), increasing cavity length to 1.67 km with the commercial SESAM-based system allows for the formation of pulses of about 1 ps with spectral widths of 5 nm, with only partial mode-locking (as visible in the inset), whereas any longer cavity fails to achieve even that. The same length of fibre in the ring with the InN SESAM leads to perfectly auto-correlated Gaussian pulses with a temporal width slightly shorter than in the 1.05 km cavity configuration (234 $\pm$ 6 fs). Optical spectra start to show some noise and the appearance of a visible shoulder at 1530 nm that can be attributed to the EDFA gain spectrum together with a lower achievable average power at the output ($\sim$26 mW) for mode-locking. Nonetheless, the integral of the areas underlying the optical spectra and the Gaussian fit curves differ by less than 1%. So, for the 1.67 km, we obtain a repetition rate at fundamental mode-locking of 124 kHz, a peak power of 0.9 MW and a pulse energy over 200 nJ.

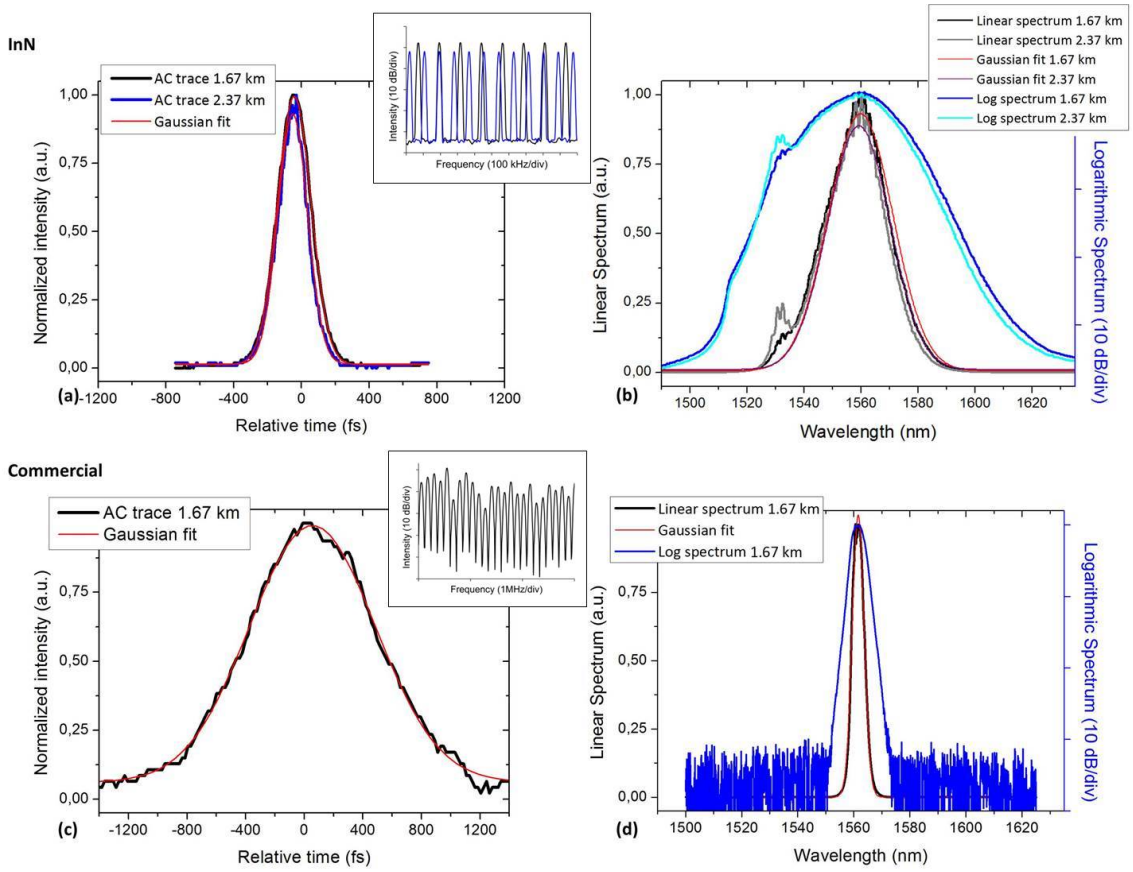

Figure 4.10: Autocorrelation traces (a, c) and optical spectra (b, d) in linear (black and grey line, Gaussian fit in red and purple) and log scale (blue and light blue line) of the 1.67 and 2.37-km-long rings configuration with InN (a, b) and commercial SESAM with linear polariser and polarisation control (c, d). Inset: corresponding RF spectrum.

Mode-locking to the fundamental mode with the InN-based SESAM can be achieved even for longer cavities, up to 2.37 km long. In spite of a clear increase of the noise, reflected in the aforementioned asymmetric shoulder in the optical spectrum around 1530 nm, the difference between spectrum and fitting is still low enough to consider most of the energy to be contained in the pulse (which goes up to 263 nJ) and, thanks to the low repetition frequency at FML (87 kHz) and short temporal width (207 $\pm$ 6 fs), the peak power overcomes the "barrier" of the megawatt (1.269 MW) -Fig.4.10 (a) and (b)-. As in the case of the 1.05 km resonator, the peak power at the entrance of the SMF fibre is in this case approximately 2.5 kW, higher than that of an ideal fundamental soliton pulse, but below the maximum peak power for $N = 2$ for the measured pulse duration. This closeness to the fundamental soliton guarantees a good preservation of the the pulse profile in its propagation across the 2.37 km of SMF.

For clarity, in Table 4.1 we have summarized the tested configurations, their specifications and the obtained results.

Table 4.1: Summary of the measured and calculated values for the different configurations.

Ring configuration	SESAM	Average power (mW)	Temporal width at FWHM (fs)	Spectral width at FWHM (nm)	Repetition frequency (MHz)	Resonator length (m)	Peak Power (kW)	Pulse Energy (nJ)
Basic	InN-based	33.2	239	24.6	5.164	38.7	26.6	6.4
Basic	commercial	32.8	263	22.6	4.650	44.5	26.8	7.0
1.05 km	InN-based	30.5	239	25.4	0.196	1053.4	650.2	155.4
1.05 km	commercial	19.0	412	13.5	0.195	1061.0	235.7	97.2
1.67 km	InN-based	26.3	234	26.7	0.124	1673.9	908.1	212.5
1.67 km	commercial	32.7	1012	5.0	∼0.12	∼1680.0	-	-
2.37 km	InN-based	23.0	207	25.7	0.087	2369.9	1269.0	262.9

4.6.4 Longer cavities: higher harmonics generation

Even with the InN SESAM set-up, stable locking to the fundamental mode can only be observed in cavities up to 2.37 km long. For longer rings, stable mode-locking to higher harmonics is reached after a noisy transition regime, by adjusting loss at the attenuator. Indeed, highly stable harmonic mode-locking at higher modes has been obtained for rings from 1.05 to 5.67 km long. This allows a broad choice of peak powers and repetition rates. In Fig. 4.11 a set of different harmonics obtained with a 5.67 km cavity are shown, with temporal widths from ∼360 fs (3^{rd} harmonic) to ∼600 fs (12^{th} harmonic) and an average output power increase from 22 mW to 31 mW as the harmonic mode increases. In the optical spectrum, the peak due to the EDFA gain spectrum around 1530 nm is here clearly visible as the spectral width at FWHM is reduced (down to 11 nm).

In Chapter 6 we will discuss the possibility to elongate even more the laser cavity and how to overcame the problem of losses in the fibre, that for a longer length could not be considered negligible anymore.

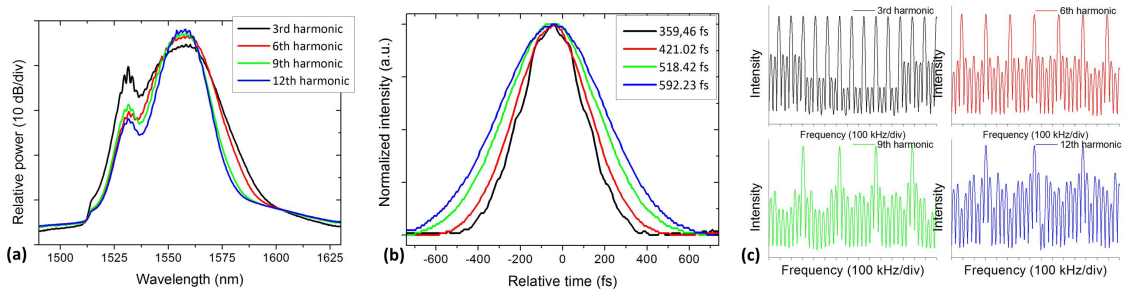

Figure 4.11: Optical spectra in log scale (a), autocorrelation traces (b) and RF spectra (c) of a 5.67 km long cavity producing higher harmonic mode locking.

4.7 Discussion of the results

Obtaining subpicosecond pulses with MW peak-power directly out of a standard telecommunication fibre-based laser oscillator represents a considerable challenge that has been overcome only thanks to the combination of two different techniques. The first one is the use of a novel, polarisation-insensitive InN SESAM that can operate at high fluences, whereas the second one is the adequate management of power and thus nonlinearities inside the cavity. The latter is achieved by attenuating the signal prior to its entrance into the SMF fibre so pulse peak power at the input of the SMF is always close to that of the fundamental soliton, as well as by reducing, if necessary, by means of a variable optical attenuator, the signal power entering the EDFA. By injecting pulses close to the fundamental soliton into the SMF, we are allowing for stable ultrashort pulse propagation over longer distances. Although some pulse breathing can be expected, pulses can adapt adiabatically to a fundamental soliton over multiple dispersion lengths. In addition, by limiting the power entering the EDFA we exert some control over both output power and signal evolution in the EDF section, obtaining limited selectivity over the harmonic to which the laser locks in.

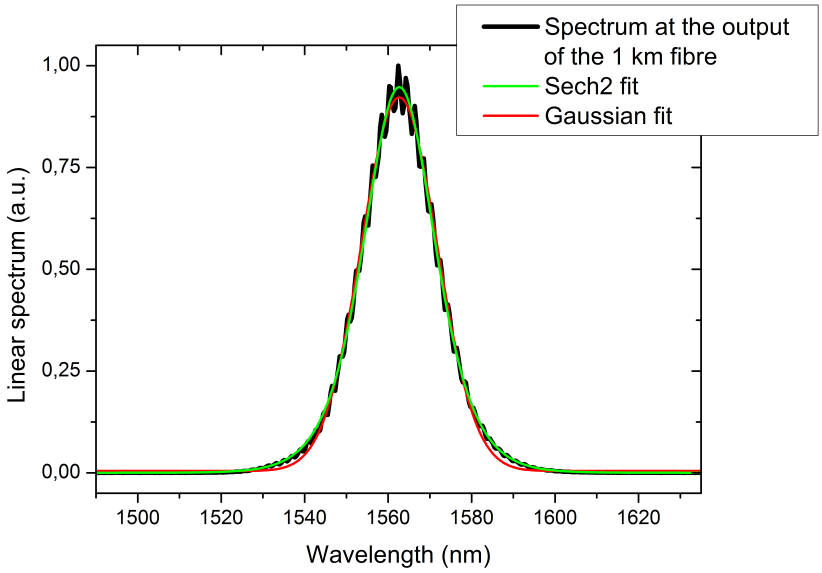

Figure 4.12: Laser spectrum at the output of the 1-km SMF (black), and respective Gaussian (red) and $sech^2$ (green) curve fits.

Figure 4.12 offers confirmation of the soliton-propagation phase by displaying the

output laser spectrum obtained through a 5% tap and measured in the optical spectrum analyser immediately after the SMF fibre for the 1 km cavity. As can be readily seen, the spectrum at this point follows a $sech^2$ profile, whereas, as we have seen in previous sections, the spectrum and the output pulse profile at the laser output, located after the amplifier stage, are closer to a Gaussian. To illustrate pulse dynamics in the SMF we have performed a simple numerical simulation using the non-linear Schrdinger equation detailing pulse evolution in the 2.37 km configuration. In this case, pulses enter the SMF fibre with a 207 fs FWHM duration and a peak power of 2.5 kW, higher than that of a fundamental soliton but lower than that of a 2^{nd} order one. As expected, the pulse relaxes into a slightly narrower soliton as it traverses the fibre, exiting as a 3.75 kW pulse with a FWHM of 112 fs (see Figure 4.13, below). The total attenuation experienced by the pulse is 0.47 dB. In this simplified model we have assumed that the pulses are initially unchirped.

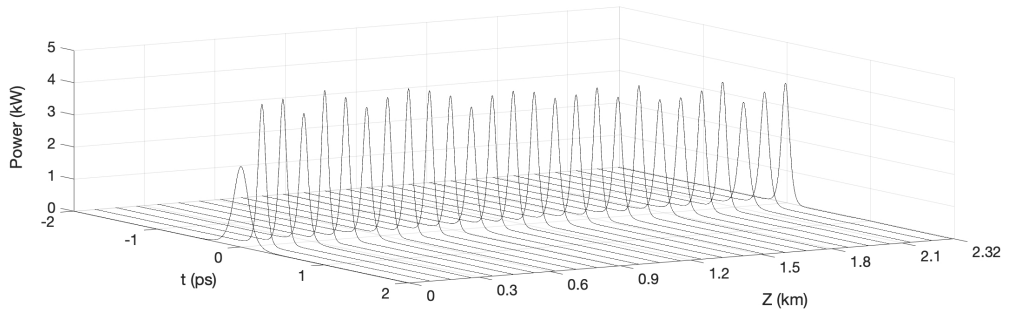

Figure 4.13: Simulated temporal pulse evolution in the SMF fibre for the 2.37 km ring configuration.

The evolution of these initially soliton-like pulses through the pumped 16 m EDF will depend strongly on fibre characteristics, as well as on the spatial and spectral gain distribution. In a normal dispersion EDF, the injected pulses can evolve into a weakly-chirped gain-guided soliton [55] with a characteristic Gaussian profile similar to the one observed in our autocorrelation traces. Similarly, a low enough dispersion EDF, whether in the normal or anomalous regime, could support stable pulse propagation over the short amplified section.

4.8 Conclusions

An inexpensive, polarisation-independent, harmonically mode-locked ultralong fibre ring laser operating at 1.56 μm based on the use of an InN SESAM has been demonstrated.

This setup is, to the best of our knowledge, the first passively mode-locked ultralong fibre master oscillator capable of achieving peak powers above 1 MW with ultrashort pulses in the fs range, without resorting to additional pulse compression or amplification stages. In particular, stable mode-locking to the fundamental mode has been achieved with a range of cavities up to 2.37 km long, while mode-locking up to the 12^{th} harmonic has been demonstrated with longer cavities. Moreover, the generated pulses are in no case transform-limited, which implies the potential for additional pulse compression (see Chapter 5).

References

[1] A. J. Demaria, D. A. Stetser, and H. Heynau, "Self mode-locking of lasers with saturable absorbers," *Appl. Phys. Lett.*, vol. 8, no. 7, pp. 174–176, 1966.

[2] C. V. Shank and E. P. Ippen, "Subpicosecond kilowatt pulses from a modelocked cw dye laser," *Applied Physics Letters*, vol. 24, no. 8, pp. 373–375, 1974.

[3] H. A. Haus, "Theory of mode locking with a fast saturable absorber," *J. Appl. Phys.*, vol. 46, no. 7, pp. 3049–3058, 1975.

[4] G. H. C. New, "Mode-locking of quasi-continuous lasers," *Optics Communications*, vol. 6, no. 2, pp. 188–192, 1972.

[5] M. E. Fermann and I. Hartl, "Ultrafast fibre lasers," *Nat. Photonics*, vol. 7, no. 11, pp. 868–874, 2013.

[6] W. H. Knox, "Ultrafast technology in telecommunications," *IEEE J. Sel. Top. Quantum Electron.*, vol. 6, no. 6, pp. 1273–1278, 2000.

[7] E. Snitzer, "Optical maser action of Nd+3 in a barium crown glass," *Phys. Rev. Lett.*, vol. 7, no. 12, pp. 444–446, 1961.

[8] M. E. Fermann and I. Hartl, "Ultrafast Fiber Laser Technology," *IEEE J. Sel. Top. Quantum Electron.*, vol. 15, no. 1, pp. 191–206, 2009.

[9] V. Ter-Mikirtychev, *Fundamentals of fiber lasers and fiber amplifiers.* Springer Series in Optical Sciences, 2014, vol. 181.

[10] G. P. Agrawal, *Applications of Nonlinear Fiber Optics.* Academic Press, 2008.

[11] L. E. Nelson, D. J. Jones, K. Tamura, H. A. Haus, and E. P. Ippen, "Ultrashort-pulse fiber ring lasers," *Appl. Phys. B Lasers Opt.*, vol. 65, no. 2, pp. 277–294, 1997.

[12] H. A. Haus, "Mode-locking of lasers," *IEEE J. Sel. Top. Quantum Electron.*, vol. 6, no. 6, pp. 1173–1185, 2000.

[13] R. Paschotta, *Field guide to laser pulse generation.* SPIE Press, 2008.

[14] U. Keller, "Recent developments in compact ultrafast lasers," *Nature*, vol. 424, no. 6950, pp. 831–838, 2003.

[15] F. X. Kärtner, J. Aus Der Au, and U. Keller, "Mode-locking with slow and fast saturable absorbers - What's the difference?" *IEEE Journal on Selected Topics in Quantum Electronics*, vol. 4, no. 2, pp. 159–168, 1998.

[16] O. E. Martinez, R. L. Fork, and J. P. Gordon, "Theory of passively mode-locked lasers for the case of a nonlinear complex-propagation coefficient," *J. Opt. Soc. Am. B*, vol. 2, no. 5, pp. 753–760, 1985.

[17] U. Keller, K. J. Weingarten, F. X. Kärtner, D. Kopf, B. Braun, I. D. Jung, R. Fluck, C. Hönninger, N. Matuschek, and J. Aus Der Au, "Semiconductor saturable absorber mirrors (SESAM's) for femtosecond to nanosecond pulse generation in solid-state lasers," *IEEE J. Sel. Top. Quantum Electron.*, vol. 2, no. 3, pp. 435–451, 1996.

[18] A. Siegman, *Lasers*. University Science Book, 1986.

[19] I. N. Duling, "All-fiber ring soliton laser mode locked with a nonlinear mirror," *Opt. Lett.*, vol. 16, no. 8, pp. 539–541, 1991.

[20] S. J. Frisken, C. A. Telford, R. A. Betts, and P. S. Atherton, "Passively mode-locked erbium-doped fibre laser with nonlinear fibre mirror," *Electronics Letters*, vol. 27, no. 10, pp. 887–889, 1991.

[21] D. J. Richardson, R. I. Laming, D. N. Payne, M. W. Phillips, and V. J. Matsas, "320 fs soliton generation with passively mode-locked erbium fibre laser," *Electronics Letters*, vol. 27, no. 9, pp. 730–732, 1991.

[22] D. J. Richardson, A. B. Grudinin, and D. N. Payne, "Passive, all-fibre source of 30 fs pulses," *Electronics Letters*, vol. 28, no. 8, pp. 778–779, 1992.

[23] M. Nakazawa, E. Yoshida, and Y. Kimura, "Generation of 98 fs optical pulses directly from an erbium-doped fibre ring laser at 1.57 μm," *Electronics Letters*, vol. 29, no. 1, pp. 63–65, 1993.

[24] T. Tsun, M. Islam, and P. Chu, "High-energy femtosecond figure-eight fiber laser," *Optics Communications*, vol. 141, no. 1, pp. 65 – 68, 1997.

[25] D. Brida, G. Krauss, A. Sell, and A. Leitenstorfer, "Ultrabroadband Er:fiber lasers," *Laser & Photonics Reviews*, vol. 8, no. 3, pp. 409–428, 2014.

[26] V. J. Matsas, T. P. Newson, D. J. Richardson, and D. N. Payne, "Selfstarting passively mode-locked fibre ring soliton laser exploiting nonlinear polarisation rotation," *Electronics Letters*, vol. 28, no. 15, pp. 1391–1393, 1992.

[27] K. Tamura, H. A. Haus, and E. P. Ippen, "Self-starting additive pulse mode-locked erbium fibre ring laser," *Electronics Letters*, vol. 28, no. 24, pp. 2226–2228, 1992.

[28] K. Tamura, E. P. Ippen, H. A. Haus, and L. E. Nelson, "All-Fiber Ring Laser," vol. 18, no. 13, pp. 1080–1082, 1993.

[29] K. Tamura, L. E. Nelson, H. A. Haus, and E. P. Ippen, "Soliton versus nonsoliton operation of fiber ring lasers," *Applied Physics Letters*, vol. 64, no. 2, pp. 149–151, 1994.

[30] K. Tamura, E. P. Ippen, and H. A. Haus, "Pulse dynamics in stretched-pulse fiber lasers," *Applied Physics Letters*, vol. 67, p. 158, 1995.

[31] K. Tamura, J. Jacobson, E. P. Ippen, H. A. Haus, and J. G. Fujimoto, "Unidirectional ring resonators for self-starting passively mode-locked lasers," *Opt. Lett.*, vol. 18, no. 3, pp. 220–222, 1993.

[32] F. Krausz and T. Brabec, "Passive mode locking in standing-wave laser resonators," *Opt. Lett.*, vol. 18, no. 11, pp. 888–890, 1993.

[33] M. Zirngibl, L. Stulz, J. Stone, J. Hugi, D. DiGiovanni, and P. Hansen, "12ps pulses from passively mode-locked laser diode pumped er-doped fibre ring laser," *Electronics Letters*, vol. 27, no. 19, pp. 1734–1735, 1991.

[34] Z. Sun, T. Hasan, F. Torrisi, D. Popa, G. Privitera, F. Wang, F. Bonaccorso, D. M. Basko, and A. C. Ferrari, "Graphene Mode-Locked Ultrafast Laser," *ACS Nano*, vol. 4, no. 2, pp. 803–810, 2010.

[35] D. Popa, Z. Sun, F. Torrisi, T. Hasan, F. Wang, and A. C. Ferrari, "Sub 200 fs pulse generation from a graphene mode-locked fiber laser," *Appl. Phys. Lett.*, vol. 97, no. 20, pp. 1–4, 2010.

[36] S. Y. Set, H. Yaguchi, Y. Tanaka, and M. Jablonski, "Laser Mode Locking Using a Saturable Absorber Incorporating Carbon Nanotubes," *J. Light. Technol.*, vol. 22, no. 1, pp. 51–56, 2004.

[37] J. Koo, J. Park, J. Lee, Y. M. Jhon, and J. H. Lee, "Femtosecond harmonic mode-locking of a fiber laser at 327 GHz using a bulk-like, MoSe_2-based saturable absorber," *Opt. Express*, vol. 24, no. 10, p. 10575, 2016.

[38] M. H. M. Ahmed, A. A. Latiff, H. Arof, and S. W. Harun, "Mode-locking pulse generation with MoS_2PVA saturable absorber in both anomalous and ultra-long normal dispersion regimes," *Appl. Opt.*, vol. 55, no. 15, p. 4247, 2016.

[39] Y. Chen, G. Jiang, S. Chen, Z. Guo, X. Yu, C. Zhao, H. Zhang, Q. Bao, S. Wen, D. Tang, and D. Fan, "Mechanically exfoliated black phosphorus as a new saturable absorber for both Q-switching and Mode-locking laser operation," *Opt. Express*, vol. 23, no. 10, pp. 12 823–12 833, 2015.

[40] J. Lee, J. Koo, Y. M. Jhon, and J. H. Lee, "Femtosecond harmonic mode-locking of a fiber laser based on a bulk-structured Bi2Te3 topological insulator," *Opt. Express*, vol. 23, no. 5, pp. 6359–6369, 2015.

[41] F. Naranjo, P. Kandaswamy, S. Valdueza-Felip, V. Calvo, M. Gonzlez-Herrez, S. Martn-Lpez, P. Corredera, J. ndez, G. Mutta, B. Lacroix, P. Ruterana, and E. Monroy, "Nonlinear absorption of InN/InGaN multiple-quantum-well structures at optical telecommunication wavelengths," *Applied Physics Letters*, vol. 98, no. 3, 2011.

[42] M. Jiménez-Rodríguez, L. Monteagudo-Lerma, E. Monroy, M. González-Herráez, and F. Naranjo, "Widely power-tunable polarization independent ultrafast mode-locked fiber laser using bulk inn as saturable absorber," *Optics Express*, vol. 25, no. 5, pp. 5366–5375, 2017.

[43] M. Jiménez-Rodríguez, E. Monroy, M. González-Herráez, and F. B. Naranjo, "Ultrafast fiber laser using inn as saturable absorber mirror," *J. Lightwave Technol.*, vol. 36, no. 11, pp. 2175–2182, 2018.

[44] H. G. Rosa and E. A. T. de Souza, "Pulse generation and propagation in dispersion-managed ultralong erbium-doped fiber lasers mode-locked by carbon nanotubes," *Opt. Lett.*, vol. 37, no. 24, pp. 5211–5213, 2012.

[45] Y. Senoo, N. Nishizawa, Y. Sakakibara, K. Sumimura, E. Itoga, H. Kataura, and K. Itoh, "Ultralow-repetition-rate, high-energy, polarization-maintaining, er-doped, ultrashort-pulse fiber laser using single-wall-carbon-nanotube saturable absorber," *Opt. Express*, vol. 18, no. 20, pp. 20 673–20 680, 2010.

[46] Y. Cai, C. Zhou, L. Chen, M. Zhang, L. Ren, P. Li, and Z. Zhang, "Sub-100kHz Repetition Rate Mode-locked Dispersion Managed Erbium-doped Fiber Laser," *CLEO/-Pacific Rim 2009*, no. 2, pp. 5–6, 2009.

[47] J. L. Dong, Z. C. Luo, W. C. Xu, A. P. Luo, L. Y. Wang, W. J. Cao, and H. Y. Wang, "Sub-100 kHz repetition rate erbium-doped fiber laser in anomalous dispersion regime," *Laser Phys.*, vol. 21, no. 6, pp. 1111–1114, 2011.

[48] P. Z. Liu, J. Hou, B. Zhang, S. P. Chen, and J. B. Chen, "Passively mode-locked fiber ring laser using semiconductor saturable absorber mirror," *Laser Phys.*, vol. 22, no. 1, pp. 273–277, 2012.

[49] A. Ivanenko, S. Kobtsev, S. Smirnov, and A. Kemmer, "Mode-locked long fibre master oscillator with intra-cavity power management and pulse energy >12 μ J," *Opt. Express*, vol. 24, no. 6, pp. 6650–6655, 2016.

[50] S. Lefrançois, K. Kieu, Y. Deng, J. D. Kafka, and F. W. Wise, "Scaling of dissipative soliton fiber lasers to megawatt peak powers by use of large-area photonic crystal fiber," *Opt. Lett.*, vol. 35, no. 10, pp. 1569–1571, 2010.

[51] L. J. Kong, L. M. Zhao, S. Lefrancois, D. G. Ouzounov, C. X. Yang, and F. W. Wise, "Generation of megawatt peak power picosecond pulses from a divided-pulse fiber amplifier," *Opt. Lett.*, vol. 37, no. 2, pp. 253–255, 2012.

[52] J. D. Ania-Castañón, T. J. Ellingham, R. Ibbotson, X. Chen, L. Zhang, and S. K. Turitsyn, "Ultralong raman fiber lasers as virtually lossless optical media," *Phys. Rev. Lett.*, vol. 96, p. 023902, 2006.

[53] I. Yarutkina, O. Shtyrina, M. Fedoruk, and S. Turitsyn, "Numerical modeling of fiber lasers with long and ultra-long ring cavity," *Opt. Express*, vol. 21, no. 10, pp. 12 942–12 950, 2013.

[54] M. Jiménez-Rodríguez, F. Gallazzi, J. D. Ania-Castañón, E. Monroy, M. González-Herraéz, and F. B. Naranjo, "Sub-200 fs mode-locked fiber laser with inn-based sesam," in *Optics InfoBase Conference Papers*, vol. Part F82-CLEO˙Europe 2017, 2017.

[55] L. M. Zhao, D. Y. Tang, and J. Wu, "Gain-guided soliton in a positive group-dispersion fiber laser," *Opt. Letters*, vol. 31, no. 12, pp. 1788–1790, 2006.

Chapter 5

Supercontinuum generation and pulse compression in single mode fibre with high peak-power femtosecond pulses

First reported by Alfano and Shapiro in 1970 [1], supercontinuum (SC) generation has attracted much attention over the past five decades due to its multiple applications, which include but are not limited to spectroscopy, microscopy, optical coherence tomography, frequency comb based metrology or telecommunications [2, 3, 4, 5, 6]. Over the past few decades, advances in laser and optical fibre technology have propelled the understanding and exploitation of SC generation in optical fibres [7, 8].

Light emitted from a laser undergoes diverse nonlinear and dispersive effects as a major spectral broadening is achieved, generating SC radiation. SC generation in a waveguide such as optical fibre can be obtained either from continuous-wave sources [9, 10, 11, 12, 13, 14, 15] or, more commonly, from the propagation of short pulses generated in an ultrafast laser [16, 17, 18, 12, 13].

In this chapter, after an introduction about supercontinuum generation in optical fibres and pulse compression, we describe a possible direct application of the ultrafast laser sources presented in Chapter 4. They have been employed as part of a simple experimental set-up for supercontinuum generation and pulse compression, which is composed by the

the high peak-power femtosecond passively harmonically mode-locked ring fibre laser, connected to reels of standard low-cost optical fibre with different length and dispersion. Finally, a possible application of the developed supercontinuum laser sources, gas sensing, is proposed and preliminary results are presented.

5.1 General introduction to supercontinuum generation

Supercontinuum generation is a complex process in which laser light is turned into light spanning a very wide spectral bandwidth (usually more than a octave), generally after propagation through a highly nonlinear medium. Supercontinuum can be efficiently achieved in optical fibres. With ultrashort high-power pulses coming from a pulsed laser, supercontinuum can be easily achieved, and its properties partially tailored by simply propagating the pulse through a nonlinear medium with suitable characteristics [19]. Conveniently, both the laser and the nonlinear medium can be fibre-based.

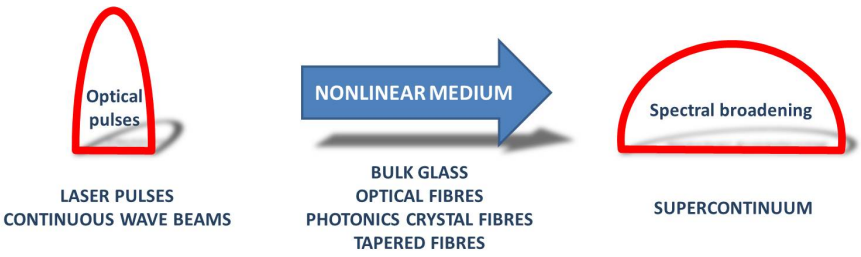

Figure 5.1: Supercontinuum generation overview.

Ultrashort pulses can display very high peak powers with moderate energies. Such optical fields will induce a nonlinear response in a transparent medium. Many nonlinear effects are observable in optical fibres. Those which influence supercontinuum generation are the ones resulting from the third order nonlinear term (Kerr effect, self focusing, FWM, SRS,...).

The generally recognized first report on supercontinuum generation is that by Alfano and Shapiro [1], in which they generated a “white light” source from 400 nm to 700 nm using picosecond pulses in bulk borosilicate glass. They immediately noticed its potential in spectroscopy, as a source useful for the measurement of transient absorption [20]. SC generation in fibres was demonstrated a few years later by Lin and Stolen [21], where the spectral broadening was mainly attributed to cascaded Raman scattering and SPM. Subsequent studies confirmed the role of Raman scattering and SPM, together with XPM

and FWM in broadening and merging the new frequency components of the generated SC [22].

The development of low loss fibres for telecommunication was important also in this area, as nonlinear optics bloomed and fibres soon proved advantageous for SC generation. In fact, in spite of silica's low nonlinear coefficient, optical fibres are especially suitable for SC because of their small effective area and considerable effective interaction length over which the optical processes may act in comparison with a bulk material [7].

5.1.1 Supercontinuum generation in optical fibres

Though the development of photonic crystal fibres (PCF), through the variability of their design, has led to a revolution in SC generation, we will focus here on conventional low-cost single mode fibres, which have been used in the experimental work reported later in this chapter.

SC generation in fibres involves a large number of linear and nonlinear effects, such self and cross-phase modulation, Raman scattering, four wave mixing and other processes resulting from the higher-order nonlinear terms. These effects are mediated by phase relations through dispersive effects, and are also dependent on fibre length, pulse duration, signal power and wavelength. If conveniently both the laser and the nonlinear medium are fibre-based, we can control to a good extent their properties to meet suitable characteristics that will define the output spectrum, as in a fibre we can control nonlinearity, chromatic dispersion and of course fibre length.

We have introduced dispersion in optical fibres in section 2.4.2. Due to its nature dispersion influences the nonlinear interactions in a fibre. In a linear regime, unchirped pulses propagating in a fibre would broaden independently of the GVD sign. This is not the same in a nonlinear regime, in which propagation varies noticeably according to the dispersion regime and the input pulses characteristics (especially pulse duration and peak power). The resulting processes can be very complexes. Very briefly, in a normal regime for sub-picosecond pulses, mainly SPM and FWM cause spectral broadening of a pulse (usually symmetrical to the pump), introducing chirp in the pulse, while longer pulses also undergo SRS, resulting in frequency shift towards longer wavelengths. In anomalous dispersion regime other dynamics are involved in the spectral broadening. For longer pulses the initial broadening is due to MI, than leading to soliton formation, which is the main

agent in the case of ultrashort pulses. In fact the interplay between the linear chirp induced by β_2 and the nonlinear chirp due to SPM can support the propagation of solitons. Higher power pulses induce other dynamics, leading to higher order solitons, where evolution is easily perturbed by other nonlinear effects, such as Raman scattering, and pulse break-up (soliton fission) may ocurr expanding the bandwidth. In addition, if a soliton propagates close to the zero dispersion wavelength of the fibre, part of its energy located in the normal dispersion regime generates a dispersive wave or Cherenkov radiation. Moreover, solitons can be displaced continuously to longer wavelengths (soliton self-frequency shift), since the soliton bandwidths overlap the Raman gain. Part of the complexity of SC generation is due to the fact that the interactions behind it generate new spectral components over a wide spectral bandwidth, which means that some parts may lay in the anomalous dispersion regime while others fall in normal regime.

To model SC generation we can go back to the NLSE in its generalised form including higher order dispersion terms, valid also for pulses with few optical cycles. It takes this form

$$\frac{\partial A(z,T)}{\partial z} - \sum_{k\geq 2} \frac{i^{k+1}}{k!}\beta_k \frac{\partial^k A(z,T)}{\partial T^k} = i\gamma\Big(1+i\tau_{shock}\frac{\partial}{\partial T}\Big)\Big(A(z,t)\int_{-\infty}^{\infty} R(T')|A(z,T-T')|^2 dT'\Big), \tag{5.1}$$

where $A(z,T)$ is the envelope of the electric field

$$E(z,T) = A(z,T)exp(-i\omega_0 T), \tag{5.2}$$

and β_k is the fibre dispersion expressed as Taylor series expansion coefficients (up to ten terms can be necessary to achieve reliable accuracy over a wide spectral bandwidth), γ is the nonlinear coefficient, τ_{shock} is the time scale and $R(T) = (1 - f_R)\delta(T) + f_R h_R(T)$ is the nonlinear response function including Kerr and Raman responses. For proper accuracy also the noise should be included.

SC generation can be produced by ultrashort femtosecond pulses, longer pulses (picosecond and nanosecond range) and also CW radiation. The underlying mechanism varies in accordance with the source and the dispersion regime is always important.

For supercontinuum generation with femtosecond pulses, SPM is usually the main cause of spectral broadening. In the anomalous dispersion regime, the input pulses are usually

higher-order solitons, which at first undergo their typical dynamics (breathing, spectral broadening and temporal compression). But they frequently depart from soliton dynamics, ending in soliton fission, due to perturbations such as higher order dispersion or SRS. If propagation occurs close to the zero dispersion wavelength, the evolution of the solitons after break up is different. A dispersive wave is generated in the normal dispersion regime and continued propagation leads to a shift towards longer wavelengths due to Raman soliton self frequency shift and XPM [23, 24]. If the input pulses propagate in the normal dispersion regime, SPM and Raman scattering are the principal sources of the broadening, but close to the zero dispersion wavelength the situation is similar to those described for the same case in the anomalous regime.

Pumping with high power picosecond or longer pulses in the anomalous dispersion regime, the higher order soliton dynamics and fission we described for femtosecond pulses is less important because the soliton fission length increases with input pulse duration. So in this case MI and FWM are more important at the beginning of the propagation. It is MI that leads to pulse break up and the evolution of the sub-pulses leads to SC generation, through dispersive wave generation and Raman soliton self frequency shift. These features can be extended to CW pump generated SC, where the partial coherence of the pump leads to field break up. In the normal dispersion regime FWM and Raman scattering induce the spectral broadening and Raman effect is especially important for strongly normal regimes. In the area close to the zero dispersion wavelength soliton dynamics already described for the femtosecond input pulses are the main cause of broadening.

We should finally mention that the possibility of generating a broadband source in the area between 1.3 μm and 1.55 μm has pushed research in the area of SC for telecommunications [6], with the objective of developing multiwavelength sources adequate for spectral slicing for wavelength-division multiplexing [25]. The challenge in this case is not in terms of total spectral bandwidth but of spectral uniformity and low noise. [12, 8, 7, 26]

5.2 Introduction to pulse compression

For an optical pulse propagating in an optical fibre we can generally say that an increase of the spectral width corresponds to a compression of the temporal width. The process of

pulse compression is again due to nonlinear effects, which can be controlled and associated with dispersive effects in a fibre. Though there had been earlier studies on optical pulse compression, the exploitation of nonlinear processes (especially SPM) started to gain importance in the 1980s, after the introduction of low loss single mode fibres.

Compression can be achieved in chirped optical pulses through propagation along a dispersive medium. Pulse chirp is considered as the time dependence of its instantaneous frequency. Up-chirping is when the frequency increases with time, while down-chirping is the frequency decrease with time. Unchirped pulses present the minimum pulse duration possible (meaning they have constant instantanoeus frequency). When pulses propagate in a medium as a fibre, they can acquire or loose chirp depending on dispersion and nonlinearities in the medium. In fact, if the input pulse is already chirped, the dispersion of the fibre will determine the outcome pulse. If GVD is opposite to the initial chirp they tend to or totally (at a specific distance) cancel each other resulting in a shorter output pulse (since GVD is linear, compression is maximum for a linearly chirped input pulse). Compression is due to the fact that different frequency components of the same pulse propagate at different velocities due to dispersion. If the quicker tail of the pulse is delayed so that it arrives with the slower tail of the pulse, the resulting pulse is compressed. So according to the chirp sign either a normal or anomalous dispersion can derive in pulse compression.

According to the mechanism, pulse compression can be divided in two general categories:

- Linear pulse compression, which is the case of already chirped pulses where compression is obtained through dechirping with dispersion compensation. Theoretically, bandwidth-limited pulses can be achieved.

- Nonlinear pulse compression, which is a two steps process. In the first, chirp is induced in the pulse through a nonlinear interaction such as SPM, while the second step is the linear compression that has just been described.

There are two main categories of pulse compressors in optical fibres, those relying on fibre grating pairs and those relying on soliton effects. We will describe more extensively this latter case as is the one of interest for this thesis. Other techniques have been used for specific applications, the most famous one probably being chirped-pulse amplification [27], which allows to obtain ultrashort pulses with very high energies.

Fibre gratings are tipically used for pulse compression in the visible and near-IR regions. The input pulse is launched in a polarisation maintaining fibre where experience spectral broadening and accumulate positive chirp. Conventional fibres usually have the zero dispersion wavelength around 1.3 μm, so they can be used to induce positive chirp only up to that wavelength, which is the usual limit of utilisation of these compressors. The pulse then passes through the gratings where is compressed by anomalous dispersion.

For pulses over 1.3 μm, which undergo both SPM and negative GVD during propagation in a conventional silica fibre, soliton effects are employed as the fibre itself can act as compressor. As we mentioned in section 2.6, higher order solitons have a periodic evolution. At the beginning of each cycle they experience some narrowing depending on the soliton order, which can be optimized by choosing appropriate fibre length.

If we ignore fibre losses, combining equation 2.42 and equation 2.47 (the propagation equation and the soliton period) and using $\beta_2 < 0$, we obtain

$$i\frac{2}{\pi}\frac{\partial U}{\partial(z/z_0)} + \frac{1}{2}\frac{\partial^2 U}{\partial \tau^2} + N^2|U|^2U = 0 \tag{5.3}$$

with N the soliton order from equation 2.43. Only for integer values of N an exact periodic pattern is possible, though for all values $N > 1$ there is an initial narrowing of the pulse. There is an optimum fibre length z_{opt} that correspond to the minimum width location. Also the compression factor can be defined as the ratio of the width at FWHM of the compressed pulse divided by that of the input pulse. Various numerical techniques have been used to derive the compression factor and z_{opt} as a function of N [28, 29]. Through numerical simulation up to $N = 50$ we can approximate

$$F_c \approx 4.1N \quad \text{and} \quad \frac{z_{opt}}{z_0} \approx \frac{0.32}{N} + \frac{1.1}{N^2}. \tag{5.4}$$

With soliton effects compressors a wide pedestal is frequently visible around the compressed pulse. This is a disadvantage of this type of compressors and it is due to the fact that SPM initially induces narrowing in higher order solitons. Since SPM induces linear chirp only in the central part of the pulse, it is only this part that is compressed through dispersion while the tails of the pulse create the pedestal.

5.3 Application of high peak-power ultrafast ring fibre lasers with InN SESAM to supercontinuum generation and pulse compression in single mode fibre

As mentioned in section 5.1, SC generated in optical fibres using ultrashort high-power pulses allows for a higher degree of temporal coherence than is achievable with CW-based solutions. SC spectral and temporal properties can be controlled more easily in the case of all fibre-based solutions, as certain advantages can be reaped in terms of improved compactness and signal characteristics, as well as control over nonlinearity, chromatic dispersion and fibre length [12, 11].

The following study tests experimentally the tunability and flexibility of supercontinuum generation and pulse compression from high-power Gaussian pulses, obtained from the lasers described in Chapter 4, propagating through standard, dispersion shifted and dispersion compensating fibre, as well as the influence of input polarisation.

5.3.1 Experimental set-up

The experimental set-up employed is depicted in Fig.5.2. The SC generation system relies on a high peak power femtosecond harmonically mode-locked ring fibre laser, which has been previously described and fully characterised in Chapter 4 [30, 31, 32]. As the nonlinear medium for SC generation we use an additional span of commercial single mode fibre, chosen from among different reels and lengths of standard single-mode fibre (SSMF), dispersion-shifted fibre (DSF) and dispersion-compensating fibre (DCF).

The master oscillator (described in Chapter 4) relies on a commercial EDFA and a novel semiconductor saturable absorber mirror (SESAM) operating in free space which is based on bulk InN. The laser cavity is completed with standard fibre optical laboratory components based on standard single mode fibre, which are displayed along the ring in Fig.5.2, and a span of SSMF is inserted between the SESAM and the EDFA (the system thus operates in the anomalous dispersion regime). The length of the SSMF can be adjusted to tailor the properties of the output pulse according to its intended application, adjusting repetition rate at fundamental mode-locking (FML) and increasing the energy per pulse. Moreover, controlling the losses in the oscillator it is possible to lock the laser to higher

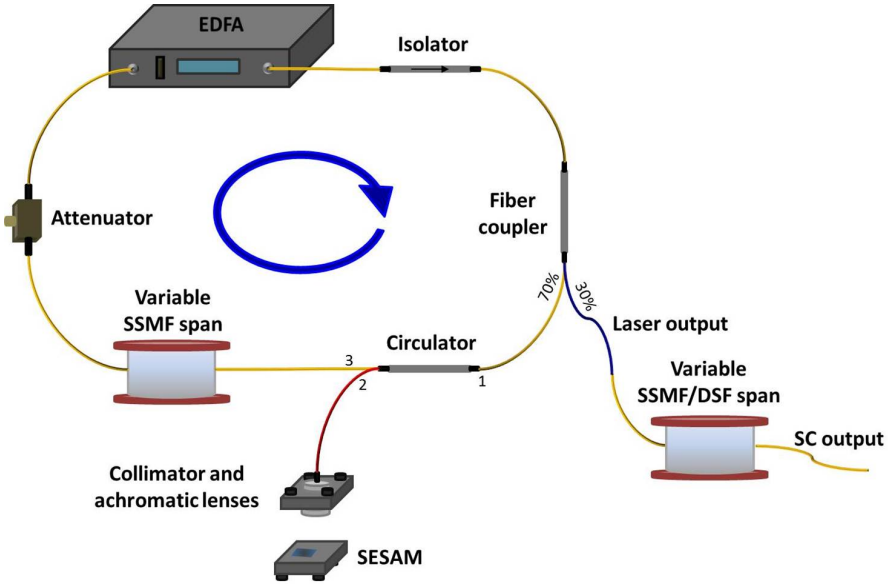

Figure 5.2: Experimental set-up of the system for supercontinuum generation and pulse compression. The fibre laser operates clock-wise.

harmonics. Selecting these last two features (length of SSMF and harmonic order), we can tune the peak power, pulse energy, repetition rate and pulse duration at the output.

At the output of the master oscillator an additional reel of single mode fibre can be been added as a nonlinear medium to study pulse propagation and the possibility of generating supercontinuum while simultaneously compressing the pulses in the time domain. The fibres used as external nonlinear medium were: two different lengths of SSMF, with a dispersion between 16.5 and 16.8 ps/(nm·km) at 1550 nm and a zero-dispersion wavelength of 1312 ± 1.3 nm; a span of DSF with a length of 4.9 km and a zero-dispersion wavelength at 1549 nm; and a narrow-core 2 km span of DCF with strongly negative dispersion at 1550 nm. The characteristics of the fibres are summarized in Table 5.1.

Table 5.1: Summary of the characteristics of the different types of single mode fibres.

Fibre type	**Zero dispersion wavelength (nm)**	**Dispersion @ 1550 nm (ps/nm·km)**	**Attenuation @ 1550 nm (dB/km)**	**Effective area @ 1550 nm (μm^2)**
SSMF	1312	16.65	0.20	84.9
DSF	1548.9	0.06	0.23	72.4
DCF	negative disp.	-30.05	1.09	28.4

5.3.2 Results and discussion

Autocorrelation traces, optical spectra, RF spectra and average power were recorded at the output of the external fibre reel. Please note that due to the specifications of the employed autocorrelator, pulses below 3 mW of average power result in noisy traces, and that the utilised optical spectrum analyser can measure only up to 1750 nm.

As we mentioned in Chapter 4 mode-locking to different harmonics can be selected in the laser source by adjusting the power entering the EDFA through a VOA. Peak power is maximum at FML and decreases at higher harmonics due to the multiplication of pulses simultaneously present in the oscillator. Peak power is also controlled trough the length of the cavity (the longer the cavity, the lower the repetition rate and the higher the peak power at FML). Two of the laser configurations have been used for SC generation: the first one is the 1,05 km resonator (see section 4.6.2), which operates at an average power of 30.5 mW, generating pulses with a peak power of 650 kW (pulse energy 155 nJ and temporal width 240 fs) and a repetition rate 196 kHz at FML, whereas the second one is the 2.4 km cavity (see section 4.6.3), which operates at an average power of 23 mW, with pulses that display a peak power of 1.27 MW (pulse energy 263 nJ and temporal width 207 fs) and a 87 kHz repetition rate in FML.

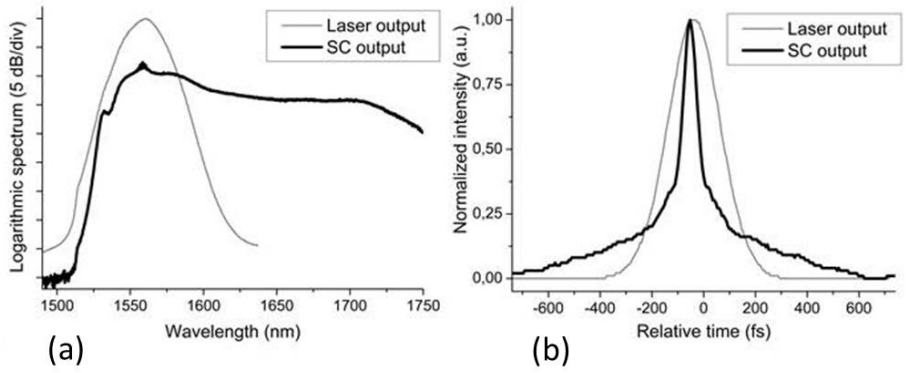

Figure 5.3: Optical spectra (b) and autocorrelation traces (c) before and after a 2.3 km SSMF span at the output of the 650 kW peak power laser.

Starting with the configuration with 650 kW pulses and 2.3 km of SSMF fibre at the laser output, we tested the actual feasibility of the system for SC generation and pulse compression. Even though SSMF is not a highly nonlinear medium, the result is a broad supercontinuum, as can be expected from the high peak powers. The initial Gaussian-like spectrum centered at 1.56 μm is broadened towards the red side to more than 200 nm

-Fig.5.3(a)-, as the high power higher-order multi-soliton structure at the input of the external fibre is differently shifted in frequency, while the pulses are compressed down to around 100 fs, passing from a Gaussian to a Lorentzian-like shape as recorded in Fig.5.3(b). The appearance of a pedestal in the autocorrelation trace can be explained with the nonlinear compression typical of soliton effects, where part of the energy is displaced to the tails of the pulse, as explained at the end of section 5.2. Despite the broadening of the spectral bandwith, the pulse structure, repetition rate and stable average output power (12.6 mW in this case) are well maintained, thus preserving the temporal coherence of the supercontinuum. The grey line in the figure displays the direct output of the laser for comparison.

In the following subsections we will explore the operation of the higher peak power laser configuration, examining the impact of fibre dispersion and harmonic order selection (e.g. repetition rate and input peak power) on pulse propagation, and thus on SC generation and pulse compression.

Results with standard single mode fibre

In the first case, 3 km of standard low-cost telecommunication SSMF are coupled to the laser output.

In Fig.5.4 we can observe the dependence of both temporal and spectral output on the order of the harmonic mode-locking at the output of the laser, as it increases from FML (at the bottom of the graphs) to the highest harmonic achievable by adjusting the variable attenuator (at the top). Mode-locking is clearly maintained in all cases, as is the wide spectral broadening of more than 200 nm towards longer wavelengths. Moreover, pulse and SC spectra intensities are temporally stable, which indicate a good preservation of temporal coherence at lower harmonics, where SC is efficiently generated. Clear, compressed pulses, down to around 50 fs for the FML case, are registered in the autocorrelator, with a shape that varies between Lorentzian-like to triangular-like to Gaussian-like (the same that is observed at the output of the laser) with growing harmonic order (lower pulse peak power) whereas supercontinuum bandwidth is at the same time reduced, and temporal width increased, as expected, reaching more than 700 fs for the 12th harmonic. Pulses are in all cases temporally compressed in comparison to the duration measured at the laser output for the same harmonic order. We can conclude that harmonic selection is a quick and

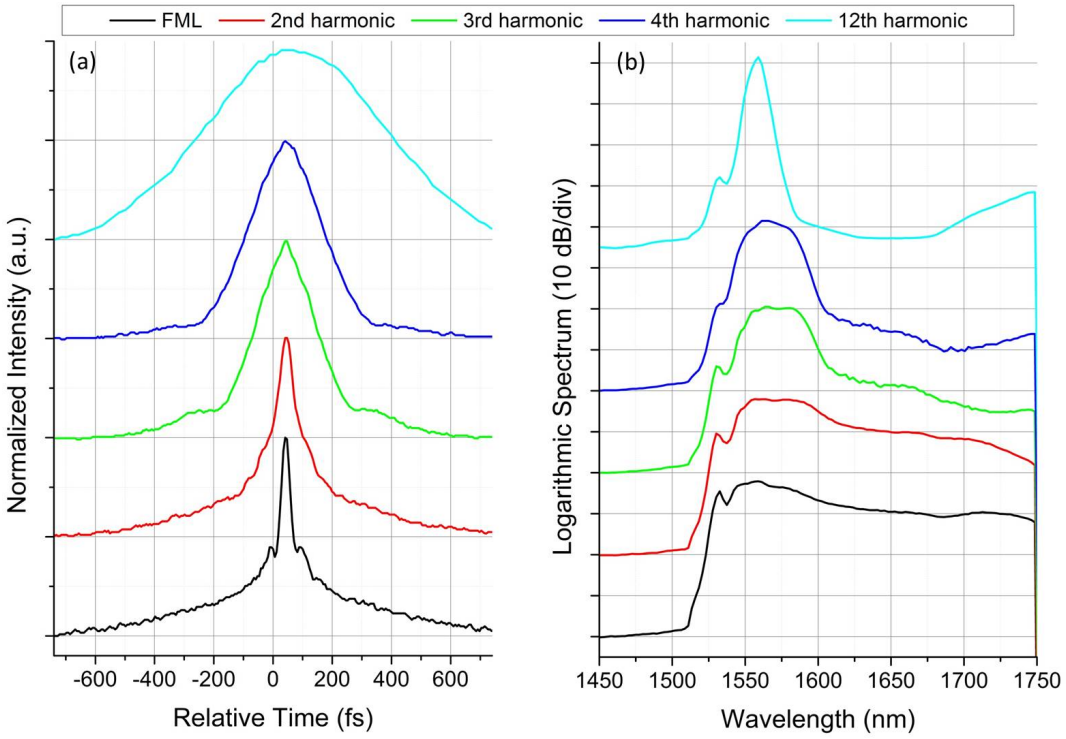

Figure 5.4: Autocorrelation traces (a) and optical spectra (b) after propagation in 3 km of SSMF at different harmonics. Average output powers are: $P_{FML} = 9$ mW, $P_{2nd} = 17$ mW, $P_{3rd} = 23$ mW, $P_{4th} = 26$ mW, $P_{12th} = 28$ mW.

efficient method for dynamically modifying the output spectrum in our set-up, dramatically affecting pulse evolution and the balance between dispersive and nonlinear effects.

Results with dispersion shifted fibre

If we modify the dispersion of the fibre at the laser output to favor four-wave mixing processes and reduce dispersion (with the pulses propagating in a slightly anomalous dispersion regime), we should expect noticeable variations in the SC spectrum. Please note that the employed DSF fibre (4.9 km long) presents a higher attenuation and insertion losses than the SSMF, reducing the average power of the output SC at FML to 1.6 mW (thus the noisy and distorted autocorrelation traces at lower harmonics -see Fig. 5.5(a), black line-).

In Fig.5.5(a) we can see how in this case the pulses experience a slightly more efficient compression at higher harmonics (down to about 70 fs), which can be related to the different dispersion and so a different propagation regime. As in [33], in Fig.5.5(b) we can observe that the pulse spectra changes considerably with peak power (in our case due

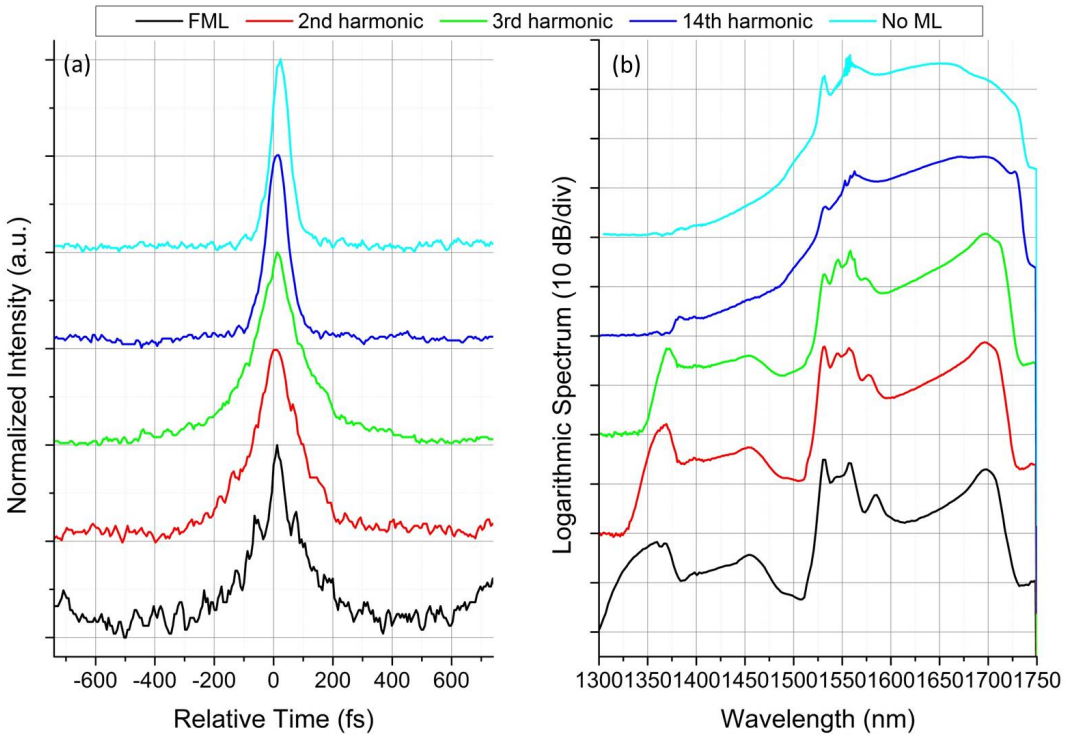

Figure 5.5: Autocorrelation traces (a) and optical spectra (b) after propagation in 4.9 km of DSF at different harmonics. "No ML (Mode Locking)" in the legend means that some locking is present, as the modes are recorded in the RF spectrum, but it is not possible to determine the order of the harmonic. Average output powers are: P_{FML} = 1.6 mW, P_{2nd} = 1.9 mW, P_{3rd} = 2.2 mW, P_{14th} = 6.5 mW, P_{NoML} = 9.6 mW.

to the selection of the harmonic). We can see that, for higher input powers, in addition to the Raman Stokes bands on the red side, also less energetic anti-Stokes bands appear shifted to shorter wavelengths, as result of the propagation of a Raman soliton [34] through the fibre. The Stokes at longer wavelengths serves to generate the continuum around 1.7 μm. Decreasing the pulse power at the input (increasing the harmonic order) only the supercontinuum at longer wavelengths is generated. In these cases temporal coherence is reduced (especially in the No ML case, purple line in Fig.5.5).

Results with dispersion compensating fibre

Finally, if we use a dispersion compensating fibre (2 km long), with both strongly normal dispersion at 1550 nm and a high nonlinear coefficient, we can expect Raman gain to become the dominant effect in the broadening of the spectrum. As was the case with the DSF, here we also have a much higher attenuation in respect to SSMF.

As visible in Fig.5.6, harmonic selection seems to have little impact over temporal and

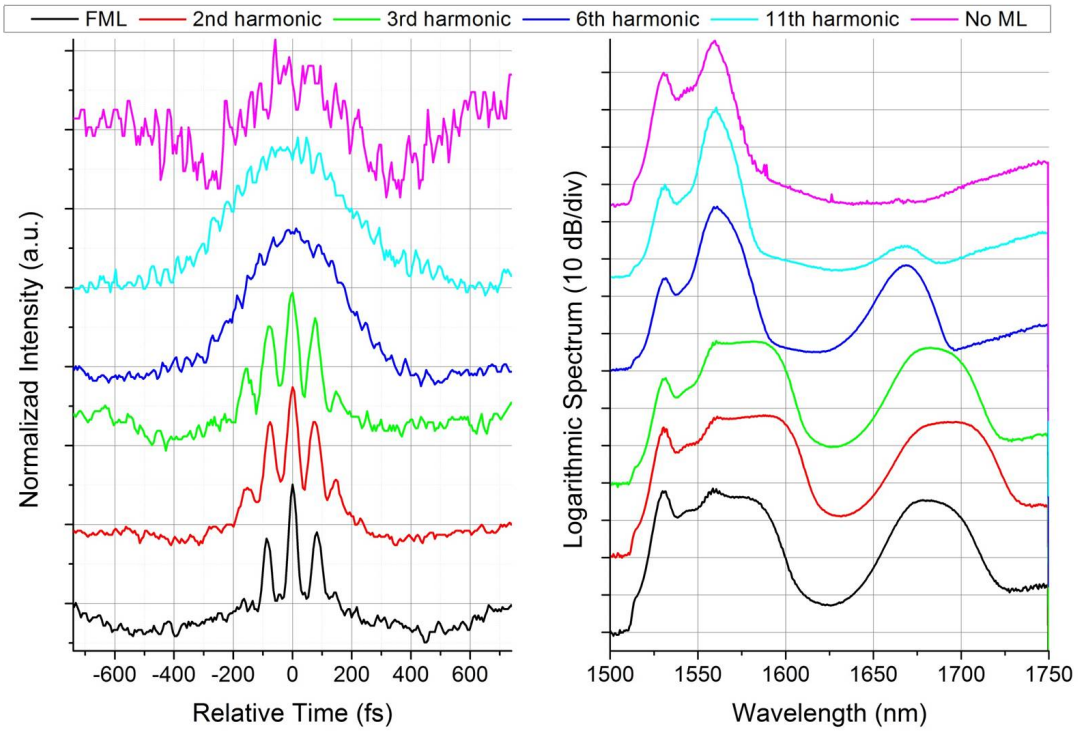

Figure 5.6: Autocorrelation traces (a) and optical spectra (b) after propagation in 2 km of DCF at different harmonics. Average output powers are: $P_{FML} = 2.2$ mW, $P_{2nd} = 3.2$ mW, $P_{3rd} = 4.2$ mW, $P_{6th} = 5.7$ mW, $P_{11th} = 6.0$ mW, $P_{NoML} = 4.3$ mW.

spectral behaviour in the case of the DCF, as long as power is high enough. No spectral broadening is noticeable for harmonics higher than the 3^{rd}, but below this threshold pulses break up into smaller structures resolvable by the autocorrelator, and the broadened spectra displays common characteristics. We can notice the broadening of the original peak at 1560 nm and the appearance of a new strong peak centered around 1700 nm -Fig.5.6(b)-, close to the Raman first Stokes wavelength, which dominates given the higher Raman gain coefficient of DCF. When input peak power is low, at higher harmonics, the Raman peak almost disappears. Also the autocorrelation trace profiles -Fig.5.6(a)- display the same threshold behaviour for the input peak power. Up to the 3^{rd} harmonic (apart from the noise in the FML case due to low average power, as in the DSF case), they present the same shape with a central more intense lobe and symmetric less intense side lobes (a first pair is clearly visible, while a second is less perceivable). From the 5^{th} harmonic up, the usual Gaussian profile is visible, slightly compressed in comparison to the pulse at the direct output of the laser with the same harmonic, probably due to the different dispersion in the fibre.

Effect of polarisation on the generation of supercontinuum

In order to add an extra degree of freedom to our system and try to better understand its potential flexibility to generate SC, we have studied the effect of pump polarisation on SC selectivity (see, for example [35, 36]). This is achieved by inserting an inline polariser and a polarisation controller at the output of the master oscillator (which was utilised in the 2.4 km higher power configuration), before the external reel of single mode fibre.

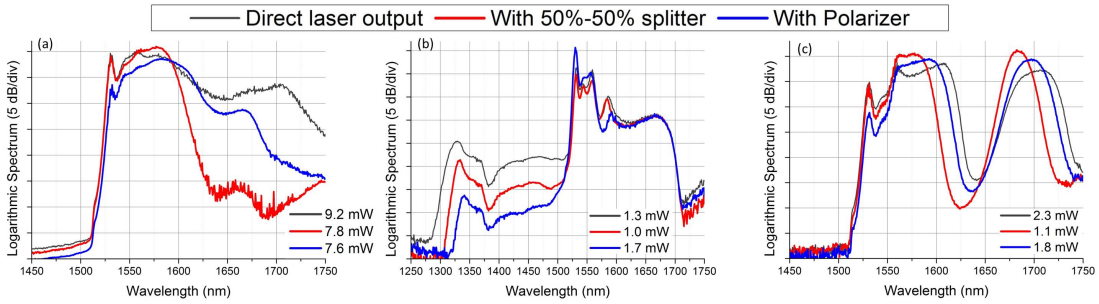

Figure 5.7: Normalized optical spectra after propagation in 2.4 km of SSMF (a), 4.9 km of DSF (b) and 2.0 km of DCF (c) at FML of the direct laser output (black line), of a 50% of the power (red line) and with an in-line polariser and polarisation controller (blue line).

In Fig. 5.7, a comparison between the supercontinua generated at FML by the direct laser output and by a polarised input into the external reel of fibre is shown for the different types of fibre. To ensure that the comparison is performed for the same average and peak power, in the case of the unpolarised laser output the signal is subjected to 3 dB attenuation (50/50 splitter) prior to its injection into the external reel of fibre.

Fig. 5.7(a) shows the results with SSMF fibre. Here it is clear that the reduction of the input power to 50% does not allow efficient SC generation. Using a polarised input we see the effect of polarisation on the Raman-induced broadening as Raman gain is highly polarisation-dependent, and thus much stronger for a polarised input than for a depolarised one. Due to this a shoulder appears at 1670 nm (close to the first Stokes), which is barely noticeable in the unpolarised case. Polarisation is not perfectly maintained during propagation through the SSMF, so the output displays a degree of polarisation (DOP) around 55% at FML. Depolarisation is reduced at higher harmonics, increasing to more than 90% for the highest ones.

Fig. 5.7(b), displays the DSF case with the pulses propagating very close to the zero dispersion wavelength. Here the impact of polarisation is less visible, with only a slight shift of the newly generated wavelengths in the supercontinuum being noticeable. The

transfer of energy producing the Raman soliton remains unchanged. The DOP at the output is around 65% at FML, and in this case decreases with increasing harmonic order.

In the case of DCF -Fig. 5.7(c)- there is little difference in the intensity of the Raman peak, while there is a difference in the spectral broadening. This is due to the fact that in all cases propagation occurs above the "threshold" that we mentioned in section relative to DCF fibre and so the difference of input peak power is less significant for the output spectra over a wider range. Also DCF has a higher Raman gain coefficient (it can be one order of magnitude higher than in SSMF [37]). So even with lower input power and polarised input, a Stokes peak is created and the only changes observable are in the spectral width of the peaks. With DCF, the DOP at the output is the lowest (around 4%) and does not change for increasing harmonics.

5.4 Application: gas sensing

The supercontinuum light sources we have described in this work may have several applications, a particularly obvious one being spectroscopy. Already Alfano at the very beginning of SC generation studies proposed it [20].

A wide broadband light source is advantageous for several gas sensing applications as they are able to simultaneously detect the spectral fingerprints of various chemical species over a wide range. Measuring numerous lines for each compound at the same time reduces interference among species. Conveniently various gases, that are important in chemical or atmospheric monitoring, have their rotational-vibrational transitions in the near-IR region and can thus be studied with this method [2, 38, 39].

5.4.1 Preliminary results

Here we present a preliminary demonstration of this gas sensing application as we measured the intensity of the supercontinuum radiation, generated with the simplest configuration of the system (the low peak-power laser from the 1.05 km long cavity and an external reel of SSMF of 2.3 km) transmitted trough an absorption cell containing a mixture of three gases: hidrogen cyanide $H^{12}C^{14}N$ (with a pressure of 5 Torr), carbon monoxide $^{12}C^{16}O$ (150 Torr) and carbon monoxide $^{13}C^{16}O$ (150 Torr) -Fig.5.8.

The cell, which has fibre-optic connectors, is composed of a glass tube 18.92 cm long,

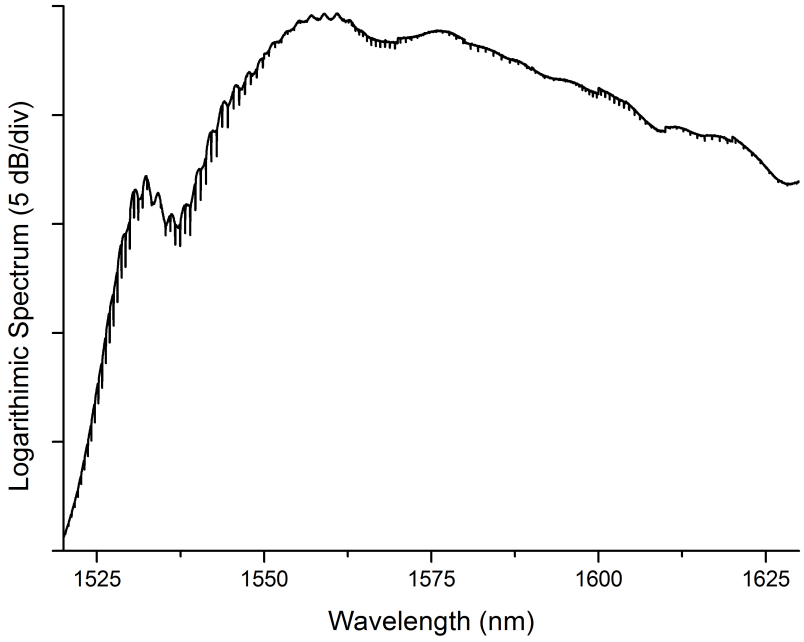

Figure 5.8: The supercontinuum spectrum transmitted through $H^{12}C^{14}N$, $^{12}C^{16}O$ and $^{13}C^{16}O$.

where, through 5 internal reflections, an optical path close to 80 cm is obtained. The rotational-vibrational transitions of the cited gases cover a bandwidth between 1520 nm and 1640 nm, which can be explored with our supercontinuum source. Though is more clearly visible for HCN -Fig.5.9- in the region between 1520 nm and 1555 nm, the spectrum of each gas shows two different areas, branch R ($\Delta J = +1$) and branch P ($\Delta J = -1$). Despite the fact that the intensity is lower, the two branches are recorded at longer wavelengths also for $^{12}C^{16}O$ -Fig.5.10(a)- between 1560 nm and 1595 nm and for $^{13}C^{16}O$ -Fig.5.10(b)-, in the region from 1595 nm to 1630 nm.

The spectra are recorded by direct absorption measurement, conducted by simply connecting the cell to the ouptut of the supercontinuum, after a fibre splitter to reduce the power entering in the cell (it is just a safety measure, it does not affect the measurement), and to an optical spectrum analyser with high spectral resolution, used as detector. The measured lines agree well with previous calibrations [40, 41, 42].

Although these are very preliminary results, they show the immediate applicability of our SC generation system to gas sensing, exploiting the advantages of a low-cost broadband laser source.

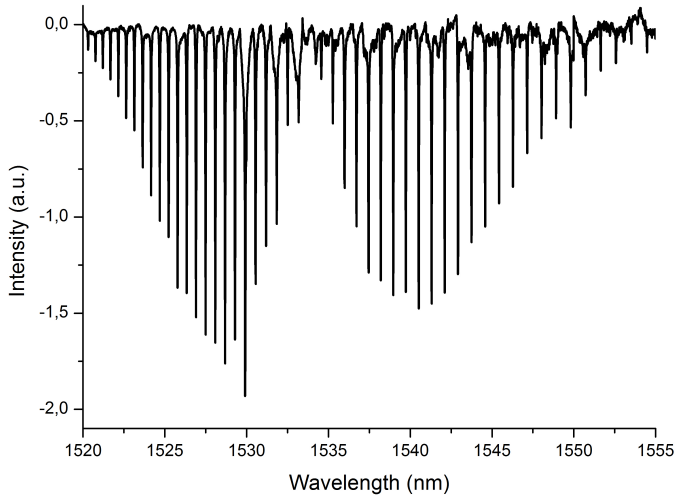

Figure 5.9: Absorbance spectrum of $H^{12}C^{14}N$ after baseline subtraction.

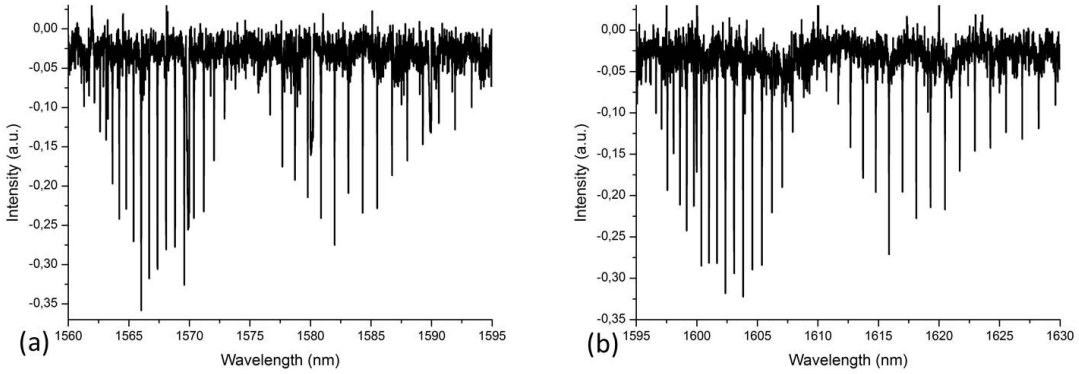

Figure 5.10: Absorbance spectrum of $^{12}C^{16}O$ (a) and of $^{13}C^{16}O$ (b) after baseline subtraction.

5.5 Conclusion

We have analysed the applicability, flexibility and tunability of supercontinuum generation and pulse compression in a low-cost system with off-the-shelf components and single mode fibres. We have experimentally demonstrated supercontinuum generation with low-cost standard telecommunication SMF over 200 nm with pulse compression down to around 50 fs, from the output of an ultrafast passively mode-locked ring fibre laser operating at 1.56 μm. With the same fibre laser, we have demonstrated the propagation of Raman solitons for higher input peak powers, when the dispersion of the propagation fibre is shifted in proximity of the wavelength of the input pulses, while a broad supercontinuum, and correspondent pulse compression down to 70 fs, is achievable with higher harmonics.

Moreover, we have observed the generation of a second peak close to the Raman first Stokes in DCF, while pulse breakup is observable in the autocorrelation trace. In addition we have tested the impact of a linearly polarised input in the external fibre, which sheds light on the mechanisms of supercontinuum generation, especially the influence of Raman scattering.

Finally, we conducted a positive first trial of one the possible applications of the resulting supercontinuum light sources, that is spectroscopy for gas sensing.

References

[1] R. Alfano and S. Shapiro, "Emission in the Region 4000 To 7000a Via Four-Photon Coupling in Glass," *Phys. Rev. Lett.*, vol. 24, pp. 584–588, 1970.

[2] C. F. Kaminski, R. S. Watt, A. D. Elder, J. H. Frank, and J. Hult, "Supercontinuum radiation for applications in chemical sensing and microscopy," *Appl. Phys. B Lasers Opt.*, vol. 92, no. 3 SPECIAL ISSUE, pp. 367–378, 2008.

[3] K. Lindfors, T. Kalkbrenner, P. Stoller, and V. Sandoghdar, "Detection and spectroscopy of gold nanoparticles using supercontinuum white light confocal microscopy," *Phys. Rev. Lett.*, vol. 93, p. 037401, 2004.

[4] W. Watanabe and K. Itoh, "Coherence spectrotomography: Optical spectroscopic tomography with low-coherence interferometry," *Opt. Rev.*, vol. 7, no. 5, pp. 406–414, 2000.

[5] B. R. Washburn, S. A. Diddams, N. R. Newbury, J. W. Nicholson, M. F. Yan, and C. G. Jørgensen, "Phase-locked, erbium-fiber-laser-based frequency comb in the near infrared," *Opt. Lett.*, vol. 29, no. 3, pp. 250–252, 2004.

[6] S. Smirnov, J. Ania-Castañón, T. Ellingham, S. Kobtsev, S. Kukarin, and S. Turitsyn, "Optical spectral broadening and supercontinuum generation in telecom applications," *Optical Fiber Technology*, vol. 12, no. 2, pp. 122 – 147, 2006.

[7] R. R. Alfano, *The Supercontinuum Laser Source. The Ultimate White Light, 3rd Ed.* Springer, 2016.

[8] J. M. Dudley and J. R. Taylor, *Supercontinuum generation in optical fibers.* Cambridge University Press, 2010.

[9] J. M. Dudley, G. Genty, F. Dias, B. Kibler, and N. Akhmediev, "Modulation instability, akhmediev breathers and continuous wave supercontinuum generation," *Opt. Express*, vol. 17, no. 24, pp. 21 497–21 508, 2009.

[10] A. K. Abeeluck, C. Headley, and C. G. Jørgensen, "High-power supercontinuum generation in highly nonlinear, dispersion-shifted fibers by use of a continuous-wave Raman fiber laser," *Opt. Lett.*, vol. 29, no. 18, p. 2163, 2004.

[11] A. E. El-Taher, J. D. Ania-Castañón, V. Karalekas, and P. Harper, "High efficiency supercontinuum generation using ultra-long raman fiber cavities," *Opt. Express*, vol. 17, no. 20, pp. 17 909–17 915, 2009.

[12] J. M. Dudley, G. Genty, and S. Coen, "Supercontinuum generation in photonic crystal fiber," *Rev. Mod. Phys.*, vol. 78, pp. 1135–1184, 2006.

[13] S. M. Kobtsev and S. V. Smirnov, "Supercontinuum fiber sources under pulsed and cw pumping," *Laser Physics*, vol. 17, no. 11, pp. 1303–1305, 2007.

[14] S. Martin-Lopez, L. Abrardi, P. Corredera, M. Gonzalez-Herraez, and A. Mussot, "Spectrally-bounded continuous-wave supercontinuum generation in a fiber with two zero-dispersion wavelengths," *Opt. Express*, vol. 16, no. 9, pp. 6745–6755, 2008.

[15] S. Martin-Lopez, P. Corredera, and M. Gonzalez-Herraez, "Cavity dispersion management in continuous-wave supercontinuum generation," *Opt. Express*, vol. 17, no. 15, pp. 12 785–12 793, 2009.

[16] M. E. Fermann and I. Hartl, "Ultrafast Fiber Laser Technology," *IEEE J. Sel. Top. Quantum Electron.*, vol. 15, no. 1, pp. 191–206, 2009.

[17] J. T. Manassah, R. R. Alfano, and M. Mustafa, "Spectral distribution of an ultrafast supercontinuum laser source," *Phys. Lett. A*, vol. 107, no. 7, pp. 305–309, 1985.

[18] S. Coen, A. H. L. Chau, R. Leonhardt, J. D. Harvey, J. C. Knight, W. J. Wadsworth, and P. S. J. Russell, "White-light supercontinuum generation with 60-ps pump pulses in a photonic crystal fiber," *Opt. Lett.*, vol. 26, no. 17, pp. 1356–1358, 2001.

[19] K. Mori, H. Takara, and S. Kawanishi, "Analysis and design of supercontinuum pulse generation in a single-mode optical fiber," *J. Opt. Soc. Am. B*, vol. 18, no. 12, p. 1780, 2001.

[20] R. R. Alfano and S. L. Shapiro, "Picosecond spectroscopy using the inverse Raman effect," *Chem. Phys. Lett.*, vol. 8, no. 6, pp. 631–633, 1971.

[21] C. Lin and R. H. Stolen, "New nanosecond continuum for excitedstate spectroscopy," *Applied Physics Letters*, vol. 28, no. 4, pp. 216–218, 1976.

[22] R. H. Stolen, C. Lee, and R. K. Jain, "Development of the stimulated raman spectrum in single-mode silica fibers," *J. Opt. Soc. Am. B*, vol. 1, no. 4, pp. 652–657, 1984.

[23] J. P. Gordon, "Theory of the soliton self-frequency shift," *Opt. Lett.*, vol. 11, no. 10, pp. 662–664, 1986.

[24] F. M. Mitschke and L. F. Mollenauer, "Discovery of the soliton self-frequency shift," *Opt. Lett.*, vol. 11, no. 10, pp. 659–661, 1986.

[25] T. Morioka, S. Kawanishi, K. Mori, and M. Saruwatari, "Nearly penalty-free, <4 ps supercontinuum Gbit/s pulse generation over 1535-1560 nm," *Electronics Letters*, vol. 30, no. 10, pp. 790–791, 1994.

[26] G. Genty, A. T. Friberg, and J. Turunen, "Chapter two - coherence of supercontinuum light," ser. Progress in Optics. Elsevier, 2016, vol. 61, pp. 71 – 112.

[27] D. Strickland and G. Mourou, "Compression of amplified chirped optical pulses," *Optics Communications*, vol. 56, no. 3, pp. 219–221, 1985.

[28] L. F. Mollenauer, R. H. Stolen, J. P. Gordon, and W. J. Tomlinson, "Extreme picosecond pulse narrowing by means of soliton effect in single-mode optical fibers," *Optics Letters*, vol. 8, no. 5, pp. 289–291, 1983.

[29] C. M. Chen and P. L. Kelley, "Nonlinear pulse compression in optical fibers: scaling laws and numerical analysis," *J. Opt. Soc. Am. B*, vol. 19, no. 9, pp. 1961–1967, 2002.

[30] M. Jiménez-Rodríguez, L. Monteagudo-Lerma, E. Monroy, M. González-Herráez, and F. Naranjo, "Widely power-tunable polarization independent ultrafast mode-locked fiber laser using bulk inn as saturable absorber," *Optics Express*, vol. 25, no. 5, pp. 5366–5375, 2017.

[31] M. Jiménez-Rodríguez, E. Monroy, M. González-Herráez, and F. B. Naranjo, "Ultrafast fiber laser using inn as saturable absorber mirror," *J. Lightwave Technol.*, vol. 36, no. 11, pp. 2175–2182, 2018.

[32] F. Gallazzi, M. Jiménez-Rodríguez, E. Monroy, P. Corredera, M. González-Herráez, F. B. Naranjo, and J. D. Ania Castañón, "Megawatt peak-power femtosecond ultralong ring fibre laser with InN SESAM," in *2019 Conference on Lasers and Electro-Optics*

Europe and European Quantum Electronics Conference. Optical Society of America, 2019, p. cf˙p˙13.

[33] P. Beaud, W. Hodel, B. Zysset, and H. P. Weber, "Ultrashort pulse propagation, pulse breakup, and fundamental soliton formation in a single-mode optical fiber," *IEEE J. Quantum Electron.*, vol. 23, no. 11, pp. 1938–1946, 1987.

[34] V. L. Kalashnikov and E. Sorokin, "Dissipative Raman solitons," *Opt. Express*, vol. 22, no. 24, p. 30118, 2014.

[35] A. Srivastava and D. Goswami, "Control of supercontinuum generation with polarization of incident laser pulses," *Applied Physics B*, vol. 77, no. 2, pp. 325–328, 2003.

[36] L. D. Boni, C. Toro, and F. E. Hernández, "Pump polarization-state preservation of picosecond generated white-light supercontinuum," *Opt. Express*, vol. 16, no. 2, pp. 957–964, 2008.

[37] C. Headley and G. P. Agrawal, *Raman amplification in fiber optical communication systems*. Elsevier Academic Press, 2005.

[38] R. S. Watt, C. F. Kaminski, and J. Hult, "Generation of supercontinuum radiation in conventional single-mode fibre and its application to broadband absorption spectroscopy," *Appl. Phys. B Lasers Opt.*, vol. 90, no. 1, pp. 47–53, 2008.

[39] J. Hult, R. S. Watt, and C. F. Kaminski, "High bandwidth absorption spectroscopy with a dispersed supercontinuum source," *Opt. Express*, vol. 15, no. 18, p. 11385, 2007.

[40] W. C. Swann and S. L. Gilbert, "Line centers, pressure shift, and pressure broadening of 1530-1560 nm hydrogen cyanide wavelength calibration lines," *J. Opt. Soc. Am. B*, vol. 22, no. 8, pp. 1749–1756, 2005.

[41] H. Álvarez Martínez, J. Galindo-Santos, J. L. D. Miguel, A. V. Velasco, and P. Corredera, "Calibración de células de absorción como referencia de longitud de onda para comunicaciones," *6 Congreso Español de Metrologia*, p. R90, 2017.

[42] W. C. Swann and S. L. Gilbert, "Pressure-induced shift and broadening of 1560–1630-nm carbon monoxide wavelength-calibration lines," *J. Opt. Soc. Am. B*, vol. 19, no. 10, pp. 2461–2467, 2002.

Chapter 6

Generation of high power ultrashort laser pulses

In this chapter a system to generate high power femtosecond pulses in ultralong fibre lasers, which makes use of the previous results presented in Chapter 3 and 4, is presented. This is the first time to our knowledge that an URFL is implemented in a pulsed fibre laser.

6.1 Introduction

As we have introduced in previous chapters, research in the field of ultrafast lasers has been pushed over the years by the multitude of applications of this technology. This has led to a great number of advances with widespread impact not only in multiple areas of physics, but also in biology, medicine or chemistry, as attested by multiple related Nobel Prize Awards over the past few decades. Among the available approaches to ultrashort pulse generation, mode-locked fibre lasers stand out as simple and inexpensive solutions. Multiple cavity architectures, simple implementation, efficiency, long interaction lengths and the possibility to manage dispersion and nonlinearities are just some of the advantages of the mode-locked fibre laser. Moreover, if we choose to operate at wavelengths around 1.55 μm, exploiting the region of minimum loss in standard telecommunication fibre, it is possible to make use of mass-produced, cost-effective and optimised optical communications components. Ultrafast passively mode-locked fibre lasers [1, 2, 3, 4] thus combine stability, efficiency, compactness and easy integrability, are nearly maintenance-free and allow for convenient output beam handling. But despite all these advantages, developing simple

fibre systems to generate high power ultrafast pulses is still a challenge, and the application of these sources is still restricted in certain areas, mostly due to their achievable pulse energy and peak power, the latter being limited in practice to the few hundreds of kW for pulses in the hundreds of fs range. As previously mentioned, a possible straightforward way to increase pulse energy and power could be increasing the length of the resonator, but this leads in general to temporal broadening into the ps range due to chromatic and polarization dispersive effects, as well as increased instability [5, 6, 7, 8, 9, 10]. In [11, 12], the challenges presented by ultralong pulsed lasers were studied numerically, showing how the increasing length of the cavity gradually reduced the region for stable generation of soliton pulses. Though mode-locking has been experimentally achieved in long lengths of fiber [13, 14, 15, 16, 17], stable mode-locking operation in the femtosecond range has proven particularly elusive. Still, as we have shown in Chapter 4, it is possible to overcome this disadvantage and achieve fundamental mode-locking of sub-250 fs in a resonator with a maximum length of 2.4 km (leading to peak powers in the order of the megawatt), as well as harmonic mode-locking in cavities up to 5.7 km [18], making use of low loss optical fibre and InN saturable absorption.

In this chapter we will demonstrate that control over the spatial distribution of signal gain/loss in the long cavity is key to controlling the balance between noise and nonlinearities in much longer cavities, and actually allows for stable harmonic mode-locking with fs-range pulse generation in fiber rings as long as 25 km, paving the way for the generation of high-power fs pulses with a broad choice of repetition rates.

Solitons are key in the operation of mode-locked lasers working in the anomalous dispersion regime. Soliton transmission generally is either achievable over short lengths of fibre, where attenuation is low, or, in theory, over a lossless transmission medium. Soliton lasers and among them soliton fiber lasers have a long history [19, 20, 21] leading to the recent focus on dissipative soliton lasers. Dissipative solitons, mentioned in section 2.6, are found not only at the balance of dispersion and nonlinearity, but also at the balance of gain and loss [22], and are extremely useful for the understanding of complex cavity and pulse dynamics, whereas mode-locked fiber lasers represent a nearly ideal sandbox for the observation and experimental study of solitonic behaviour.

As introduced in Chapter 3, URFLs operating in a continuous-wave (CW) regime were first proposed in 2004, and experimentally demonstrated in 2006 [23, 24]. When used

as distributed amplifiers, URFLs can induce simultaneous virtual spatial and spectral transparency (losslessness), which allowed for the first demonstration of fundamental soliton transmission over multiple dispersion lengths [25, 26] in standard single-mode fiber.

We will show that the combination of a classical ultrafast fiber laser ring architecture with an internal additional URFL cavity at the pulsed laser's Raman Anti-Stokes frequency provides the required control over gain-loss to permit soliton transmission and thus ultrashort pulse generation in extremely long rings. As we will see, the direct outcome of the increased effective length of the cavity is not necessarily an increase in pulse energy and peak power, due to the mode-locking of the laser at higher harmonics.

The URFL architecture integrates second order bidirectional pumping and highly reflective fibre Bragg gratings tuned to provide feedback at the Raman Stokes frequency of the pumps, which enclose a long fibre span. If pump power is high enough to achieve the requisite population inversion in the cavity, the entire transmission span is transformed into a laser at the pumps' Stokes frequency. Moreover, if the pump frequency is carefully chosen so that the Second Stokes Raman frequency coincides with that of a signal propagating through the cavity (i.e. the lasing frequency coincides with the signal's Anti-Stokes), the active cavity will provide distributed Raman gain to the signal. By balancing bi-directional pumping and adjusting total pump power to guarantee zero overall signal loss it is possible to produce a very low signal power variation along a span, virtually cancelling attenuation at every point in the fiber. As previously mentioned, this amplification system, has proved its value for unrepeatered and long-haul optical communication links [27, 28, 29] and allowed the first experimental demonstration of long-distance fundamental soliton transmission in conventional single-mode fibre. In [26] a 2^2 order URFL was implemented with a 22 km long transmission span made of standard single mode large effective area fibre (LEAF), which was pumped to obtain optimal transparency conditions. 4 ps sech^2 soliton pulses were generated with an external mode-locked fibre laser, which was made to operate with a 1.25 GHz repetition rate with a power chosen to obtain fundamental soliton conditions. Undistorted transmission was proven and pulse duration, pulse width and peak intensity were shown to remain constant along the transmission length. Output pulses consistent with a soliton profile were then obtained in cavities up to 72 km.

So, for the purpose of creating an ultralong ultrafast fibre laser, we have introduced a virtually lossless URFL transmission span (following the scheme presented in Chapter 3)

inside the cavity of a passively mode-locked fibre laser with a ring architecture, built with commercially available standard fibre optic components.

The design is based upon the the polarisation independent InN-based SESAM fiber laser oscillator presented in Chapter 4, [30, 31], with minor modifications. A variable attenuator is located just before an extended quasi-lossless transmission span reliant on the URFL architecture to create the right conditions for unperturbed soliton transmission. We are, thus, bringing together two advantageous solutions we previously introduced in this thesis as a first step towards the design of simple, flexible, compact and low-cost high peak power fibre lasers.

6.2 Results

6.2.1 Experimental set-up

Figure 6.1 represents our experimental set-up, which presents a "cavity-inside-the-cavity" type of architecture: a distributed $2^n d$ order ultra-long Raman laser amplifier is inserted in the ring of a mode-locked fibre laser relying on a SESAM for passive operation.

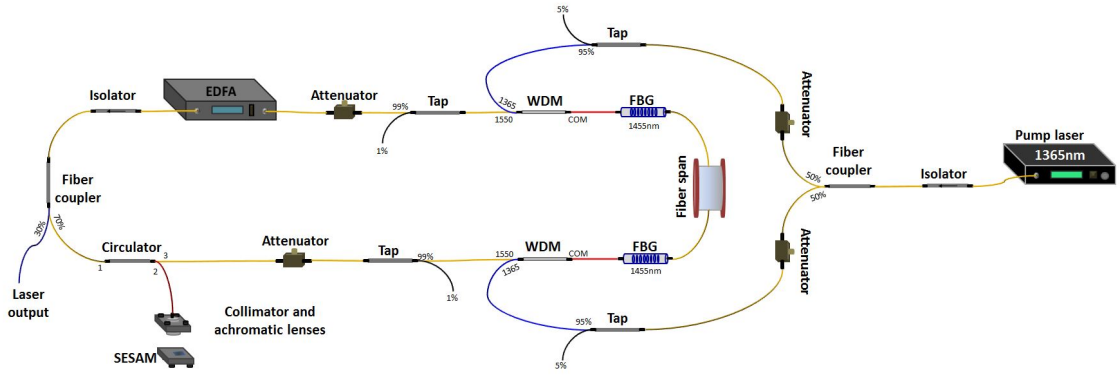

Figure 6.1: Set-up of the system. The pulses propagate along the cavity counter clockwise.

The Raman amplifier consists on a cell of standard single mode fibre (SSMF), with lengths of up to 25 km in the present study, enclosed by high reflectivity fibre Bragg gratings (FBGs) at each end of the amplified span. The URFL is pumped bidirectionally by a depolarised Raman fibre laser. The pump power is splitted by a 50/50 fibre coupler/splitter and inserted into the cavity through each end of the amplifier by means of a broadband wavelength division multiplexer (WDM). Two variable optical attenuators (VOAs) allow for control of the power balance between the two pumps, which is monitored through the

two taps located before the WDMs. In the cases considered here, they VOAs have been used to ensure identical pumping from both extremes of the cavity. The central wavelength of the FBGs is chosen to be at 1454 nm, close to the first Stokes of the Raman pump at 1365 nm, so that the URFL is able to amplify the ring laser signal centered around 1550 nm as it traverses the cavity.

The high-power ultrafast ring fibre laser is similar to the one presented in previous chapters. The whole system operates in the anomalous dispersion regime [18]. The resonator relies, as gain medium, on a commercial EDFA containing 16 m of Er-doped fibre. The EDFA displays on-off operation with a non-adjustable gain level and 24 dBm of maximum output saturated power. It uses the polarisation-insensitive InN-based SESAM described in section 4.3.1 [30, 31], as saturable absorber to achieve passive mode-locking. The SESAM section operates in free-space and is optically coupled to the fibre cavity through a circulator. As we discussed in section 4.8, the high insertion losses in the SESAM section play an important role in the pulse dynamics inside the resonator, making it possible to adjust the peak power of the laser pulses to achieve soliton conditions after the SESAM. For increased control over peak power, an additional VOA is inserted between the SESAM section and the URFL amplified section. Another VOA is inserted prior to the EDFA and an isolator is inserted after the EDFA to guarantee unidirectional propagation in the cavity. A 30% of the power is coupled out of the cavity at the laser output through a 70-30 splitter.

6.2.2 Experimental results

System performance is monitored at the laser output, where autocorrelation traces, optical spectra and RF spectra are registered. As a first step, the EDFA is turned on and the system is optimised to work without switching on amplification in the URFL-based extended. The focus of the beam on the SESAM and the attenuator before the EDFA are adjusted to achieve stable fundamental or higher-harmonic mode-locking where possible. As mentioned in Chapter 4, fundamental mode-locking is not achievable for rings longer than 2.4 km. As seen in Chapter 4, additional Raman amplification is not necessary, and indeed does not offer improvements performance in terms of energy per pulse and pulse width for ring lengths allowing for adiabatic soliton propagation. On the other hand, its effects are very relevant for lengths of 10 km and above. As second step, the continuous pump laser at

1365 nm is activated, with pump power equally splitted between the two ends of the URFL span. Power is gradually increased and the output of the system is monitored.

In Figure 6.2 we can observe the resulting pulses for a laser with a 10 km inserted fibre span. Achieving mode-locking is not immediate and may take some time (up to a couple of minutes) for the system to stabilise its output to a specific harmonic order. The system can be mode-locked between the 3^{rd} and the 10^{th} harmonic order at least (fundamental repetition rate, would be 20 kHz). Stable mode-locking with clean Gaussian pulses is more easily achieved at harmonic orders over 5. Thanks to the low attenuation of the fiber, it is still sometimes possible for the 10 km ring to achieve noise mode-locking without activating the URFL, but both stability and control over harmonic order are greatly improved by turning on the pumps and rendering the cavity quasi-lossless.

Starting with no Raman pumping (bottom black lines in Fig. 6.2), the system is stably locked to the 7^{th} harmonic -Fig. 6.2 (c). A Gaussian pulse with pulse width of 455 fs at FWHM is obtained and the optical spectrum, centered around 1555 nm, presents a shoulder around 1530 nm (due to the EDFA spectral output), indicating a large amount of ASE noise. An average output power of 24.1 mW is achieved. As the external pump power is gradually increased, the pulse width slightly narrows, down to 356 fs for a pump power of 30.7 dBm equally splitted between both ends of the 10 km fibre span. In the optical spectra we can notice how the 1530 nm shoulder clearly diminishes at 28.6 dBm, where the span reaches the "zero net gain condition, as the incoming optical power of the pulses, measured at the tap before the Raman amplification section equals the one measured at the entrance of the URFL.

The narrowest pulse and the lowest ASE are obtained with a pump power of 30.7 dBm, where the system reaches an average output power of 33 mW, which is around the same average output power that would emit the laser if we eliminated the 10 km span and the Raman amplification system, leaving a cavity which is about 40 m long. This "basic" system was described in section 4.7.1. In that case we would be able to achieve symmetric Gaussian pulses below 250 fs with a spectral width around 25 nm at fundamental repetition rate of 5.2 MHz (higher harmonic mode-locking would not be achievable). Here, utilizing the URFL-type amplification system we are able to maintain mode-locking and stability of the system for a much longer cavity, as the 10 km fibre span becomes virtually lossless [23, 32, 25]. It allows to achieve a much higher energies per pulse and peak power, which

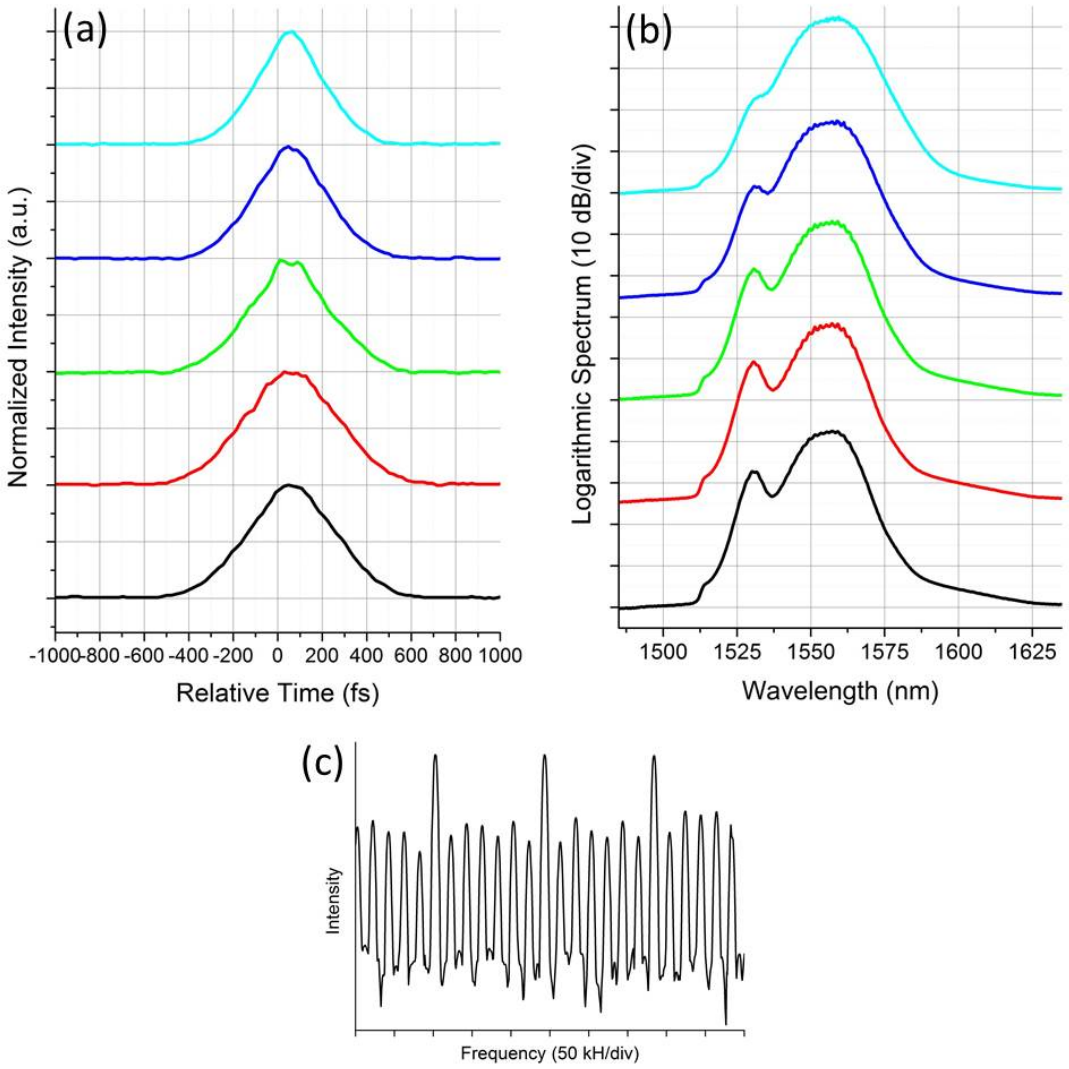

Figure 6.2: Optical spectra (a) and autocorrelation traces (b) with 10 km Raman cavity for increasing total pump power: no pump (black line), 500 mA (red line), 700 mA (green line), 900 mA (blue line, zero net gain Raman span), 1200 mA (light blue line, zero net gain system). RF spectrum (c).

can be estimated to be above 200 nJ and 650 kW respectively for a repetition rate of 140 kHz (7^{th} harmonic), keeping stable harmonic mode-locking over a long distance.

In Figure 6.3 the results for a ring laser with a 25 km URFL are summarized. Here the impact of URFL amplification is even more relevant, as it is the only means to achieve mode-locking with acceptable ASE levels. Once Raman pumping has been turned on, as in the 10 km case, it takes a few moments to lock the system, though in this situation is more difficult to fine tune the optimal focus conditions on the SESAM and loss management, as the much longer cavity leads to increased stability problems. Nonlinearity, dispersion and

attenuation are all increased, as is the total energy recirculating in the system. Anyway it is possible to mode-lock the system from the 17^{th} harmonic order up to at least the 40^{th} (fundamental repetition rate, if possible, would be 8 kHz), for the condition of no external pumping and up to 800 mA (27.6 dBm) of pump power at 1365 nm equally divided and inserted trough the WDMs at the two ends of the 25km fibre span -Fig. 6.3 (c). For higher pump powers, as noticeable in Fig. 6.3 (d), the modes are still clearly observable but it is not possible to determine to which specific harmonic order they are locked. More importantly, only in these last two cases the laser spectrum begins displaying its characteristic Gaussian shape. All other cases are noise-dominated, with an EDFA-like output spectrum. In all cases, the pulses appear more distorted temporally than in the 10-km ring. It seems a reasonable assumption to infer that the higher internal power in the system causes pulse distortion in the final section of the ring. The distortion in the autocorrelation traces at higher powers can actually suggest this, tough we still observe a single envelope.

The autocorrelation traces show Gaussian pulses with a different temporal variation following the increasing pump power. Starting from no pump power, where the temporal width at FWHM is 738 fs -black line in Fig. 6.3 (a)-, it gradually decreases to a minimum of 482 fs at 29 dBm pump power, the case in which the URFL cavity is made quasi-lossless, to increase again up to the starting width at higher power, with the lowest ASE.

Observing the optical spectra -Fig. 6.3 (b)- we can observe how the Raman amplification system is aiding the operation of the laser. Starting with no or low external pumping, we can see clearly how although mode-locking is achieved and a clear pulse is recorded, the spectrum is much close to that of the EDFA than to that of the non-extended ring. Indeed, the 1560 nm peak is partially hidden by the EDFA gain maximum at 1530 nm, suggesting most of the laser energy is contained in the noise components. Increasing pump power, the 1560 nm peak starts to intensify. Under the quasi-lossless transmission condition, when laser power at the output of the URFL Raman cell equals power at its entrance (light blue line in Figure 6.3b), the balance between pulse and ASE is reversed. And when "zero net gain" of the entire system is obtained at 29.4 dBm pump power (light blue line in Figure 6.3b) with the laser reaching the same average output power (31.0 mW) as in the basic ring configuration, the laser output spectrum becomes clearly Gaussian with just a minor shoulder at 1530 nm. A 25 km-long femtosecond pulsed fibre laser is thus obtained,

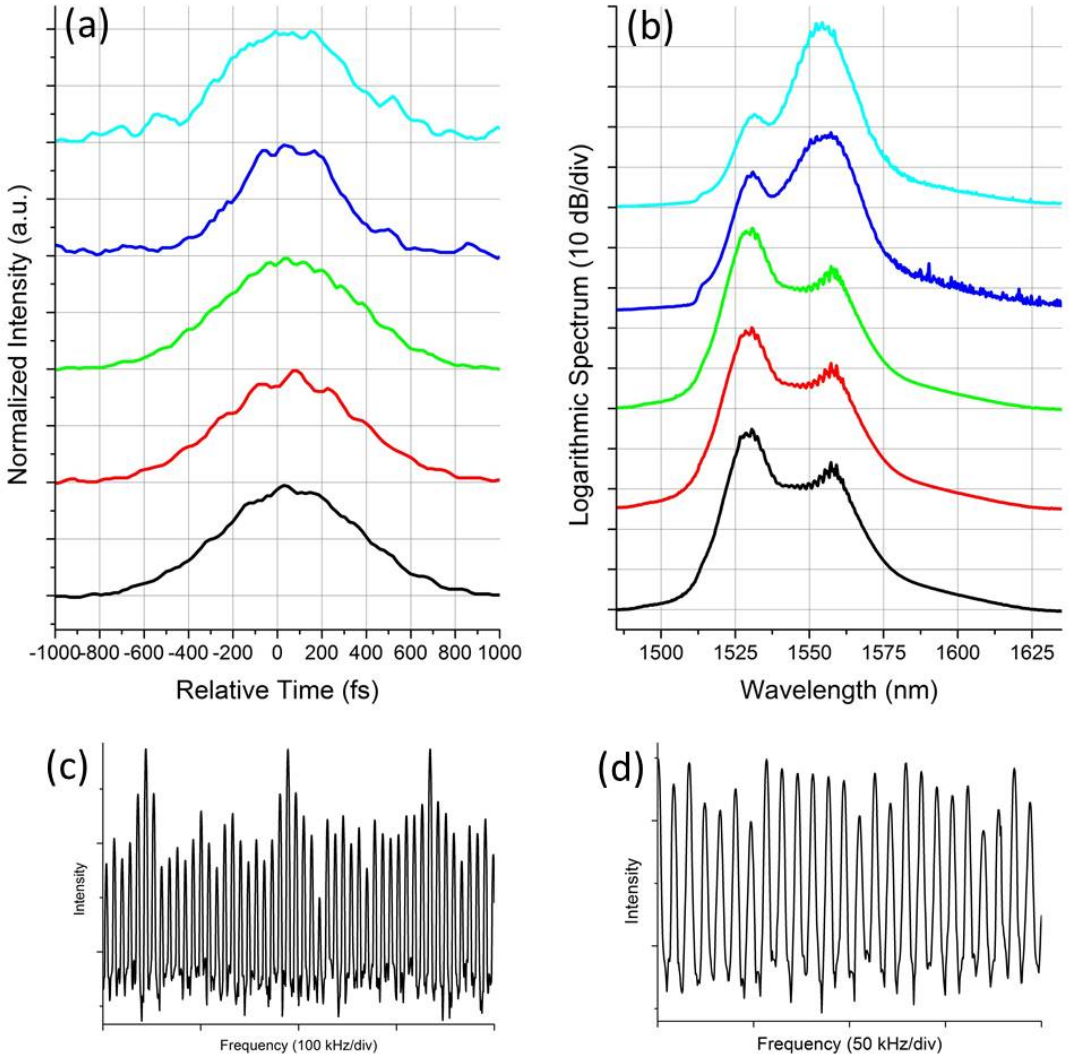

Figure 6.3: Optical spectra (a) and autocorrelation traces (b) with 25 km Raman cavity for increasing total pump power: no pump (black line), 500 mA (red line), 700 mA (green line), 950 mA (blue line, zero net gain Raman span), 1000 mA (light blue line, zero net gain system). RF spectrum below 800 mA pumping (c) and over 800 mA pumping (d).

delivering high power pulses (around 350 kW and 215 nJ can be estimated).

6.2.3 Discussion

A variety of factors lie behind the operation of the system, especially the nonlinearity and dispersion management (the system is overall operating in the anomalous dispersion regime), which, together with loss control, allows for operation in the solitonic regime. The URFL cell introduction provides spatial and spectral transparency over long fibre distances, and the use of a SESAM that combines good optical characteristics with polarisation-insensitiveness and stable operation at high fluences permits the generation of short, high

power pulses.

The design of the cavity includes the free space location of the SESAM connected to the cavity with an optical circulator and allow its use in a high energy laser system without polarisation control. Being the SESAM in free-space, the beam hits the mirror, is reflected and coupled back into the fibre. As occurred in the system described in Chapter 4, though this passage can be optimized improving the alignment, the set-up actually exploits the high insertion losses, of the order of 24 dBm. Additionally, more losses can be introduced if necessary by the following attenuator, as well as by the one prior to the EDFA, which controls the ingoing power into the amplifier. In this way, although the set-up has a high energy output, we manage to have the right power reduction such as to have the conditions for fundamental soliton propagation at the beginning of the Raman amplification section, so that the ultrashort pulse is ready to stably propagate over a long distance of fibre. Properly managing gain and losses inside the URFL-amplified section [26], and so nonlinearities in the dissipative regime, we ensure that these conditions for stable soliton propagation are maintained in the long cavity.

It has been demonstrated that in spans up to 20 km, a second order Raman amplification system, with 1365 nm pumps, is able to maintain a virtually zero signal power variation for the signal transmitted through it, even for high transmitted powers and over wide bandwidths (up to 20 nm) . Even for cells considerably longer than 20 km, this kind of systems sustain a very reduced signal power excursion, which makes them suitable for long-distance communication links [24, 25]. In the present case this behaviour is fully respected, as registered in Fig. 6.2 and 6.3, and the sub-picosecond pulses and mode-locking are maintained over 10 and 25 km.

6.3 Applicability of the system

From the results presented in this Chapter a patent has been developed [33] regarding a system and procedure for the generation of ultrashort high power pulses in lasers. Though here we have presented a specific set-up, the principle could be implemented in any type of fibre laser using conventional fibres, where the length of the cavity could be increased and a distributed amplifier could be implemented. This could be an advantageous, low-cost solution for overcoming the traditional power limitations of ultrafast mode-locked fibre

lasers, enabling their application in areas such as material processing, thanks also to the possibility of tuning the laser repetition rates.

6.4 Conclusions

For the first time to our knowledge, we have been able to experimentally design a femtosecond ultra-long mode-locked fibre laser with a maximum length of 25 km. A ring laser cavity, in which up to 25 km of standard single mode fibre is inserted, is able to sustain sub-picosecond pulse recirculation as soliton propagation is aided by a second order Raman amplification system, in the form of a ultralong Raman fibre laser that produces a virtually spatial and spectral lossless cell around the bandwidth of the laser pulse. It is thus possible to maintain the ultrafast pulse train in the soliton regime with temporal width at FWHM well below the picosecond (down to 355 fs for a 10 km long cavity and to 482 fs for 25 km). Furthermore, this approach is not limited to the specific system showcased in this chapter, but potentially applicable to any mode-locked fibre laser.

References

[1] L. E. Nelson, D. J. Jones, K. Tamura, H. A. Haus, and E. P. Ippen, "Ultrashort-pulse fiber ring lasers," *Appl. Phys. B Lasers Opt.*, vol. 65, no. 2, pp. 277–294, 1997.

[2] K. Tamura, H. A. Haus, and E. P. Ippen, "Self-starting additive pulse mode-locked erbium fibre ring laser," *Electronics Letters*, vol. 28, no. 24, pp. 2226–2228, 1992.

[3] K. Tamura, E. P. Ippen, H. A. Haus, and L. E. Nelson, "All-Fiber Ring Laser," vol. 18, no. 13, pp. 1080–1082, 1993.

[4] M. E. Fermann and I. Hartl, "Ultrafast fibre lasers," *Nat. Photonics*, vol. 7, no. 11, pp. 868–874, 2013.

[5] Y. Senoo, N. Nishizawa, Y. Sakakibara, K. Sumimura, E. Itoga, H. Kataura, and K. Itoh, "Ultralow-repetition-rate, high-energy, polarization-maintaining, er-doped, ultrashort-pulse fiber laser using single-wall-carbon-nanotube saturable absorber," *Opt. Express*, vol. 18, no. 20, pp. 20 673–20 680, Sep 2010.

[6] H. G. Rosa and E. A. T. de Souza, "Pulse generation and propagation in dispersion-managed ultralong erbium-doped fiber lasers mode-locked by carbon nanotubes," *Opt. Lett.*, vol. 37, no. 24, pp. 5211–5213, 2012.

[7] Y. Cai, C. Zhou, L. Chen, M. Zhang, L. Ren, P. Li, and Z. Zhang, "Sub-100kHz Repetition Rate Mode-locked Dispersion Managed Erbium-doped Fiber Laser," *CLEO/-Pacific Rim 2009*, no. 2, pp. 5–6, 2009.

[8] J. L. Dong, Z. C. Luo, W. C. Xu, A. P. Luo, L. Y. Wang, W. J. Cao, and H. Y. Wang, "Sub-100 kHz repetition rate erbium-doped fiber laser in anomalous dispersion regime," *Laser Phys.*, vol. 21, no. 6, pp. 1111–1114, 2011.

[9] P. Z. Liu, J. Hou, B. Zhang, S. P. Chen, and J. B. Chen, "Passively mode-locked fiber ring laser using semiconductor saturable absorber mirror," *Laser Phys.*, vol. 22, no. 1, pp. 273–277, 2012.

[10] A. Ivanenko, S. Kobtsev, S. Smirnov, and A. Kemmer, "Mode-locked long fibre master oscillator with intra-cavity power management and pulse energy >12 μ J," *Opt. Express*, vol. 24, no. 6, pp. 6650–6655, 2016.

[11] I. Yarutkina, O. Shtyrina, M. Fedoruk, and S. Turitsyn, "Numerical modeling of fiber lasers with long and ultra-long ring cavity," *Opt. Express*, vol. 21, no. 10, pp. 12 942–12 950, 2013.

[12] O. V. Shtyrina, I. A. Yarutkina, A. S. Skidin, E. V. Podivilov, and M. P. Fedoruk, "Theoretical analysis of solutions of cubic-quintic ginzburg-landau equation with gain saturation," *Optics Express*, vol. 27, no. 5, pp. 6711–6718, 2019.

[13] A. Ivanenko, "Mode-Locking in 25-km Fibre Laser," no. 1, pp. 23–25, 2010.

[14] S. Kobtsev, S. Kukarin, and Y. Fedotov, "Ultra-low repetition rate mode-locked fiber laser with high-energy pulses," *Opt. Express*, vol. 16, no. 26, p. 21936, 2008.

[15] S. M. Kobtsev, S. V. Kukarin, S. V. Smirnov, and Y. S. Fedotov, "High-energy mode-locked all-fiber laser with ultralong resonator," *Laser Phys.*, vol. 20, no. 2, pp. 351–356, 2010.

[16] X. Li, X. Liu, X. Hu, L. Wang, H. Lu, Y. Wang, and W. Zhao, "Long-cavity passively mode-locked fiber ring laser with high-energy rectangular-shape pulses in anomalous dispersion regime." *Opt. Lett.*, vol. 35, no. 19, pp. 3249–3251, 2010.

[17] N. Li, J. Xue, C. Ouyang, K. Wu, J. H. Wong, S. Aditya, and P. P. Shum, "Cavity-length optimization for high energy pulse generation in a long cavity passively mode-locked all-fiber ring laser," *Appl. Opt.*, vol. 51, no. 17, pp. 3726–3730, 2012.

[18] F. Gallazzi, M. Jiménez-Rodríguez, E. Monroy, P. Corredera, M. González-Herráez, F. B. Naranjo, and J. D. Ania Castañón, "Megawatt peak-power femtosecond ultralong ring fibre laser with InN SESAM," in *2019 Conference on Lasers and Electro-Optics Europe and European Quantum Electronics Conference*. Optical Society of America, 2019, p. cf˙p˙13.

[19] L. F. Mollenauer and R. H. Stolen, "The soliton laser," *Optics Letters*, vol. 9, no. 1, pp. 13–15, 1984.

[20] C.-J. Chen, P. K. A. Wai, and C. R. Menyuk, "Soliton fiber ring laser," *Opt. Lett.*, vol. 17, no. 6, p. 417, 1992.

[21] A. B. Grudinin and S. Gray, "Passive harmonic mode locking in soliton fiber lasers," *Journal of the Optical Society of America B: Optical Physics*, vol. 14, no. 1, pp. 144–154, 1997.

[22] P. Grelu and N. Akhmediev, "Dissipative solitons for mode-locked lasers," *Nature Photonics*, vol. 6, no. 2, pp. 84–92, 2012.

[23] J. D. Ania-Castañón, "Quasi-lossless transmission using second-order raman amplification and fiber bragg gratings," *Optics Express*, vol. 12(19), p. 43724377, 2004.

[24] J. D. Ania-Castañón, T. J. Ellingham, R. Ibbotson, X. Chen, L. Zhang, and S. K. Turitsyn, "Ultralong raman fiber lasers as virtually lossless optical media," *Phys. Rev. Lett.*, vol. 96, p. 023902, 2006.

[25] J. D. Ania-Castañón, V. Karalekas, P. Harper, and S. K. Turitsyn, "Simultaneous spatial and spectral transparency in ultralong fiber lasers," *Phys. Rev. Lett.*, vol. 101, no. 12, pp. 1–4, 2008.

[26] M. Alcon-Camas, A. E. El-Taher, H. Wang, P. Harper, V. Karalekas, J. A. Harrison, and J. D. Ania-Castañón, "Long-Distance Soliton Transmission Through Ultralong Fiber Lasers," *Opt. Soc. Am.*, vol. 34, no. 20, pp. 3104–3106, 2009.

[27] S. K. Turitsyn, "Theory of energy evolution in laser resonators with saturated gain and non-saturated loss," *Opt. Express*, vol. 17, no. 14, p. 11898, 2009.

[28] P. Rosa, J. D. Ania-Castañón, and P. Harper, "Unrepeatered DPSK transmission over 360 km SMF-28 fibre using URFL based amplification," *Optics Express*, vol. 22, no. 8, pp. 9687–9692, 2014.

[29] M. Tan, P. Rosa, I. Phillips, and P. Harper, "Extended Reach of 116 Gb/s DP-QPSK Transmission using Random DFB Fiber Laser Based Raman Amplification and Bidirectional Second-order Pumping," *Opt. Fiber Commun. Conf.*, p. W4E.1, 2015.

[30] M. Jiménez-Rodríguez, L. Monteagudo-Lerma, E. Monroy, M. González-Herráez, and F. Naranjo, "Widely power-tunable polarization independent ultrafast mode-locked fiber laser using bulk inn as saturable absorber," *Optics Express*, vol. 25, no. 5, pp. 5366–5375, 2017.

[31] M. Jiménez-Rodríguez, E. Monroy, M. González-Herráez, and F. B. Naranjo, "Ultrafast fiber laser using inn as saturable absorber mirror," *J. Lightwave Technol.*, vol. 36, no. 11, pp. 2175–2182, 2018.

[32] J. D. Ania-Castañón, S. K. Turitsyn, A. Tonello, S. Wabnitz, and E. Pincemin, "Multi-level optimization of a fiber transmission system via nonlinearity management." *Opt. Express*, vol. 14, no. 18, pp. 8065–8071, 2006.

[33] J. D. Ania-Castañón and F. Gallazzi, "Sistema y procedimiento de generación de pulsos ultracortos de alta potencia en láseres," *Spanish patent applied for*, 2019.

Chapter 7

Conclusions

We will summarize in this chapter the principal results accomplished in this thesis, regarding the study of ultralong fibre laser and amplifiers, in the CW regimes (Raman distributed amplifiers) and ultrafast mode-locked regime (femtosecond ring fibre lasers), and how, for the first time, it has been possible to integrate these kind of systems. Afterwards we will propose some possible lines for future studies.

7.1 General conclusions

The main conclusions that we can draw from this thesis are the following.

Regarding Raman distributed amplifiers for telecommunication applications:

- In a 100 km long 2^{nd} order URFL amplifier, in which it is possible to vary front-end reflectivity and pump power ratio, we have experimentally characterised RIN transfer from pump to signal. Starting from the same point in the case of total backward pumping, RIN level builds up differently in the cavity for variable and fixed pump RIN. With variable pump RIN, RIN penalty is considerably lower (at least 10 dB) when the impact of FW pumping starts to be not negligible (30% FW pumping). With fixed pump RIN, signal RIN slope steepens at a lower FW pump ratio.

- For fixed pump RIN and variable front-end reflectivity and pump split, experimental signal RIN integrated over 1 MHz increases as the FW pump power increases. For higher front-end reflectivity, the increment starts at a lower FW pump ratio and with steeper slope.

- Taking into consideration the previous results, we have analysed the impact of front-end reflectivity and FW pump ratio in a 108 km URFL, amplifying a long-haul transmission system. RIN transfer for higher (40%) FW pump ratio quickly degrades the transmission performance, which has best result with 10% and 20% FW pump ratios and 20% and 10% VRM reflectivity respectively (it allows a transmission distance of at least 5399 km with less than 0.7 dB variation among the Q-factors of the 10 channels). Using a flexible variable reflectivity module and fixed-RIN fibre laser pumps, we have demonstrated the possibility of optimizing the amplifier design to offer the best balance between ASE and RIN impairments for a 10 x 30 Gbaud DP-QPSK transmission system tested through a recirculating loop. The best performance is obtained with 20% forward pump power ratio and 10% front-end reflectivity, with a reach of 6479 km for all the 10 channels between 1542.94 nm and 1550.12 nm. This optimal balance can be expected to be dependent on both transmission format and pump RIN specifications. The results are coherent with the previous RIN transfer characterization in the cavity.

Regarding the ultrafast mode-locked lasers:

- Using as starting point a ∼40 m long ring cavity delivering a train of 239 fs symmetric Gaussian pulses at 1.56 μm at a repetition rate of ∼5 MHz with peak power of 26 kW and energy of 6 nJ, we were able to develop a simple low-cost polarisation-independent high peak-power ultrafast passively mode-locked ring fibre, laser relying on a novel InN SESAM, a commercial EDFA and standard fibre optics laboratory components, capable of achieving, for the first time to our knowledge, sub-250 fs with peak powers in the order of 1 MW in an ultralong cavity. For a 2.37 km-long SSMF-based cavity locked to the fundamental mode, our master oscillator, without additional pulse compression or amplification, delivers ∼200 fs Gaussian pulses with a repetition rate of 87 kHz and a peak power of 1.27 MW, overcoming traditionally assumed limitations and paving the way for new applications in areas such as materials processing at a fraction of its previous cost.

- The mentioned results are achieved thanks to the outstanding properties of the SESAM and the power/losses (alas nonlinearities) management in the cavity, which allow for fundamental soliton propagation at the beginning of the SSMF span inside

the resonator.

- Results are compared with a commercial GaAs-based SESAM, which needs polarisation control for stable mode-locked operation. While, with appropriate polarisation control, the basic 40 m long cavity has comparable performances with the InN-based resonator, for longer ring lengths performances soon degrade and stable mode locking is lost in cavities longer than 1 km.

- Tuning the ingoing power in the EDFA, harmonic mode-locking operation is demonstrated in cavities from 1.05 km to 5.7 km, allowing a broad choice of peak powers and repetition rates.

- Using the previously mentioned high power ultrafast lasers (either in the 1.05 km or 2.4 km long configurations) simple low-cost supercontinuum sources are developed using conventional single mode fibres (SSMF, DSF, DCF). Selection of the type of fibre, resonator length and output harmonic order partially grant control and tailoring of the generated supercontinuum. SMF-generated SC over 200 nm allows pulse compression down to 50 fs. With DSF we observe different scenarios according to the input power: Raman soliton propagation for high input power and SC generation and pulse compression (70 fs) for lower input powers. Raman scattering is the main agent in the case of DCF, where a strong new peak appear close to the Raman first Stokes frequency, whereas pulse break up is observable in the temporal trace.

- We confirm with all the types of fibre that the selection of the harmonic in the master oscillator give control on the pulse power ingoing in the external reel of fibre and so on the nonlinear and dispersive effects they experience along the fibre span.

- A proof-of-concept trial for the application of the developed supercontinuum sources to gas sensing is positively conducted. Direct absorbance spectra of $H^{12}C^{14}N$, $^{12}C^{16}O$ and $^{13}C^{16}O$ were successfully recorded.

Regarding Raman distributed amplifiers implementation in ultrafast pulsed lasers:

- For the first time to our knowledge, we have been able to experimentally design a femtosecond ultra-long mode-locked fibre laser with a maximum length of 25 km. A ring laser cavity, in which up to 25 km of standard single mode fibre is inserted, is

able to sustain sub-picosecond pulse recirculation as soliton propagation is aided by a second order Raman amplification system, in the form of a ultralong Raman fibre laser that produces a virtually spatial and spectral lossless cell around the bandwidth of the laser pulse. It is thus possible to maintain the ultrafast pulse train in the soliton regime with temporal width at FWHM well below the picosecond (down to 355 fs for a 10 km long cavity and to 480 fs for 25 km).

- Furthermore, this approach is not limited to the specific system showcased in this chapter, but potentially applicable to any mode-locked fibre laser.

7.2 Future works

For each of these lines several new studies may be proposed.

- URFLs in telecommunication have already been subject of extensive study, nevertheless further works leading to possible improvements may be suggested. First of all, the use of low RIN pumps, as finally semiconductor laser sources with the appropriate pump power are becoming available, should be tested. A lower pump RIN may improve the amount of tolerated FW pumping, approaching equal bidirectional pumping which is theoretically the best pumping solution. Also the introduction of new fibres allowing for nonlinearity management could be tested. Finally, multi-mode and multi-core fibres are acquiring more and more importance in telecommunications as possible solution to increase the bandwidth capacity, but the study of URFLs architectures, with also the possibility of polarisation multiplexing formats, with this kind of fibres has not been conducted yet and it would be interesting to undertake.

- For what regards the high peak-power passively mode-locked ultrafast lasers with InN-based SESAM, first of all a complete numerical model for the simulation of the laser should be implemented. Several other studies may be suggested both for completing the characterization and improving the performances of the system: characterise the pulses with spectral phase interferometry, measure the laser phase noise, try opearation with other configuration of the laser system and operation with autosimilar pulses, study pulse compression at the output of the resonator, use the system for polarisation attraction studies.

- In this thesis we presented some first possible applications of the high power laser system. A thorough study of supercontinuum generation may be undertaken, using also highly nonlinear fibres. Since it has been proven its feasibility, proper implementation and calibration of a spectroscopy system may be conducted. Other applications, such has material processing, could be tried.

- As it is the first time that an URFL amplifier has been implemented in a pulsed laser, this line of study is all but complete. As suggested the Raman amplifier can be tested in other laser lengths, configurations and systems and with other kind of pulses, for example parabolic pulses. A complete characterization of the pulses with spectral phase interferometry and measurement of the noise are also advisable. Finally the simulation of the total cavity can be performed.

Appendix A

List of publications

A.1 Journal publications

1. Giuseppe Rizzelli, Md Asif Iqbal, Francesca Gallazzi, Pawe Rosa, Mingming Tan, Juan Diego Ania-Castañón, Lukasz Krzczanowicz, Pedro Corredera, Ian Phillips, Wladek Forysiak and Paul Harper, *Impact of input FBG reflectivity and forward pump power on RIN transfer in ultralong Raman laser amplifiers*, Optics Express 24, 29170-29175 (2016).

2. Javier Nuño, Giuseppe Rizzelli, Francesca Gallazzi, Francisco Prieto, Concepción Pulido, Pedro Corredera, Stefan Wabnitz and Juan Diego Ania-Castañón, *Open-Cavity Spun Fiber Raman Lasers with Dual Polarization Output*, Scientific Reports 7, 13681, (2017).

3. Francesca Gallazzi, Giuseppe Rizzelli, Md Asif Iqbal, Mingming Tan, Paul Harper and Juan Diego Ania-Castañón, *Performance optimization in ultra-long Raman laser amplified 1030 GBaud DP-QPSK transmission: balancing RIN and ASE noise*, Optics Express 25, 21454-21459 (2017).

4. Francesca Gallazzi, Marco Jiménez-Rodríguez, Eva Monroy, Pedro Corredera, Miguel González-Herráez, Fernando B. Naranjo, Juan Diego Ania-Castañón, *Megawatt peak-power femtosecond passively mode-locked ultralong ring fibre lasers*, submitted.

5. Francesca Gallazzi, Laura Monroy, Javier Nuño, Pedro Corredera, Fernando B. Naranjo, Miguel González-Herráez and Juan Diego Ania-Castañón, *Tunable super-*

continuum generation with InN-SESAM based fs high-power single-mode fiber laser, submitted.

A.2 Conference contributions

1. J. Nuño del Campo, G. Rizzelli, F. Gallazzi, F. Prieto, M. C. Pulido-De Torres, P. Corredera, S. Wabnitz, and J. D. Ania-Castañón, *Open-Cavity Spun Fiber Raman Lasers with a Polarized Output*, in CLEO 2016 - Conference on Lasers and Electro-Optics, OSA Technical Digest (2016), paper SW4P.5.

2. J.D. Ania-Castañón, P. Rosa, G. Rizzelli, F. Gallazzi, J. Nuño and P. Corredera, *The role of distributed Raman amplification in the times of the 'capacity crunch'*, in 18th International Conference on Transparent Optical Networks ICTON 2016, paper Mo.D.14.

3. Md A. Iqbal, Giuseppe R. Martella, F. Gallazzi, M. Tan, P.Harper, and J. D. Ania-Castañón, *Performance improvement of broadband distributed Raman amplifier using bidirectional pumping with first and dual order forward pumps*, in 18th International Conference on Transparent Optical Networks ICTON 2016, paper Tu.P.30.

4. G. Rizzelli Martella, Md A. Iqbal, F. Gallazzi, P. Rosa, M. Tan, P. Corredera, J. D. Ania-Castañón, P. Harper, *FBG Reflectivity Impact on RIN in Ultralong Laser Amplifiers*, in ECOC 2016 - European Conference on Optical Communication, 625-627.

5. M. A. Iqbal, M. Tan, L. Krzczanowicz, G. Rizzelli, F. Gallazzi, A. E. El-Taher, W. Forysiak, P. Harper and J. D. Ania-Castañón, *Noise Performance Improvement of Broadband Distributed Raman Amplifier Using Dual Order Bidirectional Pumping*, in ACP 2016 - Asia Communications and Photonics Conference, paper AF4G.2.

6. M. Jiménez-Rodríguez, F. Gallazzi, J. D. Ania-Castañón, E. Monroy, M. González-Herráez, and F. B. Naranjo, *Sub-200 fs mode-locked fiber laser with InN-based SESAM*, in CLEO/Europe-EQEC 2017 - European Conference on Lasers and Electro-Optics and European Quantum Electronics Conference, paper CF-P.31.

7. F. Gallazzi, G. Rizzelli, M. A. Iqbal, M. Tan, P. Harper, and J. D. Ania-Castañón, *Optimal Balance of RIN and ASE Impairments in Ultra-long Raman Laser Amplified 10 x 30 GBaud DP-QPSK Transmission*, in CLEO/Europe-EQEC 2017 - European Conference on Lasers and Electro-Optics and European Quantum Electronics Conference, paper CI-2-1.

8. F. Gallazzi, G. Rizzelli, Md A. Iqbal, M. Tan, P. Harper, and J. D. Ania-Castañón, *Balancing RIN and ASE Noise in Ultra-long Raman Laser Amplified 10x30 GBaud DP-QPSK Transmission*, in Reunin Espaola de Optoelectrnica OPTOEL 2017 (awarded best student paper with II Premio Carlos Gómez-Reino).

9. F. Gallazzi, M. Jiménez-Rodríguez, E. Monroy, P. Corredera, M. González-Herráez, F. B. Naranjo, and J. D. Ania-Castañón, *Sub-250 fs, 650 kW Peak Power Harmonic Mode-Locked Fiber Laser with InN-based SESAM*, in ECOC 2017 - European Conference on Optical Communication, paper P1.SC1.3.

10. F. Gallazzi, M. Jiménez-Rodríguez, E. Monroy, P. Corredera, M. González-Herráez, F. B. Naranjo, and J. D. Ania-Castañón, *High power ultrafast mode-locked ring fibre laser with InN SESAM*, in SPIE Photonics Europe 2018, paper [10683-59] SJS.

11. F. Gallazzi, P. Corredera, F. B. Naranjo, M. González-Herráez, and J. D. Ania-Castañón, *Supercontinuum Generation and Pulse Compression from a Passively Mode-locked Ultrafast Ring Fibre Laser*, in PIERS 2019 PhotonIcs and Electromagnetics Research Symposium.

12. F. Gallazzi, M. Jiménez-Rodríguez, E. Monroy, P. Corredera, M. González-Herráez, F. B. Naranjo, and J. D. Ania-Castañón, *Megawatt peak-power femtosecond ultralong ring bre laser with InN SESAM*, in CLEO/Europe-EQEC 2019 European Conference on Lasers and Electro-Optics and European Quantum Electronics Conference, paper CF-P.13.

13. F. Gallazzi, M. Jiménez-Rodríguez, E. Monroy, P. Corredera, M. González-Herráez, F. B. Naranjo, and J. D. Ania-Castañón, *Ultrafast passively mode locked ring fibre laser with InN SESAM: overcoming the megawatt peak power*, in Reunin Espaola de Optoelectrnica, OPTOEL 2019, paper SP1.LAS10 (awarded best student paper with SPIE student prize).

14. F. Gallazzi, P. Corredera, F. B. Naranjo, M. González-Herráez, and J. D. Ania-Castañón, Ultrafast Pulse Compression, *Supercontinuum Generation and Raman Soliton Propagation in Single Mode Fibres*, in Reunin Espaola de Optoelectrnica, OPTOEL 2019, paper SP3.FIB05.

15. J. D. Ania-Castañón, F. Gallazzi, P. Corredera, M. Jiménez-Rodríguez, M. González-Herráez, and F. B. Naranjo, *Ultra-long femtosecond pulsed fibre lasers*, in 21st International Conference on Transparent Optical Networks ICTON 2019, paper Fr.C4.1.

A.3 Books

- Sara Aissati Aissati, Xoana Barcala Gosende, Clara Benedí García, Camilo Florian Baron, Francesca Gallazzi, Mario García Lechuga, Juan Luis García Pomar, Rocío Gutiérrez Contreras, Juan Luis Méndez González, Roberta Morea, Javier Nuño del Campo, Pablo Pérez Merino, Daniel Puerto García, Maria Viñas Peña (coord.), *Descubriendo la luz. Experimentos divertidos de óptica*, Editorial CSIC, Los Libros de la Catarata (Spain, 2018), ISBN 978-84-9097-536-7.

A.4 Patents

- *Sistema y procedimiento de generación de pulsos ultracortos de alta potencia en láseres*, Juan Diego Ania-Castañón, Francesca Gallazzi, 2019, *Spanish patent applied for.*